ROTAVIRUS NSP4 IN EXTRARETICULAR SITES: SUPPORT FOR ITS PATHOGENIC ROLE AS AN ENTEROTOXIN

A Dissertation

by

THOMAS FIELD GIBBONS

Submitted to the Office of Graduate Studies of
Texas A&M University
in partial fulfillment of the requirements for the degree of

DOCTOR OF PHILOSOPHY

December 2007

Major Subject: Veterinary Microbiology

ROTAVIRUS NSP4 IN EXTRARETICULAR SITES: SUPPORT FOR ITS PATHOGENIC ROLE AS AN ENTEROTOXIN

A Dissertation

by

THOMAS FIELD GIBBONS

Submitted to the Office of Graduate Studies of
Texas A&M University
in partial fulfillment of the requirements for the degree of

DOCTOR OF PHILOSOPHY

Approved by:

Chair of Committee,	Judith M. Ball
Committee Members,	Susan Payne
	Friedhelm Schroeder
	Ian Tizard
Head of Department	Gerald R. Bratton

December 2007

Major Subject: Veterinary Microbiology

ABSTRACT

Rotavirus NSP4 in Extrareticular Sites: Support for Its Pathogenic Role as an Enterotoxin. (December 2007)

Thomas Field Gibbons, B.A.A.S., Midwestern State University;

M.S., University of North Dakota

Chair of Advisory Committee: Dr. Judith M. Ball

Rotavirus non structural protein 4 (NSP4) was initially characterized as an endoplasmic reticulum intracellular receptor. Continued studies of NSP4 revealed additional functions performed by or dependent on NSP4, some of which required trafficking from the ER to other areas of the cell. Chiefly, purified NSP4 exogenously added to the PM has been shown to mobilize intracellular calcium by a phospholipase C/inositol trisphosphate signaling pathway, yet the details whereby NSP4 are able to exert enterotoxic actions are still unknown. Our initial hypothesis included the protein caveolin 1, which subsequently was proven to bind NSP4 and prompted continued investigation as to whether or not NSP4 utilized caveolin 1 for extrareticular transport and or function. Caveolin 1 is the defining protein of caveolae, a region of the plasma membrane rich in multiple molecules that function in signal transduction, including possible receptor mediated activation of the phospholipase C/inositol triphosphate pathway. To determine if NSP4 trafficked to caveolae, a novel isolation procedure was developed and utilized to show NSP4 in PM caveolae. Expanding on the caveolae/NSP4

finding, temporal and spatial analyses of NSP4 in relation to progeny virus were conducted. NSP4's appearance at the exofacial surface of the PM was carried out utilizing surface biotinylation, exofacial staining of live cells, and confocal imaging of the PM with fluorescent resonance energy transfer studies. During these studies soluble NSP4, which was isolated from RV infected cells, was also shown to interact with the PM of multiple cell lines. These studies provided confirmation of the NSP4-caveolin interaction in the presence and absence of other viral proteins. Our studies indicate the presence of full length NSP4 glycans at caveolae and the exofacial PM and are in agreement with studies indicating NSP4 traffics independent of the Golgi network. To further explore the NSP4/caveolin 1 interaction, we conducted a comparative analysis of NSP4 in relation to two separate pools of proteins. The first pool included proteins collocated with the classical secretory pathway proteins, including caveolin 1, which traffick through the Golgi. The second pool included proteins collocated with a subset of caveolin 1, which traffick independently of the Golgi.

DEDICATION

To my wife Patty,
and our wonderful kids
Alex, Katie and Ian

ACKNOWLEDGMENTS

I would like to thank my committee chair, Dr. Ball and my committee members, Dr. Payne, Dr. Schroeder, and Dr. Tizard, for their guidance and support throughout my research endeavors. I would also like to thank everyone whom I have had the pleasure and honor to work with in Dr. Ball's laboratory, Dr. Parr, Dr. Moore-Smith, Dr. Storey, Cecilia Williams, and Meagan Schroeder.

I am appreciative to the United States Air Force for selecting me to pursue a Ph.D. in microbiology at Texas A&M University. My time here has been most rewarding and I look forward to applying what I have learned while continuing to serve in the USAF.

NOMENCLATURE

aa	Amino acid
CCC	Caveolin 1 chaperone complex
DLP	Double layered particle
ds RNA	Double stranded RNA
endo H	Endo-β-N-acetylglucosaminidase H
ERCIC	Endoplasmic reticulum Golgi intermediate complex
FRET	Fluorescent resonance energy transfer
hpi	hours post infection
IDV	Integrated density value
MOI	Multiplicity of infection
mRNA	messenger RNA
NSP4	Non structural protein 4
PAPB	Poly(A)- binding protein
PIP2	Phosphatidylinositol 4,5 bisphosphate
PM	Plasma membrane
PMSF	Phenylmethysulfonyl Fluoride
RT	Room temperature
RV	Rotavirus
TLP	Triple layered particle
USAF	United States Air Force

TABLE OF CONTENTS

Page

Page

Page

Page

LIST OF TABLES

LIST OF FIGURES

FIGURE Page

FIGURE Page

1. INTRODUCTION: OVERVIEW OF ROTAVIRUS, NSP4, CAVEOLIN-1 AND THE CAVEOLIN-1 CHAPERONE COMPLEX

1.1 Rotavirus

Rotaviruses (RV) are the major viral etiologic agent of severe gastroenteritis in young children worldwide affecting approximately 70% of children before the age of 5 (27, 41, 45, 58). While mortality due to RV diarrheal disease is infrequent in US children under 5 years old, an estimated 54,000 – 55,000 hospitalizations and a financial burden of over 1 billion dollars occur annually (41). The burden of RV disease from a similar age group in developing countries has been estimated at 111 million cases and result in 440,000 deaths annually (94).

Rotavirus, family reoviradae, is a double stranded RNA virus composed of 11 segments of RNA. Each segment of RNA encodes for a single protein except for segment 11 which codes for two proteins giving a total of 12 proteins, six of which are structural and six are non structural. The 11 double stranded RNA segments are surrounded by three layers of protein coats;VP2, VP6 and VP7, (13, 49, 105) with 60 dimeric spikes composing a fourth protein, VP4, protruding from the VP7 (4). These

---

This dissertation follows the style of Journal of Virology.

four structural proteins along with VP1, which is an RNA dependent RNA polymerase (145) and VP3, which caps the rotavirus mRNA (100) comprise the nonenveloped 100 nm diameter triple layered particle (TLP) of mature RV.

To gain access to the cell, VP4 undergoes a proteolytic cleavage event. The cleavage products of VP4 remain associated with the virus, aiding the interaction with and passage through the cell membrane to the cytosol (56). Once inside the cell, the outer capsid VP7 and spikes of VP4 are lost. Without its outer capsid, rotavirus is referred to as a Double Layer Particle (DLP). The DLP, which is transcriptionally competent, begins to synthesize messenger RNA (mRNA). This synthesis occurs within the DLP with all 11 strands of the mRNA being extruded from the interior of the innermost capsid (VP2) and beyond the intermediate capsid (VP6) to the cytosol of the cell. The rotaviral mRNA strands are not polyadenylated as eukaryotic mRNA (56, 99). One of RV's six nonstructural proteins (NSP3) has an N-terminal region that interacts with a consensus sequence located in the 3 prime region of all 11 mRNAs of rotavirus. The C-terminal region of NSP3 has a region with activity similar to, but with higher affinity than cellular poly(A)-binding protein (PABP). As NSP3 levels increase in the cytosol, PABP is removed from the eukaryotic initiation factor 4E resulting in a decrease of the translation of the cellular proteins (56, 84). NSP3 also was thought to be required for rotaviral protein synthesis, (56) but recent work has suggested this may not be the case (84).

Much of the replication process for progeny rotavirus occurs in viroplasms, which are electron dense inclusion bodies within the RV infected cell. Nonstructural

proteins, NSP2 and NSP5, have been shown to drive the formation of viroplasm-like structures within the infected cell (35). The key constituent proteins (VP1,VP2,VP3 and VP6) needed to form rotavirus DLP's are concentrated within the protected environment of the viroplasm. The viroplasm also appears to be the site of nascent genomic double stranded RNA (ds RNA). Copies of the RNA strands are packaged along with VP1 and VP3 within VP2, which is in turn packaged within VP6 to form the DLP. NSP1 has virus-specific RNA binding properties (50) and it as well as many of the non structural proteins appear to play a role in the process of genome replication (56). The function of NSP6 is unknown, but has been shown to be unimportant for RV replication in cell culture (74).

The final maturation of RV requires the acquisition of VP7 and VP4, which constitutes the outer most capsid, to form the TLP. This process is mediated by NSP4, as NSP4 appears to pull the DLP from the viroplasm into the endoplasmic reticulum (ER) of the cell. As the DLP enters the ER it becomes transiently enveloped. During its exit from the ER, the envelope is lost but the proteins for the TLP are retained. RV is now ready to exit the cell and continue the infective process (25, 39).

While it is apparent that RV can affect the function of intestinal cells and cause diarrhea, there is not a single well defined mechanism as to why some RV strains induce severe diarrhea, while others cause milder asymptomatic infections. Several viral and host factors interact to determine the extent of infection and disease production. For example, RV can cause some pathological changes in intestinal epithelial cells, but these changes and subsequent inflammation are usually mild as compared to other intestinal

pathogens (109). Although the changes in the intestinal epithelial cells may contribute to diarrhea, there is no direct correlation with the pathological changes noted in the intestinal cells and the onset of diarrhea (109). NSP4 appears to play a role in decreasing the intestinal cells ability to absorb fluids from the intestinal lumen while simultaneously causing the same intestinal cells to over secrete fluids into the lumen of the intestines. In RV infection, both the malabsorption and hyper-secretion contribute to diarrhea. In human intestinal cells, NSP4 induces Ca^{++} release from the ER, activating Cl^{-} secretion resulting in water loss (30). Electrophysiological analyses of unstripped mucosa from young mice show NSP4 residues 114-135 potentiate Cl- secretion through a Ca^{++} mediated pathway (9). Digestive enzymes important for absorption are under expressed at the apical surface of RV infected enterocytes (24). It has been hypothesized that NSP4 is released from infected cells and interacts with surrounding uninfected cells. It has also been postulated that when NSP4 binds these surrounding cells, it triggers a sequence of events that leads to over secretion from these yet uninfected cells (9, 109).

1.2 NSP4

NSP4 is synthesized as a primary translation product with an approximate molecular weight of 20kD, is cotranslationally glycosylated to 29kD, and undergoes subsequent oligosaccharide processing to produce the mature 28kD protein (34). The 175 amino acid (aa) polypeptide of NSP4 consists of three N-terminal hydrophobic domains and an amphipathic α-helix that overlaps a coiled-coil region (34, 137). Topological analysis of NSP4 revealed a single transmembrane domain (aa 24-44) that orients the N-terminal 23 aa into the ER lumen and the C-terminal 130 aa as a

cytoplasmic tail (10, 21). Two N-linked high mannose glycosylation sites are located within the N-terminal, ER luminal domain at aa 8 and 18 (Fig. 1.1).

The C-terminal 14 residues of NSP4 (aa 161-175) function in viral morphogenesis by binding the outer coat of immature viral particles (VP6) and mediating the budding of these particles through the ER membrane into the ER lumen (81). NSP4 aa 112-148 function in the binding of the spike protein VP4 which decorates the outer layer of RV (6), aa 129-175 bind microtubules (143), and NSP4 aa 114-135

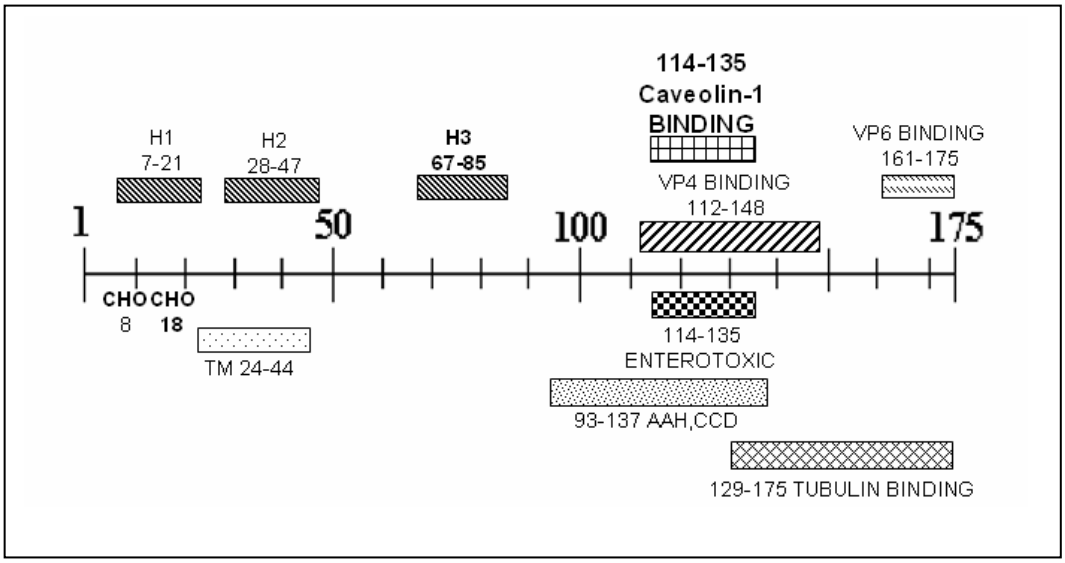

Fig. 1.1 Linear schematic of NSP4 H1,H2, and H3 indicate the three, N-terminal hydrophobic domains. CHO indicates glycosylation sites in the ER lumen. TM indicates ER transmembrane domain. AAH,CCD indicates amphipathic alpha helical region that folds as coiled coil domain.

bind caveolin-1 (95). NSP4 also has been shown to function as a modulator of viral transcription (121). Silencing gene 10, which encodes NSP4, in RV infected cells

dramatically decreases viroplasm formation (73, 121) while simultaneously increasing viral transcription (121). Exogenous addition of NSP4 or its enterotoxic peptide, $NSP4_{114-135}$, induces a specific, age and dose-dependent diarrhea in mouse pups. The diarrheal response is mediated by the mobilization of $[Ca^{2+}]_i$ and results in Cl^- secretion and substantial fluid accumulation in mouse pup intestinal loops in the absence of histological alterations (9). NSP4 induces $[Ca^{2+}]$i mobilization through phospholipase C activation and inositol 1,4,5-tri phosphate (IP3) production in human intestinal HT-29 cells (30). The viral enterotoxin also appears to disrupt tight-junction biogenesis and epithelial integrity in polarized canine kidney MDCK cells (133). NSP4 and $NSP4_{114-135}$ interact with caveolae-like model membranes with high curvature and high relative concentrations of cholesterol and anionic phospholipids (52).

Due to the Endo-β-N-acetylglucosaminidase H (endo H) sensitivity of the NSP4 carbohydrate moieties and NSP4's role in viral particle morphogenesis at the ER, early studies designated NSP4 as a resident ER transmembrane glycoprotein (10, 34, 57, 136). Ample evidence show that NSP4 is not exclusively localized to the ER, but traffics from the ER by a pathway that likely bypasses the Golgi (10, 12, 15, 26, 91). A C-terminal NSP4 fragment (aa 112-175) has been isolated from the culture media of NSP4-recombinant baculovirus-infected Spodoptera frugiperds (Sf9) insect cells and virus-infected mammalian cells (146). Subcellular localization of NSP4 also has been noted in the ER-Golgi intermediate compartments (ERGIC) of stable transfected human intestinal cells (143). In section 2 of this work, we show that NSP4 has been isolated with PM caveolae of infected cells that have undergone an isolation procedure that removes ER

resident proteins (132). NSP4 also has been shown to co-localize with viroplasm markers in infected cells (11). Lastly, NSP4 has been isolated from the media of infected CaCO2 cells (19). We have shown that NSP4 is exposed at the exofacial surface of the PM of infected cells as early as 3 hours post infection (hpi) in HT29.f8 cells and 7 hpi in MDCK cells (section 3 of this work). Soluble NSP4 that has been clarified of virus binds the membranes of non-infected cells (section 3 of this work).

1.3 Caveolae

The plasma membrane (PM) of an eukaryotic cell is composed of a lipid bilayer with differing concentrations of proteins and lipids, for example anionic phospholipids, neutral phospholipids, cholesterol, sphingolipids and glycolipids are exposed on the cytosolic or the exofacial leaflet at different concentrations (29, 120). The PM, besides having heterogenetic differences in the leaflets, also possesses differences in lateral regions, such as rafts. Rafts are detergent resistant membranes rich in saturated hydrocarbons, sphingolipids and cholesterol relative to the rest of the PM. A specific subset of rafts are caveolae, which are small (50-100 nm diameter), cholesterol-dependent PM microdomains present in most cells that function in intracellular transport and signaling events (3, 44). The interactions of Ras proteins (127), G protein-coupled receptors (70), and Src family kinases (69) with caveolae in the PM indicate an active role for this microdomain in compartmentalizing and integrating a wide range of signal transduction processes. The partitioning of IP3 receptors (37), the PM Ca^{2+} pump (36), and nearly half of the cellular phosphatidylinositol 4,5 bisphosphate (PIP2) (48, 103) to

caveolae, indicate that caveolae may function as a specialized apparatus for signal-mediated $[Ca^{2+}]_i$ fluctuations and Ca^{2+}-mediated signal transduction.

Caveolin-1 is a protein 178 amino acids in length, and is the central protein controlling caveolae (130). Caveolin-1 regulates the signaling activity of resident caveolae proteins (22, 36, 37, 48, 69, 103, 127) and the transport of cholesterol to and from caveolae (67, 88, 125, 140, 143). Caveolin-1 is inserted in the cytofacial leaflet of the PM with amino acids 102 – 134 forming a hairpin in the PM bilayer leaving the N and C terminal domains exposed to the cytoplasm (97, 107). Caveolin-1 is synthesized in the ER, and there are two primary routes of trafficking from the ER to the PM. One follows the well established secretory route while the other follows a non secretory trafficking route. Caveolin-1 binds cholesterol and plays a key role in cholesterol transport from the ER to the PM. This caveolin-mediated cholesterol transport starts in the ER, progressing through the endoplasmic reticulum Golgi intermediate complex (ERGIC), the cis-to trans-Golgi, and caveolae-like vesicles to the PM (67, 88, 143). A cytosolic subset of caveolin-1 (investigated in relation to NSP4 in section 4 of this work) which is part of the heat-shock-protein immunophilin chaperone complex consisting of caveolin-1, heat-shock protein 56, cyclophilin 40, cyclophilin A, and cholesterol (caveolin-1 chaperone complex) is involved in transporting newly synthesized cholesterol directly from the ER to PM caveolae (125, 140).

In this work, PM caveolae are isolated from RV infected cells and analyzed for the presence of NSP4. Extending the PM caveolae work, a temporal analysis for the presence of NSP4 at the exofacial PM in relation to virus release from infected cells was

accomplished. This study was performed utilizing a variety of methods, including, surface biotinylation and live cell staining of RV infected cells. We also developed two novel immunofluorescent and confocal analysis techniques which allowed us to probe individually RV infected cells for the exofacial presence of NSP4. Additionally we investigated the interaction between naïve cells and exogenously added NSP4. Lastly we investigated NSP4 and its relation to selected marker proteins of two trafficking pathways.

The data produced in this work challenges the longstanding dogma which regards NSP4 solely as an ER transmembrane protein. Instead, the data shows that NSP4 not only resides in the ER but leaves via a Golgi-by-passing trafficking pathway. NSP4 is present at the exofacial surface of the PM, is secreted from cells, and binds the PM of naïve cells. NSP4 also likely traffics with the caveolin-1 chaperone complex proteins.

2. FULL-LENGTH, GLYCOSYLATED NSP4 IS LOCALIZED TO PLASMA MEMBRANE CAVEOLAE BY A NOVEL RAFT ISOLATION TECHNIQUE*

2.1 Overview

Rotavirus NSP4, initially characterized as an endoplasmic reticulum intracellular receptor, is a multifunctional viral enterotoxin that induces diarrhea in murine pups. There have been recent reports of the secretion of a cleaved NSP4 fragment (residues 112 to 175) and of the association NSP4 with LC3 positive autophagosomes, raft membranes and microtubules. To determine if NSP4 traffics to a specific subset of rafts at the plasma membrane, we isolated caveolae from plasma membrane-enriched material that yielded caveolae membranes free of endoplasmic reticulum and non-raft plasma membrane markers. Analyses of the newly isolated caveolae from rotavirus-infected MDCK cells revealed full-length, high-mannose glycosylated NSP4. The lack of Golgi-specific processing of the caveolar NSP4 glycans support studies showing NSP4 bypasses the Golgi. Confocal imaging showed co-localization of NSP4 with caveolin-1 early and late in infection, elucidating the temporal and spatial NSP4-caveolin-1 association during infection. These data were extended with fluorescent resonance energy transfer (FRET) analyses refining the NSP4 and caveolin-1 association to within 10 nm of each other during infection. Cells transfected with NSP4 showed patterns of staining and colocalization with caveolin-1 similar to those of infected cells. This study

* Reprinted with permission from "Full-Length, Glycosylated NSP4 Is Localized to Plasma Membrane Caveolae by a Novel Raft Isolation Technique" by Stephen M. Storey, Thomas F. Gibbons, Cecilia V. Williams, Rebecca D. Parr, Friedhelm Schroeder, and Judith M. Ball, 2007, Journal of Virology 81:5472-5483

presents an endoplasmic reticulum contaminant-free caveolae isolation protocol, the presence of full-length, endoglycosidase H-sensitive NSP4 in plasma membrane caveolae, confirmation of the NSP4-caveolin-1 interaction, and a final plasma membrane destination for Golgi-bypassing NSP4 transport.

2.2 Introduction

Rotaviruses (RV) are the leading viral etiologic agents of severe pediatric gastroenteritis worldwide affecting nearly all children before the age of 5 with 2 million cases resulting in 444,000 deaths annually (77, 78, 94). RV non-structural protein 4 (NSP4) initially was characterized as an endoplasmic reticulum (ER) transmembrane glycoprotein due to the protein's high mannose glycosylation and its critical function as an intracellular receptor for translocation of subviral particles into the ER during virion morphogenesis (5, 10, 33). However, the identification of NSP4 and NSP4 amino acids (aa) 114-135 ($NSP4_{114-135}$) as enterotoxic and the redistribution of RV-encoded proteins upon NSP4 silencing led to a re-evaluation of NSP4 function(s) and subcellular localization(s) (9, 73).

A cleaved NSP4 fragment, aa 112-175, is secreted from RV-infected epithelial cells implicating that some portion of NSP4 traffics from the ER to the plasma membrane (PM) (146). Co-localization of $NSP4_{114-135}$ and the extracellular matrix proteins laminin-β3 and fibronectin at the basement membrane of small intestinal epithelia from RV EDIM-infected mouse pups also supports NSP4 transport to the PM during host infection (15). While both studies demonstrate that at least a fragment of NSP4 leaves the ER of infected cells, neither confirms the presence of full-length NSP4

at the PM nor reveals the specific distribution of the viral glycoprotein in PM lipid microdomains. The detection of NSP4 in Triton X-100-resistant 'lipid rafts' isolated from RV-infected Caco-2 cells indicates the viral enterotoxin may be a resident of cellular lipid rafts during infection (25, 114).

The biophysical structure and composition of cellular lipid rafts remain controversial as they are primarily defined operationally as a collection of cellular membranes insoluble in non-ionic detergents at 4^{o}C. These detergent-resistant membranes (DRM) have a unique lipid composition, enriched in cholesterol, sphingomyelin and glycolipids, producing a liquid-ordered or gel-phase 'raft' with a light buoyant density on sucrose gradients (38, 124). Ganglioside M1 (G_{M1}), glycerophosphatidylinositol-anchored proteins, flotillin, and caveolins have been used as markers for measuring enrichment of DRM following isolation from cell lysates or membrane fractions (118, 119). Yet the ability of detergents to both cluster and remove cellular membrane proteins and lipids illustrate that DRM do not represent the actual composition of all rafts in the cell (47, 128).

Caveolae are a subset of lipid rafts defined by the presence of caveolin proteins (caveolin-1, -2, or -3) (115, 116). Despite the recent use of detergent-free isolations, caveolae composition is nearly as controversial as that of rafts due to the confusing and often conflicting data resulting from the use of different cell types and isolation procedures (102). Using a high pH sodium carbonate homogenization buffer and sucrose gradients to isolate caveolae from myocytes yield a caveolin-3-enriched fraction without detectable clathrin, Na/K-ATPase (non-raft PM marker) and mannosidase II

(Golgi marker) (144), whereas utilizing the same protocol with a PM-enriched material from another cell type yields a caveolin-1-enriched fraction that contains both clathrin and Na/K-ATPase (46). Other caveolae isolation protocols, such as anti-caveolin affinity chromatography and density gradient fractionation of caveolae sheared from silica-coated PM successfully extract caveolin-containing membranes, but these fractions have yet to be assayed for a similar range of organelle- and vesicle-specific markers (118, 126, 129).

We have reported that NSP4 may specifically partition into caveolae during infection. NSP4 and $NSP4_{114-135}$ preferentially interact with highly-curved model membranes enriched in cholesterol and anionic phospholipids (51, 52). Specific secondary structure alterations (increased helical content) upon interacting with different model membranes demonstrate NSP4 and $NSP4_{114-135}$ associate with membranes that mimic caveolae (51). Although this study utilizes model membranes lacking proteins, we also show co-localization of NSP4 with caveolin-1 at both intracellular sites and at the periphery of RV-infected MDCK and Caco-2 cells, as well as a direct interaction between NSP4 and caveolin-1 by yeast two-hybrid, *in vitro* binding, and co-immunoprecipitation assays (95). Based on these data, we hypothesize full-length NSP4 traffics from the ER to PM caveolae during RV infection of epithelial cells. To examine this hypothesis, we generated a detergent-free isolation method optimized to produce a PM caveolae-enriched fraction from epithelial cells that contained caveolae markers and were devoid of detectable Golgi, ER, clathrin-coated pit, and liquid-phase (non-raft) PM markers. Analysis of the PM caveolae isolated in this manner from RV-infected cells

revealed that full-length NSP4 was present and was double-glycosylated with high-mannose glycans.

2.3 Materials and Methods

2.3.1 Antibodies and reagents

Antibodies directed against Na/K-ATPase α (mouse anti-sheep Na/K-ATPase α; Affinity BioReagents, Inc., Golden, CO), calnexin (rabbit anti-canine calnexin aa 575 to 593; Stressgen Biotech, Victoria, BC Canada), Golgin-97 (mouse anti-human golgin-97; Molecular Probes, Eugene, OR), giantin (rabbit anti-human giantin aa 1 to 469, Covance Research Products, Inc, Princeton, JN), flotillin-1 (mouse anti-mouse flotillin-1 aa 312 to 428) and clathrin (mouse anti-rat clathrin heavy chain aa 4 to 171; BD Transduction Lab, Lexington, KY), and cholera toxin (rabbit anti-Vibrio cholerae toxin; Sigma Aldrich, Saint Louis, MO) were purchased from the indicated commercial sources. Horseradish peroxidase (HRP; goat anti-rabbit and anti-mouse immunoglobulin G; Southern Biotech Assoc, Inc, Birmingham, AL), and alkaline phosphatase-conjugated goat anti-rabbit IgG (Sigma Aldrich) were purchased commercially. Linked antibodies and fluorescent molecules included goat anti-mouse IgG-Texas Red (Rockland Immunochem, Inc, Gilbertsville, PA), the $F(ab')_2$ fragment of goat anti-mouse and anti-rabbit antibody-Cy2 (Jackson ImmunoResearch), and goat anti-rabbit IgG-fluorescein isothiocynate (IgG-FITC; KPL, Inc, Gaithersburg, MD). Antibodies specific to the NSP4 peptide aa 150 to 175 ($NSP4_{150\text{-}175}$; deduced from the simian rotavirus SA11 NSP4 sequence) were generated in rabbits by using peptide cross-linked to keyhole limpet hemocyanin as an antigen (95).

Purified cholera toxin B subunit (CT-B; Sigma Aldrich), 5-bromo-4-chloro-3'-indolyphosphate p-toluidine (BCIP)/nitro-blue tetrazolium chloride (NBT) premixed electrophoresis reagent (Sigma Aldrich), Concanavalin A-(ConA)-Sepharose 4B (Amersham Pharmacia Biotech, Piscataway, NJ), α-methyl-D-mannopyranoside (Acros Organics/Fisher Sci Intl, Inc, Hampton, NH), endo-β-N-acetylglucosaminidase H (endo H; New England BioLabs, Ipswich, MA), protease inhibitor cocktail set III (Calbiochem, Darmstadt, Germany), and 0.45 μ pure nitrocellulose (GE Osmonics Labstore, Minnetonka, MN) were acquired from commercial sources.

2.3.2 Generation of anti-NSP4$_{150\text{-}175}$ Fab segments

NSP4$_{150\text{-}175}$ specific antibodies were affinity purified before use in confocal microscopy, and Fab fragments were generated for fluorescent resonance energy transfer (FRET) analyses to reduce the distances of the fluorophores from the target proteins. Rabbit anti-NSP4$_{150\text{-}175}$ was affinity purified on an NSP4$_{150\text{-}175}$ peptide column prepared with preactivated cyanogens bromide Sepharose 4B beads by following the instructions of the manufacturer (Pharmacia Biotech) (7). The bound peptide IgG was eluted by altering the pH (134). The ImmunoPure F(ab)$_2$ preparation kit (Pierce, Rockford, IL) was utilized, and the recommended protocol was followed with the exception that immobilized papain was substituted for immobilized pepsin to produce Fab versus F(ab)$_2$ (142). Cy3 monofunctional reactive dye was conjugated to the affinity-purified NSP4$_{150\text{-}175}$ Fab fragment for FRET analyses exactly as described by the manufacturer (Amersham Bioscience).

2.3.3 Cultured cells and virus

MDCK (American Type Culture Collection, Manassas, VA) and HT29.f8 cells, a spontaneously polarizing cell line derived from the human adenocarcinoma HT29 intestinal line (83), were grown in maintenance media (Dulbecco's Modification of Eagle's media [DMEM] with 4.5 g/L glucose, L-glutamine, and sodium pyruvate; Mediatech, Inc., Herndon, VA) supplemented with 2 mM L-glutamine (200 mM; BioWhittaker/Cambrex), 1 mM sodium pyruvate (Cambrex), 0.1 mM non-essential amino acids (Mediatech, Inc.), 100 U/L penicillin, 100 μg/L streptomycin, 0.25 μg/L amphotericin (10,000 U penicillin-10,000 U of streptomycin- 25 μg/liter amphotericin B; Cambrex), 43.9 mM sodium bicarbonate (GIBCO), 5% fetal bovine serum, and 5% Serum Supreme (Cambrex) at 37^{o}C in 5% CO_2. MDCK cell stocks were maintained in 175 cm^2 flasks and expanded into 500 cm^2 trays or 2 cm^2 multiwell plates (Corning, Inc, Corning, NY) for caveolae isolation. MDCK cells were infected with SA11 clone 4F (gift of Mary Estes, Baylor College of Medicine, Houston, TX) at a multiplicity of infection (MOI) of 2 PFU/cell. Briefly, the virus was sonicated (5 minutes using a cuphorn attachment ice bath in a Misonix Sonicator 3000; Misonix, Inc, Farmingdale, NY) and incubated in serum-free DMEM with 5 μg/ml trypsin for 30 minutes (min) at 37^{o}C, then incubated with the cells for 60 min at 37^{o}C in 5% CO_2. The inoculum was replaced with serum-free DMEM supplemented with 1 μg/ml trypsin and the cells incubated for an additional 7.5 or 24 hours. The HT29.f8 cells were grown on glass cover slips for confocal imaging and FRET analyses. Prior to infection, the cells were starved for FBS for 10- 16 hours. RV SA11 4F was treated with trypsin at a

concentration of 10μg/ml for 30 min and then applied to cells for 1 h at an MOI of 2 PFU/cell.

2.3.4 NSP4 transfection

MDCK and HT29.f8 cells were transiently transfected with pcDNA3.2D $NSP4_{1-175}$ plasmid DNA using nucleofection, a delivery system in which DNA is delivered directly into the nuclei of the cells. The Nucleofector II device and Nucleofector I kits were used following the protocols designed by Amaxa Biosystems (Cologne, Germany). Briefly, the cells were grown to 60-70 % confluency (~3.5 x 10^5cells/cm^2 for MDCK cells and~5.5 x 10^5cells/cm^2 for HT29.f8 cells), and the appropriate numbers of cells ($5x10^5$ MDCK cells and $1x10^6$ HT29.f8 cells) were harvested, and mixed with the cell-type specific Nucleofector solution and $NSP4_{1-175}$ plasmid DNA, subjected to nucleofection (using Nucleofector programs A-024 and W-017 for MDCK and HT29.f8 cells, respectively), plated on 10 mm cover slips and incubated for 20 hours. After the removal of the growth media and washing with phosphate-buffered saline (PBS), the transfected cells were fixed and permeabilized with ice-cold methanol:acetone (1:1).

2.3.5 DRM isolation

DRM were isolated from MDCK cells as previously described (114). Briefly, four 500 cm^2 trays of cells were grown to confluency (~ 6 x 10^7 cells/tray), washed with PBS, and scraped into a 4 ml final volume of TNE buffer (20 mM Tris-HCl pH 7.4, 150 mM NaCl, 1 mM EDTA, 0.2 μM Phenylmethlysulfonyl fluoride [PMSF] and 1% Triton X-100). The suspended cells were passed 10 times through a 22-gauge needle and the homogenate incubated for 30 min at 4^{o}C before mixing with 2.5 M sucrose to a density

of 40%. A 40%- 35%-5% discontinuous sucrose density gradient was centrifuged at 180,000 X g, 4^{o}C for 18 hours (by using a Beckman SW41Ti rotor and Optima LE-80k Ultracentrifuge) and the DRM were recovered from the 35%-5% interface. For Western blot analyses, the DRM and detergent-soluble membrane (DSM) proteins (40% gradient layer) were further processed by ultracentrifugation (190,000 X g for 1.5 hours with a Beckman SW41Ti rotor) in Tris buffer (10 mM Tris, 1 mM EDTA), suspended in PBS for protein quantification or in PBS containing 0.2 μM PMSF and 1 μl/ml protease inhibitor cocktail set III for cold storage at -80^{o}C. All membrane isolations were completed on ice unless otherwise noted.

2.3.6 Cavitation-sucrose chromatography (CSC) caveolae isolation

PM-derived caveolae were isolated with a sucrose density gradient and ConA affinity chromatography as described previously (38). Briefly, MDCK cells were grown in 4-8 trays (500 cm^2), washed twice with PBS, and scraped into 8 ml final volume. Cells were pelleted for 5 min at 1,000 X g at room temperature (RT), suspended in 2 ml of 0.25 M sucrose, 1 mM EDTA, 20 mM Tris-base, pH 7.8, and homogenized by nitrogen gas cavitation (15 min at 40 lb/in^2) (2, 63). The nuclei and remaining intact cells were pelleted by centrifugation for 10 min at 1,000 X g at RT. The original cell supernatant and post nuclear supernatant (PNS) were floated on a discontinuous sucrose density gradients (0.5 ml, 55%, 1.5 ml, 40%, 1.5 ml, 35%, 1.5 ml, 32%, 1.5 ml, 29%, 1.5 ml, 27%, and 1.5 ml, 20%; [all wt/vol] in 1 mM EDTA-20 mM Tris-base pH 7.8), and centrifuged for 90 min at 192,000 X g at 4^{o}C. ER-enriched fractions (35%-40% and 40%-55% interface bands) from the supernatant gradient were pooled, pelleted for 2

hours at 190,000 X g at 4^{o}C, and suspended in PBS containing 0.2 μM PMSF and 1 μl/ml protease inhibitor cocktail set III for storage at -80^{o}C. The PNS-derived PM fractions (27%-29%, 29%-32%, and 32%-35% interface bands) were pooled, sonicated briefly (three 1 second pulses at 5 second intervals in a Misonix Sonicator with cuphorn attachment at power level 3) and added to a slurry of ConA-sepharose 4B prewashed in Buffer 1 (0.14 M KCl, 0.01 M HEPES, 1 mM $MgCl_2$, 1 mM $MnCl_2$, [pH 7.8] with KOH). The PM-containing slurry was mixed for 2 min by nitrogen bubbling, incubated for 10 min at RT for binding, transferred to a glass preparative column and washed with 75 ml of Buffer 1. Buffer 2 (0.5 M α-methyl-mannopyranoside in buffer 1) was added, mixed by nitrogen bubbling and the ConA-binding material drained from the column. Fluid from a total of six sequential 14 ml Buffer 2 washes were collected, centrifuged for 14 hours at 111,000 X g at 4^{o}C, and the resulting caveolar membrane pellets suspended in small volumes of Buffer 2 for protein quantification or Buffer 2 containing 0.2 μM PMSF and 1 μl/ml protease inhibitor cocktail set III for storage at -80^{o}C.

2.3.7 Protein quantification

Micro bicinchoninic acid (BCA) protein assay and SilverSNAP Stain II kits (Pierce) were used to quantify the protein concentration of the isolated membrane fractions. The Micro BCA kit was used with bovine serum albumin standards per manufacturer's protocol to calculate an initial protein concentration for each membrane fraction. To ensure the differences in sample solvents did not alter the analysis of marker enrichment, equivalent amounts of each fraction as calculated above were resolved by sodium dodecyl sulfate-polyacrylamide gel electrophoresis (SDS-PAGE)

and silver stained using SilverSNAP. Densitometry scans of the stained proteins in each lane were used to correct the BCA protein concentrations based on the difference (n-fold) from the lysate (Triton X-100 fractions) or homogenate (CSC fractions) absorption units.

2.3.8 EM of isolated caveolae

CSC caveolae were negatively stained with 2% phosphotungstic acid, pH 7.0, as described previously but with slight alterations and were examined by electron microscopy (EM), with a Zeiss EM 10C (40). In brief, CSC caveolae were adsorbed onto a Formvar coated film grid (Electron Microscopy Sciences, Fort Washington, PA) for 1 hour at RT. The adsorbed sample was stained with phosphotungstic acid and images were captured at 8,000 fold magnification. The captured images were scanned and processed with Image J (developed at NIH and is available at http://rsb.info.nih.gov/ij) for scale (3 fold digital zoom for a resolution of 1.52 pixels per nm), threshold, and manual discrete object separation. The processed images were analyzed in Adobe Photoshop by Feret's function to quantify the maximal diameter of visible discrete membranes.

2.3.9 Endoglycosidase reactions

For endo H cleavage, 1 μg aliquots of total protein from fractionated caveolae isolated from uninfected and RV-infected (MOI of 2 PFU/cell) MDCK cells at 24 hours post infection (hpi) were used. The glycoproteins were denatured and diluted per protocol of the manufacturer (New England Biolabs). Either 1 μl of sterile water (mock cleavage) or 1 μl of endo H was added to the control or sample set from mock and

infected cells. The cleavage reaction was performed for 1 hour at 37°C, and the proteins were resolved by SDS-PAGE and visualized by Western blotting.

2.3.10 Western blot analyses

A series of Western blots were utilized to monitor the enrichment of each of the isolated membrane fractions with specific organelle markers and to identify those fractions containing NSP4. Two micrograms of total protein from each fraction (or 1 μg of each glycosidase cleaved sample) was resolved on 12% polyacrylamide minigels and transferred to nitrocellulose filters (0.45 μ pure nitrocellulose[GE Osmonics]) according to the manufacturer (Mini-PROTEAN II or Trans-Blot respectively; BioRad). The filters were blocked in 10% (wt/vol) non-fat dry milk in PBS (10% BLOTTO) for 1 hour at RT and reacted with the primary antibody in 2.5% BLOTTO for 14 hours at 4°C with rocking. The filters were incubated an additional 1 hour at RT with primary antibody, then washed once in 0.5% BLOTTO, twice in 0.5% BLOTTO with 0.05% Tween-20, and once in 0.5% BLOTTO with rocking (10 min per wash). Secondary antibodies were diluted in 2.5% BLOTTO and incubated with the filters for 1 hour at RT with rocking. The filters were washed as above, rinsed with PBS, and reacted with SuperSignal West Pico or Femto chemiluminescent substrates as per the manufacturer's protocols (Pierce). The marker-specific bands were visualized by exposure to and development of x-ray film and the resulting signals were analyzed by densitometry scan.

2.3.11 Cholera toxin G_{M1} binding assay

A dilution series of purified G_{M1} (0 to 100 ng) and equal amounts of total protein from each isolated fraction were spotted onto nitrocellulose filters, air dried, and rinsed twice in PBS. The filters were blocked in 3% (wt/vol) BSA in PBS for 30 min at RT, rinsed twice gently with PBS, and incubated with 1 μg/ml cholera toxin subunit B (CT-B) in PBS for 2 hours at RT. Excess CT-B was removed with 2 PBS rinses and the filters were incubated with 1:500 rabbit anti-CT-B in PBS for 1 hour at RT. Following two rinses with PBS, the filters were incubated with goat anti-rabbit IgG conjugated to alkaline phosphatase in PBS (1:7,500) for 30 min at RT, and rinsed twice in PBS. The filters were washed in alkaline phosphatase reaction buffer (1 M Tris, 0.1 mM NaCl, 10.5 mM $MgCl_2$ pH 9.0) for 5 min at RT and the G_{M1}-CT-B signals developed in BCIP-nitroblue tetrazolium chloride. The filters were rinsed twice in water, dried, and laminated before analysis of the resulting signals by densitometry scan.

2.3.12 Confocal microscopy

Mock and SA11-infected MDCK cells were grown on glass coverslips and processed at 7.5 or 24 hpi for fluorescent imaging. The infected cells were rinsed in PBS, fixed and permeabilized in methanol:acetone (1:1, vol/vol) for 10 min at -20^{o}C, and non-specific binding sites were blocked with 3% BLOTTO(3% dry milk in PBS) at RT for 45 min. The infected and uninfected cells were incubated with primary antibodies (NSP4 and caveolin-1 peptide-specific, affinity-purified IgG) diluted in 1% BLOTTO-PBS at RT for 45 min. The cells were washed four times in 0.5% BLOTTO-PBS for 10 min each and incubated with Cy2, Texas Red, or Cy5-labeled secondary

antibody diluted in 1% BLOTTO-PBS for 45 min in the dark. The cells were washed again as above but in the dark and mounted with fluorescent mounting media (KPL Inc.) onto glass slides. The resulting fluorescent images were captured with a MRC-1024MP BioRad laser scanning confocal microscopy system (BioRad, Hercules, CA) using a Zeiss inverted Axiovert microscope (Carl Zeiss, Inc., Thronwood, NY), a 63 X Zeiss oil apochromat objective, and the 488- 568- and 647-nm-wavelength excitation lines of an argon/krypton ion laser source. LaserSharp 3.0 (BioRad), Confocal Assistant 4.02 (Brelje TC/BioRad) and Adobe Photoshop 7.0 (Adobe Systems Inc., San Jose, CA), respectively, were used to capture the pixilated fluorescent data, to calculate co-localization values and to adjust contrast curves to construct the final images.

2.3.13 Indirect immunofluorescence with digital imaging

Following the transfection of HT29.f8 and MDCK cells with pcDNA3.2D $NSP4_{1\text{-}175}$ plasmid DNA, cells were fixed, permeabilized (as described above) and blocked with BLOTTO (2% powdered milk in PBS) with rocking overnight at 4°C. After blocking, the cells were probed with mouse anti-$NSP4_{150\text{-}175}$ and rabbit anti-caveolin-1 at room temperature for 30 min with rocking. The cell monolayers were washed 4 times (10 min each) with PBS, followed by treatment with goat anti-rabbit IgG-Texas Red and goat anti-mouse IgG-FITC, covered with aluminum foil, and incubated at room temperature for 30 min with rocking. Following a single wash with PBS, the cells were stained with Hoechst 33342 to visualize the nuclei and the wash repeated. The cover slips were air-dried, mounted inverted on a microscope slide using mounting solution and sealed with enamel. To examine the colocalization of caveolin-1

with $NSP4_{1-175}$ in the transfected MDCK and HT29.f8 cells and to examine the distribution of NSP4 when expressed alone, cells were visualized using a Stallion Digital Imaging workstation (Carl Zeiss MicroImaging, Inc. Thornwood, NY) equipped with a 300W xenon fluorescent light source with rapid switching (<2msec) between excitation wavelengths. Images were collected using a 63X objective, 0.75 N.A., and a ROPER CoolSnap HQ camera. The Stallion system filter set includes excitation/emission suitable for color staining including DAPI (4',6'-diamidino-2phenylindole)/Hoechst (365:445/50 nm), FITC/Cy2 (470/20:505 to 530 nm), and Texas Red/Cy3 (560/40:590 nm). The images were processed using Image J (public domain software from NIH Image).

2.3.14 FRET by acceptor photobleaching

FRET is a process by which non-radiative energy transfer occurs from one fluorophore to another if the two fluorophores(or proteins) are within 10 nm of each other (60). Acceptor photobleaching is one of the simpler and more effective FRET techniques whereby the acceptor fluorophore is bleached then an increase in the donor fluorophore is assessed to determine if two proteins interact (59). RV-infected HT29.f8 cells were labeled with Cy3-linked $NSP4_{150-175}$ Fab and caveolin-1-specific IgG, followed by Cy2-linkged secondary antibody. A series of images were taken both before (488 and 568nm; 10% power) and after the photobleaching the Cy3 fluorophore. The cells were photobleached at 568 nm at 100% power for 3 min. An increase in the Cy2 signal (488 nm) was assessed following photobleaching to determine if the two fluorophores were in close proximity (less than 10 nm apart) and there was a positive

FRET reaction (59). Image analysis was accomplished using Image J software, a public domain Java image-processing program inspired by NIH Image. Image J has a large and increasing number of plug-ins, which are functional programming updates to Image J designed to perform a specific task. The FRETcalc plug-in (http://rsb.info.nih.gov/ij/plugins/fret/fret-cal.html) was utilized to assess the FRET data, as this plug-in is specific to acceptor photo-bleaching.

2.4 Results

2.4.1 Triton X-100-resistant lipid rafts

NSP4 expression at 12 hpi has been detected in both Triton X-100-resistant and -soluble fractions isolated from RV-infected Caco-2 cells (114). To examine the DRM fraction for the presence of full-length NSP4, the resistant fraction should contain caveolae-specific markers without detectable ER or non-raft PM markers. The presence of even a trace of ER contamination, a known reservoir of NSP4 during RV infection, in the raft/caveolae fraction could introduce NSP4 as an artifact of the isolation methodology. For analyses of the detergent resistant and soluble membrane fractions isolated from MDCK cells, DRM were extracted using Triton X-100. Equal amounts of lysate, DRM, and DSM proteins (Fig. 2.1, lanes 1-3 respectively) were resolved by SDS-PAGE and assayed by Western blotting for each caveolae/raft and non-caveolar marker. Caveolae markers, caveolin-1 (112, 115, 124) (Fig. 2.1A), flotillin-1 (14, 87) (Fig. 1B) and G_{M1} (96) (Fig. 2.1C), were present in the DRM fractions. A densitometry analysis of the caveolin-1 bands indicated that this key caveolae protein is enriched approximately 3.5 fold in the DRM fractions when compared to lysate levels (data not shown).

However the contaminant marker profiles revealed calnexin (ER marker) (Fig. 2.1D) (31, 55, 108) and Na/K-ATPase α (non-raft PM marker), (Fig. 2.1E) (46, 72, 92, 144) were also were present in the DRM fraction. The presence of ER and non-raft PM markers preclude use of DRM for determining if full-length NSP4 traffics to PM caveolae.

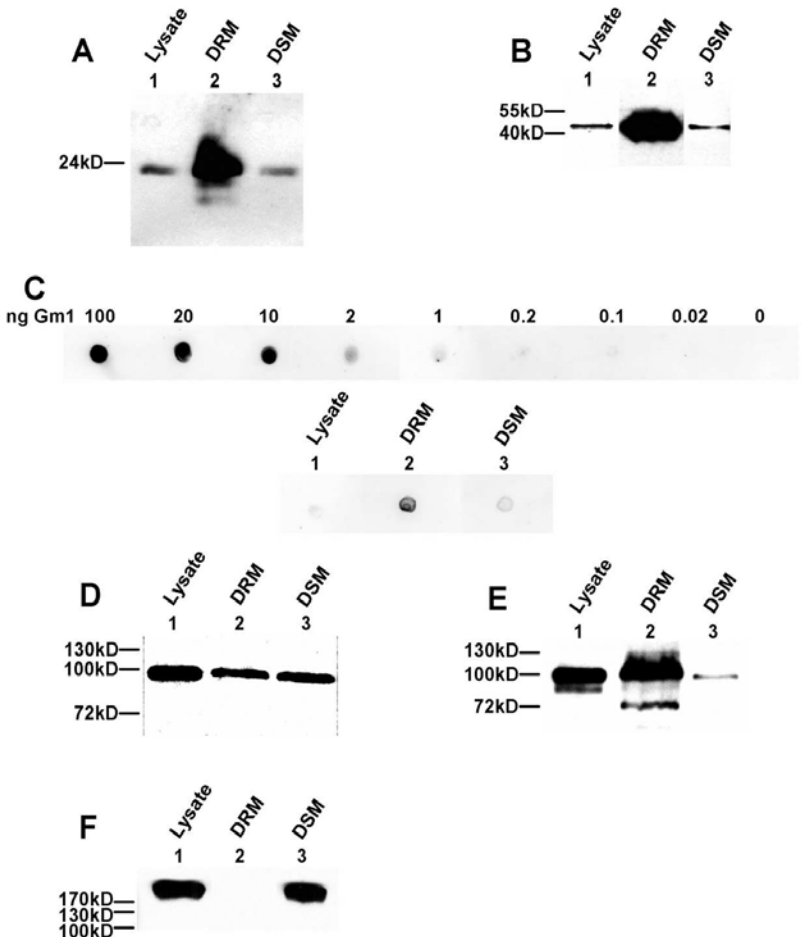

Figure 2.1. Distribution of intracellular protein and lipid markers in Triton X-100-extracted (DRM) fractions. Equal amounts of total protein from the cell lysate, DRM, and DSM fractions of MDCK cells were assayed for the presence of specific cellular markers (Table 2.1) by Western blotting. Peptide-specific antisera were used to detect caveolin-1 (A) and flotillin-1 (B). (C) CT-B and CT-B-specific antisera were used to detect the levels of the caveola-localized lipid G_{M1} by dot blotting. (D,E, and F) Marker-specific antisera identified the distribution of contaminating ER membrane (calnexin) (D), non-lipid raft PM (Na/K-ATPase αsubunit) (E), and clathrin coats (clathrin heavy chain) (F).

2.4.2 Isolation of PM-enriched caveolae from epithelial cells in the absence of ER or non-raft PM marker

The recovery of PM-enriched material was optimized for MDCK cells from a previously reported nitrogen cavitation and sucrose gradient fractionation technique (38). These PM fractions were utilized to isolate caveolae free of contaminants relative to NSP4, in particular ER contaminants. Following cell homogenization, the nuclei and intact cells were pelleted and the post-nuclear supernatant (PNS) was fractionated on discontinuous sucrose gradients. Equal volumes of sequential fractions from the gradient were resolved by SDS-PAGE and examined by Western blotting for the presence of caveolin-1, Na/K-ATPase α, and calnexin (data not shown). The resulting marker profiles indicated that the gradient layers between the 27% and 29% sucrose interface and the 32% and 35% sucrose interface were enriched in both caveolae and PM markers with a minimal amount of ER marker. This PM-enriched fraction was briefly sonicated to disrupt large membrane sheets, further purified by ConA affinity chromatography, tested for caveolae and non-caveolae markers, and designated cavitation-sucrose-chromatography (CSC) caveolae.

2.4.3 Differential protein composition and membrane structure in DRM and CSC caveolae fractions

To determine if the global protein composition of the CSC caveolae fraction was similar to that of DRM, equivalent amounts of Triton X-100-extracted and CSC-isolated membrane fractions were resolved by SDS-PAGE and examined by silver staining. As anticipated, there were distinct banding patterns for both DRM and CSC caveolae with

unique and similar bands at different mol wt (Fig. 2.2). The predominant DRM bands were present at 24 kDa and above, while the major bands of CSC caveolae were below 24 kDa. Hence there was a striking difference in the overall protein content of the DRM and CSC caveolae.

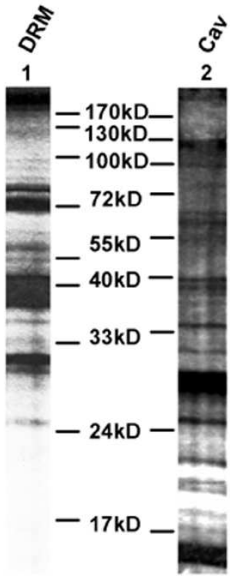

Figure 2.2 Silver stain analysis of DRM and CSC caveolae. Equal amounts of total protein from Triton X-100 extracted DRM and isolated CSC caveolae (Cav) were resolved by 12% SDS-PAGE and evaluated by silver staining.

EM images of CSC caveolae showed vesicular membrane structures (Fig. 2.3A) with an average diameter of 99 nm (n=61). Separation of these objects into 10 nm diameter groups showed that a majority of these isolated membranes were within the expected range of intact caveolae (50-100 nm diameter) or appeared to be broken structures(Fig. 2.3B).

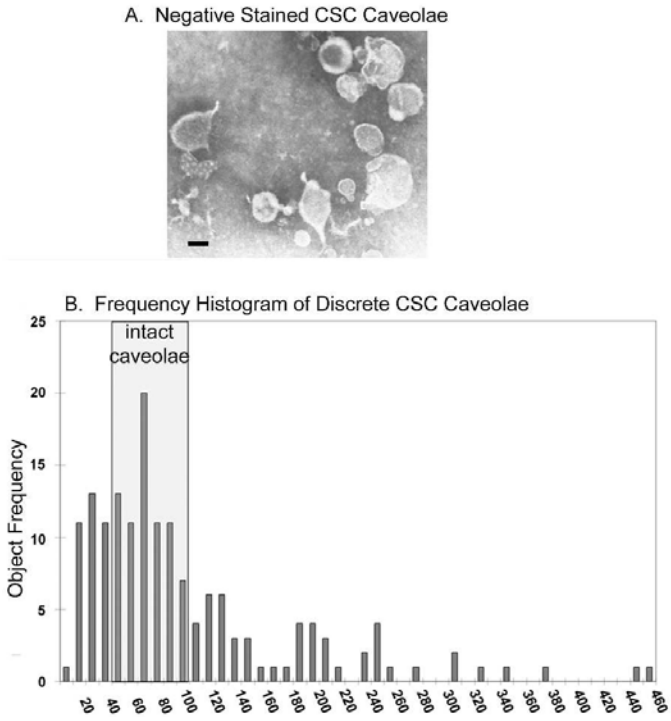

Figure 2.3. EM imaging and analyses of CSC caveolae. CSC caveolae were negatively stained with 2% phosphotungstic acid and imaged by EM. (**A**) A three-fold digital magnification was used to resolve the ultrastructure of the membranes to a resolution of 1.52 pixels per nm (bar indicates 100 nm). (**B**) The manual separation of discrete objects and analysis of maximal object diameter by Feret's function resulted in the quantification of the diameter contained in the CSC caveolae fraction. The diameters were segregated into groups including all the diameters within a 10-nm range, and the representative values (*x* axis) were plotted against the number of objects observed with diameters in the corresponding range. Analyses of161 discrete objects revealed the size distribution of the membranes in CSC caveolae.

2.4.4 CSC-isolated caveolae contained caveolae markers in the absence of detectable ER and non-raft PM markers

To test for the presence of caveolae, ER and non-raft PM in the CSC caveolae, equivalent amounts of homogenate, PNS, ER, PM, and CSC caveolae fractions were resolved by SDS-PAGE and analyzed by Western or dot blot for the corresponding cellular markers (Table 2.1). Specific bands corresponding to caveolin-1 and flotillin-1, and specific spots for G_{M1} confirmed the presence of each caveolae marker in the CSC

caveolae (Fig. 2.4A-C). The contaminant marker profiles (Fig. 2.4D to F) showed that the protein composition of CSC caveolae differed from that of DRM isolated from the same cells (Fig. 2.1). The absence of calnexin in CSC caveolae (Fig. 2.4D) demonstrated that this isolation method yielded membranes lacking detectable ER contamination endemic to the DRM technique. Thus the CSC caveolae preparation was more suitable for our studies to detect NSP4 in PM caveolae. The relatively intense bands corresponding to clathrin (61, 117, 131) and Na/K-ATPase α in the CSC PM fraction and the absence of detectable amounts of either protein in CSC caveolae indicated that these non-caveolar protein markers were absent in the final CSC caveolae isolated from the PM-enriched material (Fig. 2.4E and F).

TABLE 2.1. Intracellular organelle and membrane markers

Marker	Subcellular distribution	Comment (s)	References(s)
Caveolin-1	Caveolae, ER, Golgi apparatus	Defining caveola marker; hairpin structure with C and N termini exposed	112, 115, 124
Flotillin 1	Lipid rafts	Potentially involved in caveola localization; peripheral membrane protein	14, 87, 129
Ganglioside M1	PM caveolae	Glycolipid; primary cholera toxin receptor	96
Calnexin	ER	Integral membrane protein; ER chaperone	31, 55, 108
Giantin	Cis-medial Golgi network	Integral membrane protein	71
Na/K-ATPase α subunit	Nonraft PM	Integral membrane protein; one reporter of caveola localization in cardiac cells	72, 92, 144
Clathrin heavy chain	PM-coated pits, trans-Golgi network, endosomes	Membrane-association protein	61, 117, 131

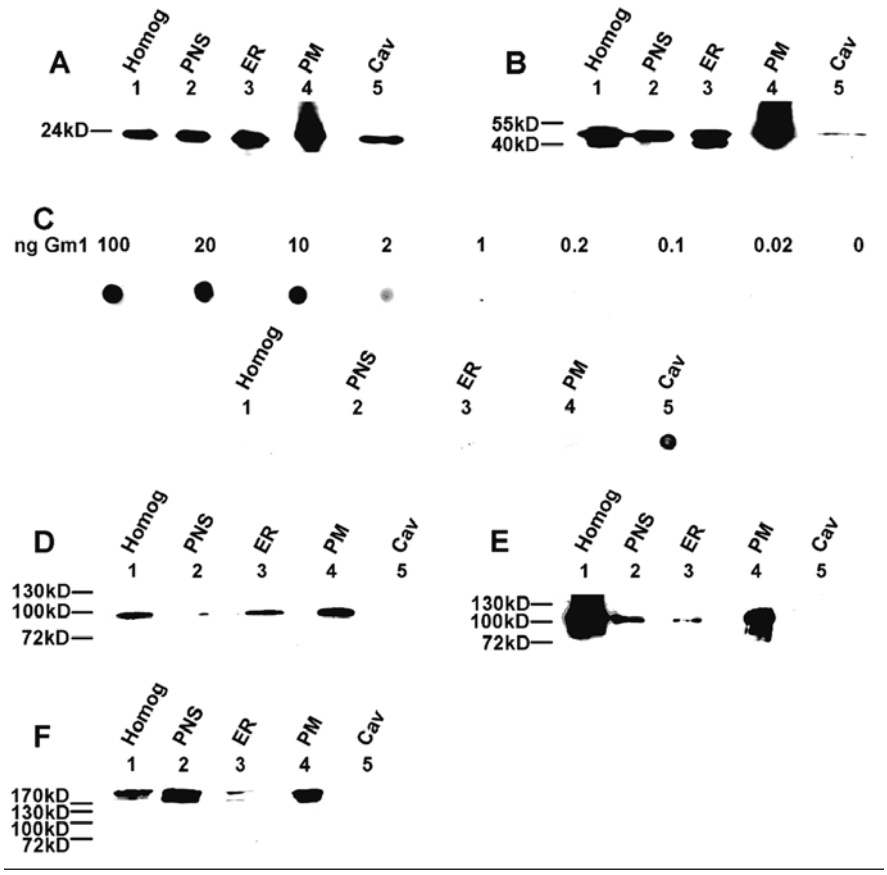

Figure 2.4. Distribution of intracellular protein and lipid markers in CSC-isolated membrane fractions. Equal amounts of total protein from homogenate (Homog), PNS, ER, PM, and caveola (Cav) fractions isolated from MDCK cells by CSC isolation were assayed for the presence of the corresponding markers (Table I). Peptide-specific antisera were used to detect caveolin-1 (**A**) and flotillin-1 (**B**) by Western blotting. (C) CT-B and CT-B-specific antisera were used to detect the levels of the caveolae-localized lipid G_{M1} by dot blotting. (D,E, and F) Marker-specific antisera and western blots identified the distribution of contaminating ER membrane (calnexin), non-lipid raft PM (Na/K-ATPase α subunit,) and clathrin-coated membranes (clathrin heavy chain) in each of the membrane fractions.

2.4.5 RV infection did not affect marker distributions in CSC caveolae

To ensure that the presence of NSP4 in CSC caveolae was not due to redistribution of ER or non-raft membranes into the caveolae fraction by viral infection, CSC fractions were isolated from RV-infected MDCK cells at 24 hpi and analyzed by Western blot for the same protein markers (Table 2.1). The caveolae marker profiles

showed that the infected CSC caveolae contained both caveolin-1 and flotillin-1 (Fig. 2.5A and B), but lacked calnexin (Fig. 2.5C). Since clathrin and Na/K-ATPase α were also absent in the infected CSC caveolae fraction (Fig. 2.5D and E), RV infection did not redistribute intracellular organelles or non-raft PM membranes into the CSC caveolae at the time point examined.

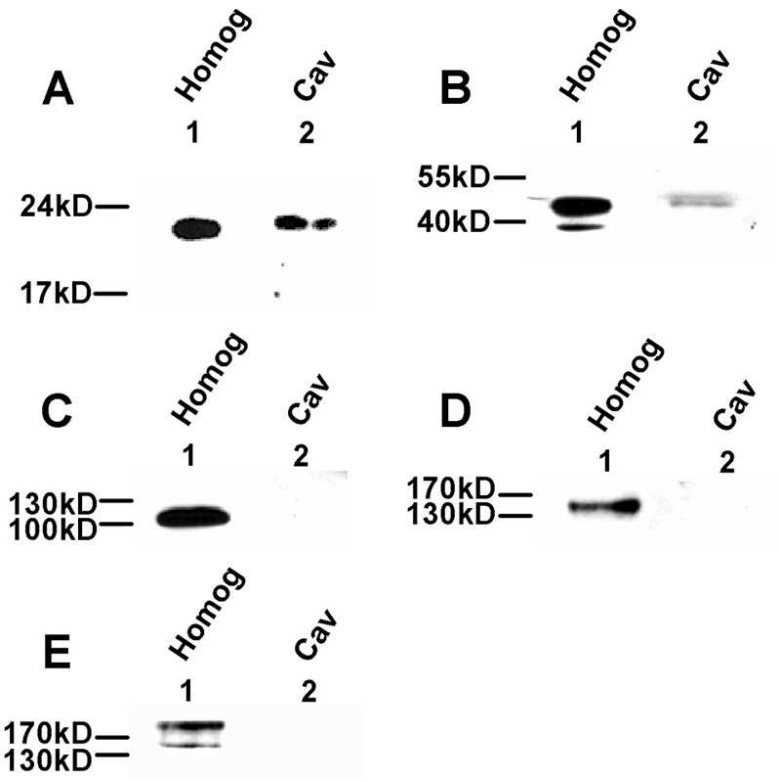

Figure 2.5. Distribution of the intracellular markers in CSC caveolae from RV-infected cells. Equal amounts of total protein from homogenate (Homog) and caveolae (Cav) fractions isolated from RV-infected MDCK cells were assayed for a panel of cellular markers (Table 1). Peptide-specific antisera were used to detect caveolin-1 (**A**) and flotillin-1 (**B**) by Western blotting. Marker-specific antisera and western blots were used to identify the distribution of contaminating ER membrane (calnexin) (C), non-lipid raft PM (Na/K-ATPase α subunit) (D) and clathrin-coated membranes (clathrin heavy chain) (E) in each membrane fraction.

These data indicated if NSP4 was present in the infected CSC caveolae, its presence would not be from cross-contamination of other intracellular organelles, but from transport of NSP4 to PM caveolae.

2.4.6 Full-length, Endo H-sensitive NSP4 was present in CSC caveolae isolated from RV SA11-4F-infected epithelial cells

To evaluate the presence of NSP4 in PM caveolae during RV infection, CSC fractions were isolated from mock or RV-infected MDCK cells, resolved by SDS-PAGE, and analyzed by Western blot. NSP4-specific bands were present at 28, 24, and 20 kDa, the expected mol wt of doubly, singly and unglycosylated full-length enterotoxin, in the homogenate, and the ER and PM fractions with NSP4-specific bands (Fig. 2.6A, lanes 6, 8, and 9, respectively) (33). Of these, the 28 kDa NSP4 was present in CSC caveolae, and the 24- and 20-kDa bands were absent (Fig. 2.6A, lane 10). A smaller protein of approximately 16 kDa also was visible in all preliminary fractions and in CSC caveolae when blots were overexposed (Fig. 2.6A, lane 11). This 16 kDa band was presumed to be a single cleaved fragment (residues 42-175) or dimers of the 7.5 kDa (aa 112-175) NSP4 cleavage product (146).

The endo H-sensitivity of NSP4 was used to verify the 28 kDa bands seen in the homogenate and CSC caveolae were due to the glycosylation state of NSP4 (Fig. 2.6B), and that both termini of NSP4 were present. The presence of the N-terminus of NSP4 was established by the presence of glycosylation sites (at aa 8 and 18) and the of the C-terminus was confirmed by using a C-terminal peptide-specific antibody (anti-$NSP4_{150-175}$) (16). Endo H pretreatment of the infected homogenate resulted in a significant loss

of the 28 kDa NSP4-specific band with a coinciding increase in intensity of the 20 kDa (unglycosylated) NSP4 band (Fig. 2.6B, lanes 5 and 6). In addition, endo H pretreatment of the CSC caveolae resulted in a shift of the NSP4 28 kDa band to the unglycosylated 20 kDa form (Fig. 2.6B, lanes 7 and 8). The smaller 16 kDa band was

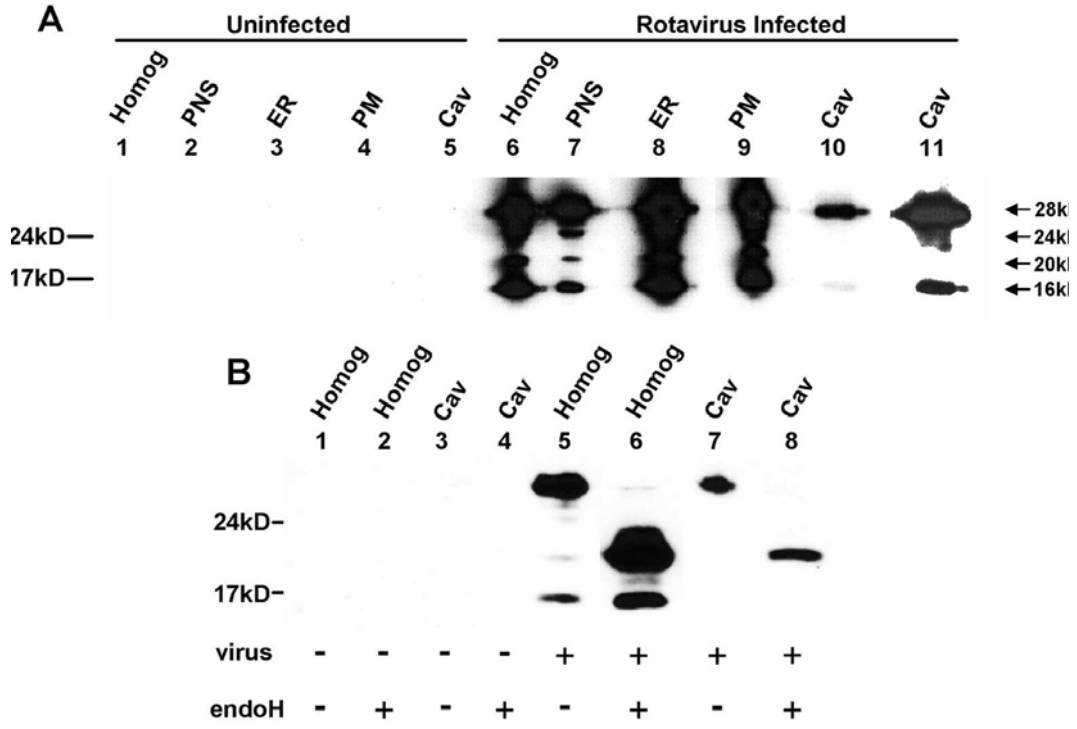

Figure 2.6. Detection of full-length, endo H-sensitive NSP4 in CSC caveolae isolated from RV-infected MDCK cells. (**A**) Equal amounts of total protein in homogenate (Homog), PNS, ER, PM, and CSC caveolae (Cav) isolated from mock- and RV-infected MDCK cells were assayed for the presence of NSP4 with $NSP4_{150\text{-}175}$-specific antisera. Homogenate, PNS, ER and PM fractions showed NSP4-specific banding profiles consistent with full-length, double-, single-, and unglycosylated NSP4 (28, 24, and 20 kDa respectively) in addition to a ~16 kDa band that may be a dimer of the NSP4 cleavage fragment (aa 112 to 175). CSC caveolae (lane 10) contained predominately the doubly-glycosylated 28 kDa form of NSP4 with a relatively small amount of the 16 kDa band observed when the film was significantly overexposed (lane 11). (**B**) The homogenate and CSC caveolae (lanes 3 and 4) fractions from uninfected cells were mock and endo H treated to determine if the enzyme treatment altered the specificity of NSP4 staining that was observed in panel A. The homogenate and CSC caveolae from RV-infected MDCK cells were similarly mock and endo H treated to confirm that the multiple forms of NSP4 were due to differences in the glycosylation state of the full-length protein and the absence of Golgi-specific mannosidase trimming. +, present; -, absent.

unaffected by endo H digestion (data not shown). The absence of the single-glycosylated NSP4 and presence of the non-glycosylated 16 kDa fragment in the CSC caveolae indicated that the inclusion of full-length, double-glycosylated NSP4 in the PM caveolae was not due to NSP4 glycans simply binding ConA.

2.4.7 NSP4 associates with caveolin-1, but not Golgi-localized proteins at early and late stages of infection

The endo H sensitivity of NSP4 in CSC caveolae isolated from MDCK cells at 24 hpi suggested the enterotoxin bypassed the endomannosidase-rich Golgi apparatus during transport from the ER (43, 53, 68, 85). We therefore examined RV-infected MDCK cells for the colocalization of NSP4 and caveolin-1 at both the early and late time points postinfectioin (Fig 2.7, colored panels). An examination of the subcellular distribution of NSP4 at perinuclear sites, in cytoplasmic vesicular-like structures, and at the cells periphery (Fig 2.7) and an increase in the NSP4 signal at 24 hpi compared to that at 7.5 hpi. In contrast, the levels of the caveolin-1 signal at both time points appeared to be essentially the same. Similarly, colocalization at the cell periphery and in vesicular-like structures in the cytoplasm was seen (Fig. 2.7, right panels). At the same times postinfection, the association of giantin, a cis-medial Golgi network marker, and NSP4 was evaluated (data not shown). These data revealed an absence of colocalization with the cis-medial Golgi network marker, in agreement with a recent report showing the NSP4-enhanced green fluorescent protein (EGFP) and giantin fail to colocalize (11). The specificity of each antibody set was corroborated using mock infected cells, as well as secondary antibody controls (Fig. 2.7 top panels).

While caveolin-1 traffics directly between the ER and PM caveolin caveolae in specific chaperone complexes, the only experimentally defined caveolin-1 vesicular pathway transits through the Golgi apparatus and buds from the trans-Golgi network, albeit other vesicular pathways have been suggested, including direct transport between the ER and the PM (23, 101, 140). Therefore, the subcellular distribution of the trans-

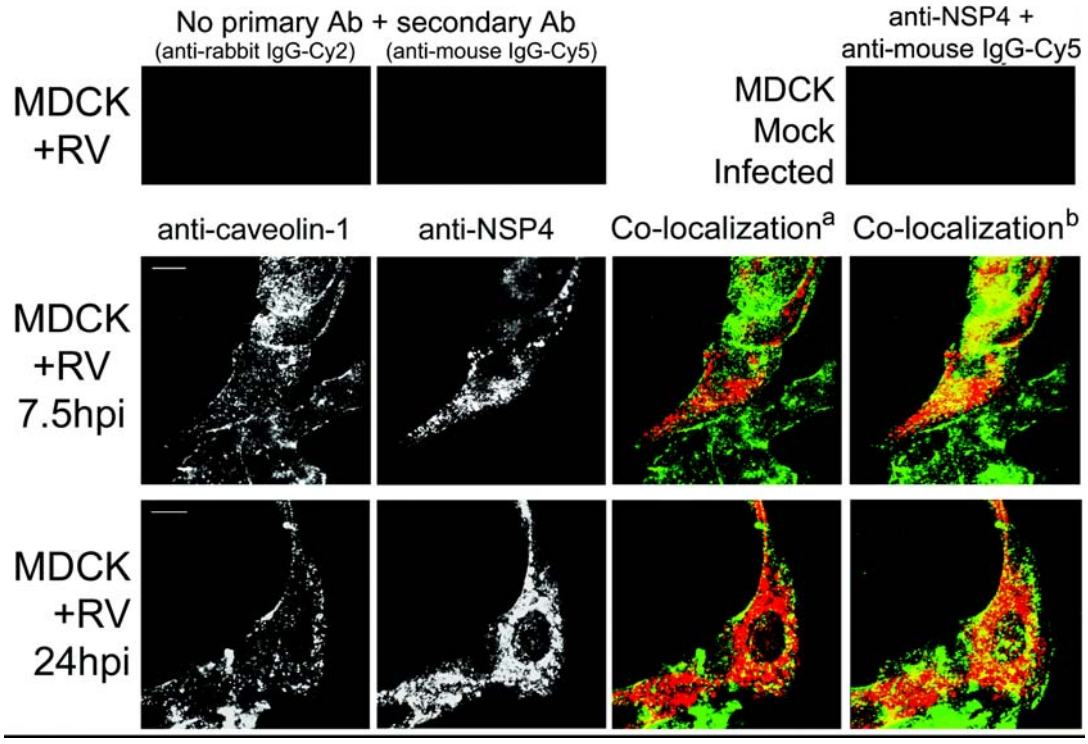

Figure 2.7. Association of NSP4 with caveolin-1 during early and late rotavirus infection. RV-infected MDCK cells were probed with the indicated primary antibodies. Fluorescently tagged secondary antibodies were imaged with 488-nm- and then 647-nm-wavelentgh excitation sources to capture Cy2 and Cy5 data, respectively, and to control for Cy2 signal bleed-through into the Cy5 images. Images from mock (right upper panel)- and RV (left and center upper panels)-infected cells in the absence of the indicated primary antibodies were used to control for the stain specificity and nonspecific binding of each antibody set. Shown are the data acquired for caveolin-1 and NSP4 and the merged images (co-localization[a]; caveolin-1 is in green, and NSP4 is in red). To optimize the visualization of the relative amounts of colocalized NSP4 and caveolin-1, a merged set of 8 z-series images (taken at 0.75-µm intervals) is also shown (co-localization[b]). The images shown are representative of results from four experiments.

Golgi network-localized golgin-97 (31, 75) in CSC-isolated membrane fractions was examined by Western blotting (Fig 2.8). Analogous to the lack of NSP4 colocalization with a cis-medial Golgi network marker, there was an absence of golgin-97 in the caveolae fraction (Fig. 2.8 lane 5). Hence, fluorescence imaging and Western blotting failed to detect cis-medial and trans-Golgi network marker, respectively.

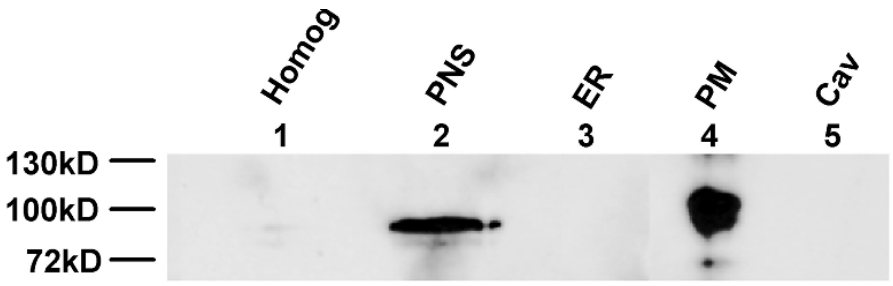

Figure 2.8. Distribution of Golgin-97 in CSC-isolated membrane fractions. Equal amounts of total protein from homogenate (Homog), PNS, ER, PM, and CSC caveolae (Cav) fractions isolated from RV-infected MDCK cells by CSC isolation were assayed for the presence of the trans-Golgi marker golgin-97. Golgin-97 was undetectable in the CSC caveolae fraction by Western blotting.

2.4.8 NSP4 expression was sufficient for colocalization with caveolin-1

To determine if additional viral proteins were required for the intracellular NSP4-caveilin-1 association, epifluorescence was utilized with NSP4-transfected cells. In the absence of other viral proteins, NSP4 had the same subcellular distribution patterns in MDCK and HT29.f8 cells as those observed during RV infection (Fig. 2.9 central panels). Both cell lines stained for caveolin-1, whereas only one of the HT29.f8 cells (of the two shown) was transfected, as indicated by the presence of NSP4 (Fig. 2.9, upper panels). Additionally, the NSP4 and caveolin-1 proteins in the transfected cells

colocalized (Fig. 2.9, far-right panels) at intracellular sites similar to those observed in RV-infected cells (compare Fig. 2.7). These results confirmed that the NSP4 protein is sufficient in and of itself to associate with the key caveolar structural protein caveolin-1 in two different cell types.

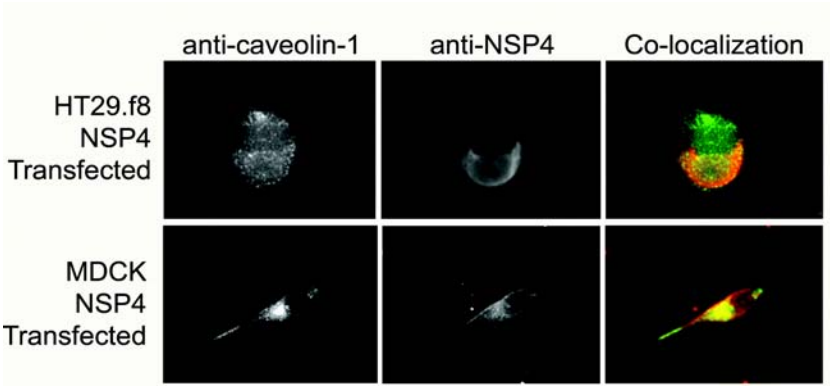

Figure 2.9. Colocalization of NSP4 with caveolin-1 in transfected cells. HT29.f8 (top panels) and MDCK (bottom panels) cells were transfected with pcDNA3.2D $_{NSP4150\text{-}175}$ plasmid DNA and probed with the indicated primary antibodies. Fluorescently tagged secondary antibodies were imaged with 48-nm and then 560-nm wavelength excitation source to capture Cy2 and Texas Red signals, respectively (n = 4). Caveolin-1 left panels) and NSP4 (center panels) distributions are shown. Note that only one of the two HT29.f8 cells shown was transfected (NSP4 signal). The panels on the far right are merged images showing the colocalization of NSP4 (red) and caveolin-1 (green).

2.4.9 NSP4-caveolin-1 association was resolved to within a 10-nm radius in MDCK cells during RV infection

The colocalization of NSP4 and caveolin-1 during RV infection or NSP4 transfection resolved the proteins to within about 200 nm, whereas FRET analyses with Cy2- and Cy3-labeled probes resolved the NSP4-caveolin-1 interaction to an area of less than 10 nm in radius (Fig. 2.10, boxes 1) (113). Figure 2.10A and B show the labeled

NSP4 (acceptor) before and after photobleaching (large boxes) in MDCK cells. Likewise, panels C and D illustrate the caveolin-1 (donor) signal prior to and after the photobleaching of the acceptor. The caveolin-1 donor (Cy2) signal emission increased by 7.83% (Table 2.2) and was FRET strongly positive in areas where NSP4 was extensively bleached (Fig. 2.10, boxes 1). Cells in the control areas of the same fields of view, where NSP4 was only partially bleached (boxes 2) or where NSP4 was not present (boxes 3), failed to show an increase in the donor (caveolin-1) signal (Table 2.2).

TABLE 2.2 Mean fluorescence values from FRET analyses[a]

	Mean fluorescence value for NSP4		Mean fluorescence value for caveolin-1		
Photoacceptor status	Prebleach	Post bleach	Pre beach	Postbleach	% Change in caveolin-1 mean fluorescence[b]
Bleached with 100% power	111	4	115	124	7.8
Bleached with 32% poser	107	73	65	46	-29.2
Not present	0	0	71	46	-35.2

[a]Mean fluorescence intensities are expressed in arbitrary units as acquired from Image J. Data correspond to boxes (bleached with 100% power), 2 (bleached with 32% power), and 3 (not present)

[b]Amount of increase or decrease (-) in Cy2-labeled caveolin-1 after bleaching of Cy3-labeled NSP4

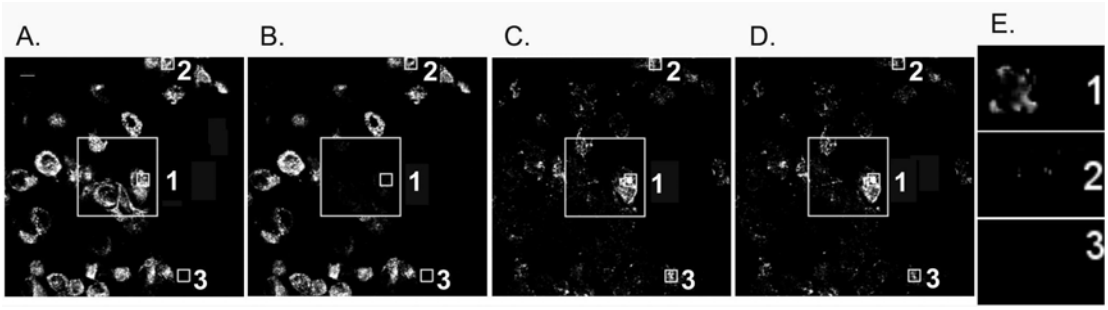

Figure 2.10. FRET analysis by acceptor photobleaching. NSP4 was probed with Cy3-linked Fab prepared from anti-NSP41$_{50\text{-}175}$ IgG and caveolin-1 was probed with anti-caveolin 1 followed by Cy2 conjugated goat ant-rabbit antibody in RV-infected HT29.f8 cells. The Cy3 and Cy2 images were acquired with the 568nm and 48 nm-wavelength lasers (panels A and C are prebleach images of NSP4 and caveolin-1 respectively). Subsequently, an area highlighted by the large boxes in panels A to D was photobleached wit 568 nm-wavelength laser at 100% power for 3 min. Cy3 and Cy2 signals were reimaged following the photobleaching of he acceptor signal (panels B and D are postbleach images of NSP4 and caveolin-1). Panel B demonstrates the efficient photobleaching of the acceptor within the large box. To monitor FRET efficiency, three small areas were selected and closely examine for FRET (box1, area where NSP4 was extensively bleached; box 2, area where NSP4 was partially bleached; and box 3, area where NSP4 was not present). On the far right (panel E) images corresponding to the small boxes are enlarged to visualize the percentage of FRET that varied from no signal when NSP4 was absent (box 3) to a significant amount when NSP4 was bleached (box 1).

As anticipated, those areas corresponding to boxes 2 and 3 showed weak or negative FRET AS the Forester radius of the Cy2-Cy3 fluorophore pair is 5 to 6 nm and the calculated probe-to-probe radius is dependent on the inverse sixth power of the intermolecular separation, the NSP4 and caveolin-1 labels must be no more than 10 nm from each other for the detection of a FRET reaction (59, 60), i.e., a positive FRET reaction placed at least some portion of the NSP4 and caveolin-1 protein pools within 10 nm of each other, highly indicative of a protein-protein interaction.

2.5 Discussion

By utilizing a newly developed PM caveolae isolation protocol and RV-infected MDCK cells, our data showed the presence of full-length, high-mannose glycosylated

NSP4 in PM caveolae that lacked an ER marker, but contained caveolin-1, flotillin-1 and G_{M1}. Several reports have implicated the association of NSP4 with lipid rafts. First, a preferential interaction between NSP4 and $NSP4_{114-135}$ with anionic, cholesterol-rich, caveolae-like model membranes has been shown by circular dichroism and a filter-binding assay (51, 52). Second, RV particles, VP4 (the RV spike protein), and NSP4 are associated with DRM in RV-infected cells (114). Third, infectious RV particles and NSP4 are detected in Triton X-100-insoluble fractions and sensitive to drugs that compromise lipid raft integrity (26). Fourth, NSP4 directly binds caveolin-1 with the binding site mapping to NSP4 residues 114 to 135 (95). Taken together these data strongly indicate an association of raft membranes with NSP4 for intracellular transport from the ER to the PM. However, these data are inconclusive, as DRM contain a large quantity of ER-specific markers.

There are several reported raft/caveolae isolation protocols that have been extensively utilized to study the composition and interactions specific to raft membrane microdomains (101, 102). For our purposes, it was critical to isolate PM caveolae free of even a trace of ER contamination. The ER is a known reservoir of NSP4 during RV infection and the presence of ER membranes could non-specifically introduce NSP4 into caveolae in the absence of NSP4-raft association (10). We recognize this concern may be unique to NSP4 and other ER-localized proteins in that a trace of ER contamination would not influence the conclusions of other studies.

A recent report has revealed that NSP4 bypasses the Golgi in route from the ER to the cell periphery using a NSP4-EGFP fusion protein (11). In that study, the NSP4-

EGFP fusion protein failed to localize with Golgi apparatus marker, giantin, but co-localized with the autophagosomal marker LC3 and accumulated close to, but not within, the PM cytoplasmic leaflet. In the present study, we show fully glycosylated, endo H-sensitive NSP4 in CSC caveolae. This discrepancy in PM localization may be due to inherent differences in virally expressed NSP4 versus expression of a NSP4 expressed with a large fusion partner (EGFP) or the use of alternate analysis techniques. Nonetheless our data agree with the study by Berkova et al. (11) on several key points, including the presence of NSP4 in cytoplasmic, vesicular-like structures that bypass the Golgi in transport to the cell surface and the presence of non-ER NSP4 intracellular pools with apparently distinct functions.

Caveolae can function as vesicular carriers containing key fusion complex proteins that mediate vesicle formation, docking and fusion, including GTPases, annexins, N-ethylmaleimide-sensitive fusion factor, soluble N-ethylmaleimide-sensitive fusion factor attachment proteins, and soluble N-ethylmaleimide-sensitive fusion factor attachment protein receptors (110, 118, 119). It remains unclear if CSC caveolae interact with fusion-competent caveolae vesicles. The autophagosomes carrying NSP4 apparently do not fuse with other membranes such as the PM (11). Hence, distinct, functionally divergent NSP4 pools may be uniquely transported, as suggested by Berkova et al. (11).

NSP4 and caveolin-1 co-localized at multiple sites within infected cells (this study and reference (95)). Although co-localizations via merged confocal images are widely used to determine if two or more molecules are in close proximity, the resolution

of these co-localized molecules is approximately 200 nm (79). Given that caveolae are 50-100 nm in diameter, imaging data alone are inconclusive, necessitating a second, confirmatory technique. Hence we evaluated the composition of caveolae (free of ER) and performed FRET analyses of NSP4 and caveolin-1, which brings the resolution to within 10 nm (113).

Caveolin-1 and G_{M1} are established markers for raft/caveolae fractions (112, 126, 129). Flotillin-1, a 45 kDa membrane-associated protein enriched in isolated lipid rafts as defined by Triton X-100-extracted DRM, is also detected in sodium carbonate (high pH)-extracted caveolae, but is absent from immunopurified caveolae (87, 128, 129). In our hands, flotillin-1 was present in CSC caveolae along with the other two caveolae markers, although the protein markers were not enriched in CSC caveolae when compared to the PM. Our focus was on obtaining pure, ER-negative PM caveolae rather than acquiring large quantities of raft membranes. We discovered there was a trade off between purity and recovery with a probable loss of some portion of the PM caveolae during processing. Alternatively, the brief sonication used to disrupt the large membrane sheets before ConA-affinity isolation may have sheared a portion of the peripheral and membrane associated protein populations. In that instance, the presence of full-length NSP4 in CSC caveolae would suggest NSP4 crosses the PM bilayer rather than interacting through a peripheral association. Additional studies are needed to distinguish these precise protein-lipid interactions.

To ensure the presence of NSP4 in CSC caveolae was not due to co-isolation of a contaminant membrane, calnexin (ER), Golgin-97 (Golgi), clathrin (clathrin coated pits),

and Na/K-ATPase α (non-raft PM) marker proteins were examined. These proteins are commonly utilized to indicate the presence of the corresponding membranes in cell fractionation experiments due to their association with specific intracellular membranes (31, 72, 75, 108). The resultant marker profiles indicated the CSC caveolae fraction was void of detectable ER, Golgi, and clathrin-coated membranes, as well as non-raft PM domains.

The recent identification of NSP4 in DRM isolated from RV -infected colon cells prompted us to define the composition of identical DRM isolated from MDCK cells and provide further insight into the presence of NSP4 in lipid rafts and caveolae (26, 114). While clathrin was not detected in MDCK DRM, significant amounts of the ER and non-raft PM markers were present. Due to the ER and non-raft PM contaminants, previous identification of NSP4 in DRM is indicative, but not conclusive, of NSP4 caveolae localization.

The critical intracellular receptor function of NSP4 in RV morphogenesis stresses the importance of a NSP4 pool in the ER during infection (5, 10). NSP4 in CSC caveolae extracted from a PM-enriched material devoid of detectable ER contamination indicates the presence of a second pool of NSP4 that is transported to PM caveolae during infection. Third and fourth pools present in LC3-containing autophagosomes and radiating from the ER-Golgi intermediate compartment have been detected previously (11, 143). It is reasonable to propose the RV multifunctional enterotoxin is transported by multiple cellular pathways to different intracellular locations due to interactions with

different host molecules. Further, more than one pathway may direct NSP4 to the same intracellular site.

The visualization of NSP4 in transfected cells showed a similar pattern to that seen following a virus infection. These data indicated NSP4 traffics to distinct intracellular locations in the absence of other viral proteins. While it remains unknown if the structure or the primary sequence of NSP4 facilitates its transport, transfected NSP4 still co-localized with caveolin-1 in the absence of other viral proteins. Positive FRET analyses further confirmed the specific interaction of NSP4 and caveolin-1 during RV infection.

In summary, NSP4 is a multifunctional, complex glycoprotein that uniquely interacts with host cell molecules. The data presented herein confirms the presence of full-length NSP4 in PM caveolae and the lack of Golgi network association in transport to the PM. Additional studies are needed to determine if NSP4 transport is dependent on caveolin-1 or caveolae intracellular movement and to fully elucidate the many roles of NSP4 during infection.

3. NSP4 IS EXPOSED AT THE EXOFACIAL SURFACE OF THE PM OF ROTAVIRUS INFECTED CELLS AND BINDS TO THE PM OF NON-INFECTED CELLS

3.1 Overview

Rotavirus NSP4, the first described viral enterotoxin, has been shown to be a multi-functional glycoprotein localized to several intracellular sites. The focus of this study was a pool of full-length NSP4 that bypassed the Golgi *en route* to the plasma membrane that appeared on the exofacial surface early post-infection, subsequently was released into culture media, and boung to naïve cells. Employing two distinct cell lines, NSP4 was noted at the exofacial leaflet of the plasma membrane between 2–3 and 4-8 hpi in HT29.f8 and MDCK cells, respectively, and was detectable in un-concentrated media of HT29.f8 and MDCK cells at 8 hpi. Corresponding viral growth curves reveaedl RV was not released at these early time points and the absence of NSP5 and caveolin-1 at the exofacial surface of the PM indicated the cells were intact. The endogenously-expressed, released and exogenously added NSP4 molecules were 28 kD and sensitive to endoglycosidase H digestion.

3.2 Introduction

Rotavirus (RV) NSP4 is synthesized as a primary translation product with an apparent molecular weight of 20 kD, is co-translationally glycosylated to 29 kD, and undergoes subsequent oligosaccharide processing to the mature 28 kD protein (34). The 175 amino acid (aa) polypeptide backbone of NSP4 consists of 3 N-terminal hydrophobic domains, yet topological analyses reveal a single transmembrane domain that traverses the

endoplasmic reticulum (ER) bilayer such that the N-terminal 23 aa are in the lumen of the ER and residues 45-175 form an extended, cytoplasmic domain (10, 21, 137). Two *N*-linked high mannose glycosylation sites are located within the short ER luminal domain (10). These glycan moieties remain sensitive to endoglycosidase H (endo H) digestion supporting the lack of exposure to Golgi enzymes (10, 16, 57). Within the cytoplasmic domain, there is an extended amphipathic α-helix that folds as a coiled-coil (aa 93-137) and overlaps the enterotoxic and oligomerization domains, as well as several cellular and viral protein binding domains(9, 15, 17, 82, 95, 137, 143). It is well established that NSP4 functions in viral morphogenesis at the ER by serving as an intracellular receptor to double layered particles (DLPs) (6, 137). RNA silencing (siRNA) studies of NSP4 expression disclose several additional functions (73, 121). In the absence of NSP4, there is: i) an abnormal distribution of viral proteins in the viroplasm; ii) little to no infectious virus particles present in the cell, iii) an accumulation of empty (no viral RNA) viral particles , and iv) an up regulation of viral transcription (121). Thus NSP4 also functions in viral transcription regulation, viroplasm formation and distribution of viral proteins in infected cells. Several reviews summarize the multiple roles of NSP4 and discuss in detail the disruption of Ca^{2+} homeostasis that influences RV assembly (8, 20, 76). The exclusive ER localization of NSP4 first came into question with the discovery of its enterotoxic function (9). In this study, purified NSP4 or NSP4 peptides were added exogenously to cell culture or to mouse pup intestines to elicit the enterotoxic effect prompting the authors to speculate NSP4 leaves the ER. Since then it has become clear that NSP4 is not exclusively localized to the ER and has been localized radiating from the ERGIC along

microtubules (143), associated with autophagosomes (11), in PM caveolae (132), and in culture media as a cleavage product (146) or as large 32 kD product (19). Autophagosomes typically traffic via a cytoplasm to vacuole or lysosomal pathway that by-pass the Golgi (1) supporting the absence of Golgi glycan trimming in this pool of NSP4 (11). In addition, co-localization with caveolin-1 places NSP4 in the cytosol and at the cell periphery (95). Collectively these data confirm NSP4 is not exclusively in the ER, but found throughout the cell and released from the cell. Evidence of vesicle fusion or the presence of classical fusion proteins involved in secretion is lacking.

In this report, we examined the exofacial surface of the PM to determine both the timing of NSP4 exposure post RV infection and verified the endo H sensitivity of the exposed enterotoxin's glycan moieties. We also determined the kinetics of NSP4 appearance in culture media and evaluated the subsequent binding to naïve cells. Our results revealed that full-length, endo H-sensitive enterotoxic NSP4 was exposed on the exofacial cell surface early post RV infection, dependent on the cell line. Hence, both endogenously expressed and exogenously added NSP4 associate with the exofacial PM surface of cells. We compared the timing of NSP4 exposure and release to RV growth curves in the same cell lines (MDCK and HT29.f8) and verified the lack of infectious virus above input virus in the media. Lastly, we showed NSP4 at the exofacial surface of naïve cells when exposed to NSP4-containing culture media. These data may explain how endogenously expressed NSP4 induces specific signaling events that are initiated at the PM.

3.3 Materials and Methods

3.3.1 Antibodies and reagents

Antibodies directed against rabbit caveolin-1 (anti-caveolin-1, Cell Signaling, Danvers, MA), mouse caveolin-1 (anti-caveolin-1, BD Transduction Laboratories, San Jose California) cyclophilin A (rabbit anti-cyclophilin A, Affinity Bioreaents, Golden, CO) giantin (rabbit anti-human giantin aa 1 to 469; Covance Research Products, Inc., Princeton, NJ), protein disulfide isomerase (mouse anti-PDI, Medical & Biological Laboratories Co. LTD., Woburn, MA) and horseradish peroxidase (HRP; goat anti-rabbit immunoglobulin G; Pierce Biotechnology, Rockford, IL), were purchased commercially from the indicated sources. Linked antibodies and fluorescent molecules included Alexa Fluor 350 conjugated streptavidin (Molecular Probes Eugene, OR), goat anti-mouse IgG-Texas Red (Rockland Immunochem, Inc, Gilbertsville, PA), goat anti-mouse-Cy5 conjugated, and the $F(ab')_2$ fragment of goat anti-rabbit-Cy2, and Cy3 conjugated Streptavidin (Jackson ImmunoResearch, West Grove, PA), and goat anti-rabbit IgG-fluorescein isothiocynate (IgG-FITC; KPL, Inc, Gaithersburg, MD). Antibodies specific to the NSP4 peptide aa 150 to 175 ($NSP4_{150-175}$; deduced from the simian rotavirus SA11 NSP4 sequence) were generated in rabbits by using peptide cross-linked to keyhole limpet hemocyanin as an antigen. Rabbit anti NSP5 was a gift from Dr Susan Lopez (Developmental Genetics and Molecular Physiology Department of the Institute of Biotechnology, National Autonomous University of Mexico).

3.3.2 Generation of anti-NSP4$_{150–175}$ F(ab)$_2$ segments

NSP4$_{150–175}$-specific antibodies were affinity purified against the inoculating peptide before use in confocal microscopy, and F(ab)$_2$ fragments were generated for fluorescent resonance energy transfer (FRET) analyses to reduce the distances of the fluorophores from the target proteins. Rabbit anti-NSP4$_{150–175}$ was affinity purified on an NSP4$_{150–175}$ peptide column prepared with preactivated cyanogen bromide Sepharose 4B beads by following the instructions of the manufacturer (Pharmacia Biotech, Piscataway, NJ) (7). The bound peptide IgG was eluted by altering the pH (134). The ImmunoPure F(ab)2 preparation kit (Pierce, Rockford, IL) was utilized, and the recommended protocol was followed to produce F(ab)$_2$ (142). Cy5 and Cy3 monofunctional reactive dye was conjugated to the affinity-purified NSP4$_{150–175}$ F(ab)$_2$ to produce aliquots of Cy3 and Cy5 conjugated NSP4$_{150–175}$ F(ab)$_2$ for FRET and exclusive colocalization analyses exactly as described by the manufacturer (Amersham Bioscience, Piscataway, NJ).

3.3.3 Cultured cells and virus

MDCK (ATCC, Manassas, VA) and HT29.f8 cells, a spontaneously polarizing cell line derived from the human adenocarcinoma HT29 intestinal line (83), were grown in maintenance media (Dulbecco's Modification of Eagle's media [DMEM] with 4.5 g/L glucose, L-glutamine, and sodium pyruvate; Mediatech, Inc., Herndon, VA) supplemented with 2 mM L-glutamine (200 mM; BioWhittaker/Cambrex), 1 mM sodium pyruvate (Cambrex), 0.1 mM non-essential amino acids (Mediatech, Inc.), 100 U/L penicillin, 100 μg/L streptomycin, 0.25 μg/L amphotericin (10,000 U penicillin-10,000 U of streptomycin- 25 μg/liter amphotericin B; Cambrex), 43.9 mM sodium

bicarbonate (GIBCO), 5% fetal bovine serum, and 5% Serum Supreme (Cambrex) at 37^{o}C in 5% CO_2. Cells were infected with SA11 clone 4F (gift of Mary Estes, Baylor College of Medicine, Houston, TX) at a multiplicity of infection (MOI) of 2 PFU/cell. Briefly, the virus was sonicated (5 minutes at a setting of 3.5, using a cuphorn attachment ice bath in a Misonix Sonicator 3000; Misonix, Inc, Farmingdale, NY) and incubated in serum-free DMEM with 10 μg/ml trypsin for 30 minutes at 37^{o}C, then incubated with the cells for 60 min at 37^{o}C in 5% CO_2. The inoculum was replaced with serum-free DMEM and the cells incubated for specified periods.

3.3.4 Western blot analyses

Equal amounts of total protein as assessed by BCA and Coomassie staining of gels were resolved on 12% polyacrylamide minigels and transferred to nitrocellulose filters (0.45 μ pure nitrocellulose; GE Osmonics) according to the manufacturer (Mini-PROTEAN II and Trans-Blot respectively; BioRad). The filters were blocked in 10% (wt/vol) non-fat dry milk in PBS (10% BLOTTO) for 1 hour at RT and reacted with the primary antibody in 2.5% BLOTTO for 14 hours at 4^{o}C with rocking. The filters were incubated an additional 1 hour at RT (room temperature) with primary antibody, then washed once in PBS, twice in PBS with 0.05% Tween-20, and once in PBS with rocking (10 min per wash). Secondary antibodies were diluted in 2.5% BLOTTO and incubated with the filters for 1 hour at RT with rocking. The nitrocellulose filters were washed as above, and reacted with Immobilon Western chemiluminescent substrates as per the manufacturer's protocols (Millipore, Billerica MA). The marker-specific bands were visualized by exposure to and development of x-ray film.

3.3.5 Confocal microscopy

Mock and SA11-infected cells were grown on glass coverslips and processed at specified periods of times post infection for fluorescent imaging. The infected cells were rinsed in PBS, fixed and permeabilized in methanol:acetone (1:1, vol/vol) for 5 min at -20^{o}C, and non-specific binding sites were blocked with 4% BLOTTO(4% dry milk in PBS) at RT for 45 min. The infected and uninfected cells were incubated with primary antibodies ($F(ab)_2NSP4_{150-175}$-Cy5, $NSP4_{150-175}$ or caveolin-1 peptide-specific, affinity-purified IgG) diluted in 2% BLOTTO-PBS at RT for 45 min. The cells were washed four times in PBS for 10 min each and incubated with Cy2, Texas Red, or Cy5-labeled secondary antibody diluted in 1% BLOTTO-PBS for 45 min in the dark. When applicable, proteins located on the exofacial surface of the PM were biotinylated and then labeled with streptavidin conjugated to Cy2 or Cy3. The cells were washed again as above but in the dark and mounted with fluorescent mounting media (KPL Inc.) onto glass slides. The resulting fluorescent images were captured with a MRC-1024MP BioRad laser scanning confocal microscopy system (BioRad, Hercules, CA) using a Zeiss inverted Axiovert microscope (Carl Zeiss, Inc., Thornwood, NY), a 63 X Zeiss oil apochromat objective, and the 488- 568- and 647-nm-wavelength excitation lines of an argon/krypton ion laser source. LaserSharp 3.0 (BioRad), Confocal Assistant 4.02 (Brelje TC/BioRad) and Image J were used to capture the pixilated fluorescent data, and to adjust contrast curves to construct the final images.

3.3.6 FRET by acceptor photobleaching

Fluorescent Resonance Energy Transfer (FRET) is a process by which nonradiative energy transfer from one fluorophore to another occurs if the two fluorophores (or proteins) are within 10 nm of each other (60). Acceptor photobleaching is one of the simpler and more effective FRET techniques whereby the acceptor fluorophore is bleached and then an increase in the donor fluorophore is assessed for to determine if the two proteins interact (59). The biotinylated cell surface proteins from RV-infected MDCK cells were labeled with Streptavidin-Cy3 and the entire cell was labeled with $NSP4_{150–175}$ $F(ab)_2$ specific IgG-Cy5 or Mouse anti-caveolin-1/goat anti-mouse-Cy5. A series of images were taken both before (568 and 647 nm; 10% power) and after the photobleaching of the Cy5 fluorophore. The cells were photobleached at 647 nm at 100% power for 3 min. An increase in the Cy3 signal (568 nm), indicating a positive FRET reaction which could only occur if the two fluorophores were in close proximity (less than 10 nm apart) (60) was assessed for. For each time point (4 and 7 hpi), a minimum of 10 fields were analyzed and percent FRET was calculated. Briefly, the integrated density value (IDV) for the Cy3 labeled surface proteins, both before and after bleaching the Cy5 labeld protein (either NSP4 or caveolin-1) were collected. The percent FRET was calculated by first subtracting the Cy3 IDV pior to photobleaching the Cy5 from the Cy3 IDV after photobleaching the Cy5. Second, this value (post Cy3 IDV – pre Cy3 IDV) was divided by the post Cy3 IDV rendering the percent FRET. As an internal control, the Cy3 (cell surface proteins) in a 500 by 100 pixel area outside of the region undergoing photobleaching of Cy5 labeled NSP4 or caveolin-1 was also

utilized to calculate a percent FRET and was referred to as the control area for each anlzyzed cell witin a given field of view. The percent FRET for RV infected cells from any field of view that contained a control area with a calculated percent FRET greater thatn +/- 10% was not utilized. The average percent FRET was calculated from 20 analyzed fields taken from 2 independent experiments for each time point. Image analysis was accomplished using Image J software, a public domain Java image-processing program inspired by NIH Image. Image J has a large and increasing number of plug-ins, which are functional programming updates to perform a specific task.

3.3.7 Surface biotinylation for isolation of cell surface proteins or visualization by confocal microscopy

Mock and infected cells were grown in 12 well plates or 8 well coverslips and reacted with 0.5mg/ml of membrane impermeable Sulfo-NHS-SS-Biotin (PIERCE #21331,) for 20 min at 4°C. Excess biotin was quenched with cold cell culture media (DMEM with serum). Following washes, cells on 8 well coverslips were fixed and permeabilized for Cy3 and Cy5 labeling and FRET analyses by confocal microscopy. Cells in the 12 well plates were lysed with RIPA buffer (150mM NaCl, 50 mM Tris-base, 1% SDS, 0.5% DOC, pH 8.0) containing protease inhibitors (0.2 μM PMSF and 1 μl/ml protease inhibitor cocktail set III) for 5 min at 4°C. To extract the biotin-labeled proteins, 30 μl of streptavdin-agarose slurry (Pierce # 20347D) per ml of lysate was incubated overnight at 4°C with constant rotation. The streptavidin-agarose-bound proteins were pelleted by centrifugation at 4°C. Each pellet was washed 3 times with 1 ml of RIPA buffer, the supernatants removed, and the remaining pellet suspended in

sample reducing buffer and separated by SDS-PAGE then electro-transferred to nitrocellulose membranes. Mock biotinylated samples were used to control for non-specific binding of proteins to the strepavidin beads and for non specific Streptavidin-Cy3 signal in LSCM analysis.

3.3.8 Protein quantification

Micro bicinchoninic acid (BCA) protein assay (Pierce) was utilized to quantify the protein concentrations with bovine serum albumin standards per manufacturer's protocol.

3.3.9 Live cell staining

For NSP4 exposure on intact cells present 24h post infection, mock and infected live cells were rinsed in DPBS then incubated with 1% BLOTTO/DMEM and anti-$NSP4_{150\text{-}175}$ at 4°C, rinsed in DPBS and fixed with cold methanol only. The fixed cells were then processed as for confocal microscopy utilizing secondary antibodies only. Cells were compared with permeabilized controls cells which were processed as for confocal microscopy with primary and secondary antibodies.

3.3.10 Growth curves

HT29.f8 and MDCK cells were grown to 80% confluency in 35mm tissue culture plates. Cells were incubated in complete DMEM minus sera for 12 hours prior to incubating with trypsin-activated SA11 4F for 1 h at 37°C in 5% CO_2 at a MOI of 2, after which the cells were washed two times with DMEM minus sera and 1250µl of DMEM with 1µg/ml trypsin was added. At specified points post infection either media or cells and media were collected. Media was spun at 1000g for 2 min to pellet any

cellular debris and immediately stored at -80°C. Cells and media were collected by carefully freezing the plate in liquid nitrogen followed by thawing and removing both cells and media, and immediately stored at -80°C. Titers were determined by indirect immunofluorescent staining of infected MA104 cell monolayers inoculated with serial dilutions of the samples. Virus titers were expressed as the number of fluorescing cell-forming units per ml.

3.3.11 Production of soluble NSP4 for exogenous addition to cells

MA104 cells were infected with RV SA114F at an MOI of 2 in a 175 cm^2 tissue culture flask. Cells were incubated for 14 hours, all cells and media were removed to 5 mls of Tricine consisting of 1 mM EDTA and 20 mM Tricine ph 7.8 buffer with protease inhibitors. Cells, media and lysates were spun at 3,000 rpm for 5 min and the PNS was removed and spun @ 39,000 rpm (192,000g) in SW 41Ti rotor for three hours. The supernatant from the high speed spin was collected and a portion was concentrated using an iCON^{TM} 7 ml/9k Concentrator (PIERCE #89884) approximately 10-fold before diluted 6-fold in DMEM and applied to MDCK or HT29.f8 cells for specified periods of time.

3.3.12 Exclusive colocalization of NSP4 with exofacial PM proteins in RV-infected HT29.f8 cells

Because the ER spreads throughout the eukaryotic cell and in many cases towards the inner surface of the PM, it is difficult to ascertain when NSP4 actually leaves the ER and arrives at the exofacial surface of the PM by IFA analysis. Resolution under 200 nm by light microscopy currently can not be achieved. Given that the PM of a cell is only 5nm thick, it is difficult to determine if NSP4 located within 100 nm of the PM is located on the external face of the PM or even at the PM, or if the NSP4 is still residing in the ER. In an effort to resolve this problem, a series of colocalization studies performed on the same HT29.f8 RV infected cells at 3 hpi and 11 hpi was accomplished. HT29.f8 cells were biotinylated then fixed and permeabilized and labeled for NSP4, a cytoplasmic protein Cyclophilin A, PDI as an ER marker and exofacial PM by Alexa-350 linked Streptavidin. Images were taken of each marker and colocalized signals corresponding to NSP4 and the PM, NSP4 and Cyclophilin A , and NSP4 and ER were selected using Image J. Again utilizing Image J, each of the colocalized pixels were pseudo-colored and merged with each other to determine if any pixels showed exclusive colocalization of NSP4 with the exofacial PM. Cells were examined at 40% confluency to increase the chance of evaluating independent cells. All cells in 5 fields of view for each experiment were analyzed with an average of 3 cells per field analyzed. Cells were visualized using a Stallion Digital Imaging workstation (Carl Zeiss MicroImaging, Inc. Thornwood, NY) equipped with a 300W xenon fluorescent light source with rapid switching (<2msec) between excitation wavelengths. Images were collected using a 63X

objective, 0.75 N.A., and a ROPER CoolSnap HQ camera. The Stallion system includes excitation/emission filter sets suitable for color staining including DAPI and Hoechst (365:445/50 nm), FITC and Cy2 (470/20:505-530 nm) and TX Red and Cy3 (560/40:590 nm) and Cy5 (600/50:685/50 nm). The images were processed using Image J.

3.3.13 Endoglycosidase reactions

For endo H cleavage, equal aliquots of protein samples from cell lysates and surface biotinylated proteins of the exofacial PM of cells were denatured and diluted per protocol of the manufacture (New England Biolabs, Ipswich, MA). Either 1 µl of sterile water (mock endo H treated) or 1 µl of endo H was added to the control or the sample. The cleavage reaction was performed for 1 hour at 37°C, and the proteins were resolved by SDS-PAGE and visualized by Western blotting

3.4 Results

3.4.1 Rotavirus growth curve analysis in HT29.f8 and MDCK cells

We performed a careful temporal analysis of the presence of NSP4 at the exofacial surface of the PM of RV infected cells, as well as its appearance in the media and interaction with the PM of non-infected cells. To more accurately interpret our findings, and to expose any possible differences in the intestinal cell line (HT29.f8) versus the kidney cell line (MDCK) we determined the RV growth curve in both cell lines. At specified time points starting at 2 hpi through 48 hpi either media (to detect virus release) or media and cells were collected and titered. Our results for both cell lines

(Fig 3.1 and Table 3.1) were similar and resembled RV SA11 growth curve analysis performed in a previous study (135). Of particular interest is the fact that virus release did not occur until sometime after 6 hpi in either cell line.

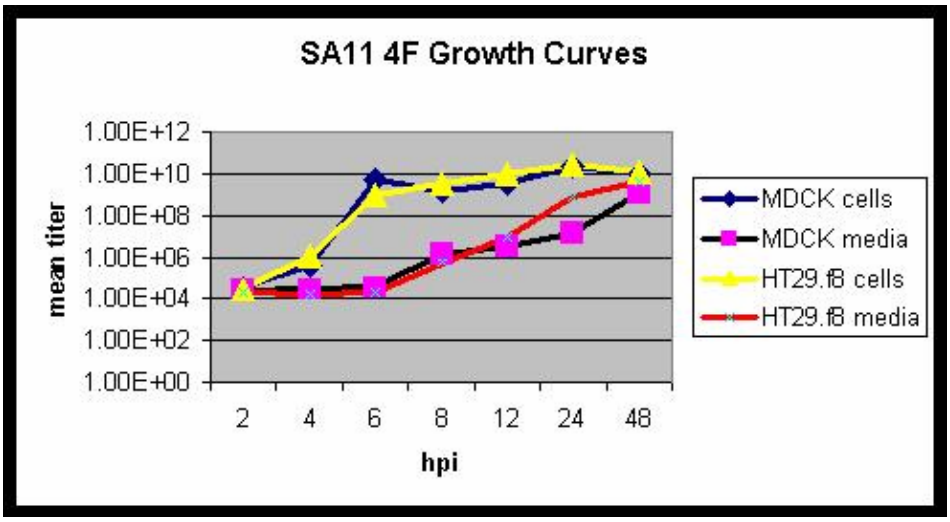

Figure 3.1 Rotavirus SA11 4F growth curves in MDCK and HT29.f8 cells are very similar. At time points from 2 to 48 hpi the media was collected to assess for virus exit from cells, and cells and media were collected to assess for appearance of progeny virus. Samples were tittered for RV and the average from three different 35 mm plates for each time point are annotated in the table 3.1 and graphically above.

TABLE 3.1 Mean RV titer from MDCK and HT29.f8 media or cells at various times post infection. Hours post infection are shown in the top row.

Hpi	**2**	**4**	**6**	**8**	**12**	**24**	**48**
MDCK media	2.27E+04	2.82E+04	3.60E+04	1.60E+06	3.33E+06	1.47E+07	1.27E+09
HT29.f8 media	2.00E+04	1.53E+04	2.00E+04	5.67E+05	1.00E+07	8.67E+08	4.60E+09
MDCK cells	3.33E+04	4.27E+05	5.87E+09	1.53E+09	3.40E+09	2.33E+10	1.07E+10
HT29.f8 cells	2.67E+04	1.20E+06	9.67E+08	3.74E+09	1.00E+10	2.80E+10	1.37E+10

3.4.2 NSP4 was exposed on the exofacial surface of MDCK and HT29.f8 cells early post infection

We examined the surface expression of NSP4 in RV-infected MDCK and HT29.f8 cells at several time points early post infection to determine when NSP4 was first exposed on the cell surface. Utilizing early time points also helped ensure a minimum of cytopathic effects and that the PM was intact. Bugarcic et al (19) observed secretion of NSP4 by 16 hpi in Caco-2 cells infected with the UK strain of bovine RV at a moi of 10, however NSP4 appears post-translationally processed to approximately 32kD with a partial endo H-resistant population as well. Initial experiments were completed to establish the presence of NSP4 on the surface of both MDCK and HT29.f8 cells at 8 hpi (data not shown). We then tested for the presence of NSP4 at 7 and 4 hpi and found that in MDCK cells, NSP4 was only exposed at 7 hpi indicating in these cells NSP4 reached the cell surface after 4 hpi (Fig. 3.2 A bottom panel, lane 2).

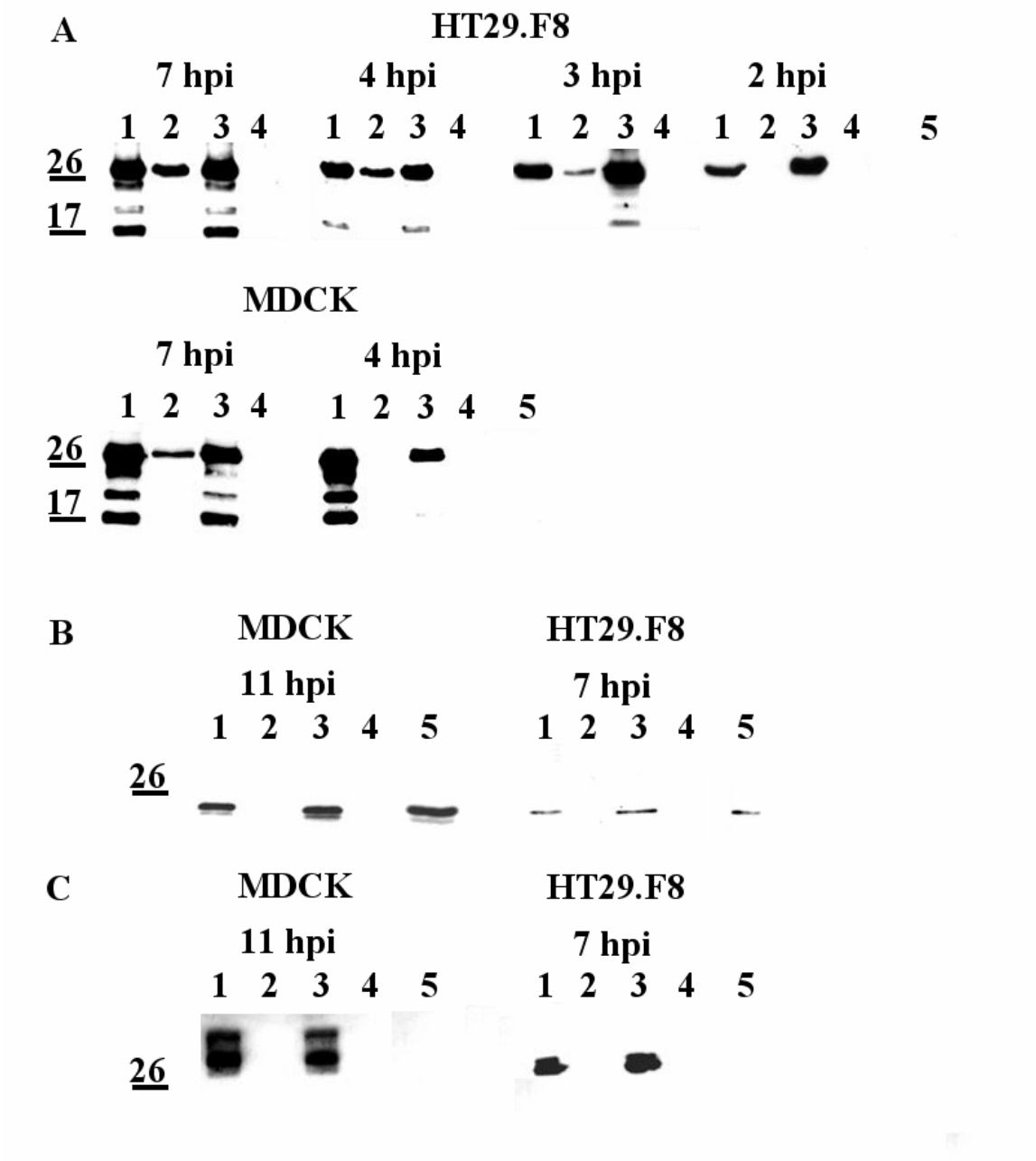

Figure 3.2. Western blot analyses of surface biotinylated proteins. MDCK and HT29.f8 cells were infected with RV SA11.4F at a moi of 2 for specified times, surface biotinylated and precipitated with streptavidin agarose. The cell lysates and precipitated surface proteins were separated by SDS-PAGE and analyzed by Western blot using anit-$NSP4_{150\text{-}175}$ A. anti-caveolin-1 B. or anti-NSP5 C. For all blots 1 = lysates from biotinylated cells, 2 = streptavidin pull down of biotinylated exofacial proteins, 3 = lysates from no biotin control, 4 = streptavidin pull down of mock biotinylated exofacial proteins, and 5 = lysates from no RV cell control.

In the HT29.f8 cells, NSP4 was surface biotinylated at 7, 4 and 3 hpi, but not at 2 hpi (Fig.3.2 A top panel, lane 2) indicating NSP4 was exposed after 2 hpi in this cell line. Two control antibodies were employed in RV infected cells with both cell lines 4 hours later than the point in which NSP4 was first detected at the exofacial surface of the PM, corresponding to 7 hpi for HT29.f8 cells and 11 hpi for MDCK cells. These antibodies were utilized to assess for the presence of NSP5 which is a marker of the perinuclear located viroplasm (35, 74) and for caveolin-1 which is located at the endofacial surface of the PM (130). Neither caveolin-1 nor NSP5 were detected at the cell surface (Fig 3.2B and 3.2C lane 2). These data showed the PM to be intact and placed NSP4 at the exofacial PM leaflet between 2-3 hpi in HT29.f8 intestinal cells and between 4-7 hpi in MDCK kidney cells.

3.4.3 Cell-surface exposed NSP4 was endo H sensitive

To determine if the cell surface-exposed NSP4 molecules were sensitive to endo H, RV-infected MDCK and HT29.f8 cells were surface biotinylated and the biotinylated proteins subjected to endo H digestion (Fig. 3.3). The lysates for lanes 1 show the mobility of NSP4 in the cell lysates of the biotinylated cells, and lanes 2 correspond to the lysates of the biotinylated cells that have been mock endo H-treated. As previously reported, 3 distinct NSP4-specific bands of approximately 28, 24, and 20kD (double-, single-, and unglycosylated NSP4) (95) were detected by Western blot (Fig 3.3, lysate lanes 1 and 2) in the untreated and mock treated cell lysates at 7 hpi. The HT29.f8 cells also were evaluated at 4 hpi. When the lysates were digested with endo H (lysates, lanes 3), a shift of NSP4 electrophoretic mobility was noted with the 28 kD double-

glycosylated band shifting to ~20 kD. There was no change in mobility of the unglycosylated 20 kD NSP4 band. NSP4 endo H sensitivity of the infected lysates agree with our previous results (95, 132). When the surface biotinylated fraction was pulled downs with streptavidin coated agarose beads and was examined by Western blot, only the doubly-glycosylated, 28 kD NSP4 was seen (Fig. 3.3, PM lanes 1 and 2) illustrating only the fully glycosylated protein is exposed on the cell surface. Surface NSP4 was endo H sensitive with the 28 kD migrating at 20 kD (Fig. 3.3, PM lanes 3).

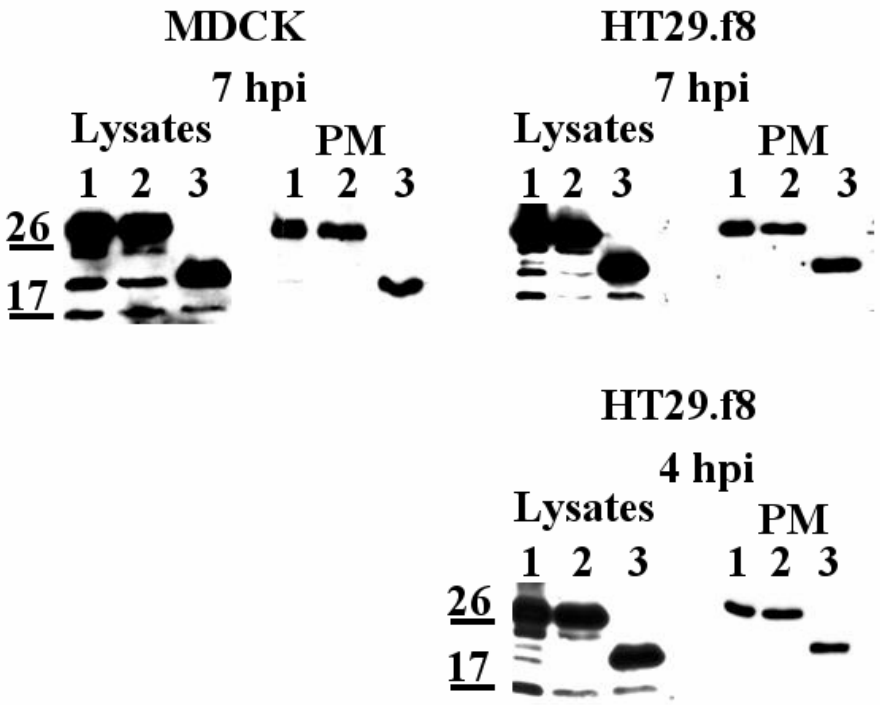

Figure 3.3. Endo H of lysates and precipitated surface proteins from MDCK cells at 7 hpi and from HT29.f8 cells at 7 and 4 hpi. Western blot analyses using anti-$NSP4_{150-175}$. Lane 1 = pre endo H 2 = Mock endo H treated 3 = endo H treated.

3.4.4 NSP4 was detected on the exofacial PM by a live cell staining method

To verify the results of NSP4 at the exofacial leaflet of the PM, an alternative biochemical method in addition to surface biotinylation of all exofacial PM proteins was employed. Two sets of MDCK cells were RV infected or mock infected for 11 hours. At 10.5 hpi, both the mock infected and RV infected cells were incubated for 20 minutes at 4°C with DMEM including anti-$NSP4_{150\text{-}175}$, washed twice with media and incubated an additional 20 minutes at 4°C with DMEM including a biotinylated goat anti-rabbit. After washing the cells twice again with media, processing resumed as when the cells were surface biotinylated (see above). Western blot analyses with anti-$NSP4_{150\text{-}175}$ revealed a 28 kd band in the RV infected cells but not in the mock infected cells treated with the anti-$NSP4_{150\text{-}175}$ (Fig. 3.4 lane 4 and 6). The 28 kD band corresponded to the same size band seen in surface biotinylated RV infected cells (Fig 3.4, lane 2).

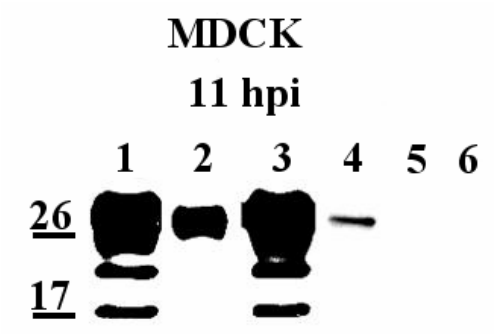

Figure 3.4. Western blot analyses of surface biotinylated proteins. MDCK cells were infected with RV SA11.4F at a moi of 2 for 11 hours and surface biotinylated or live cell stained with anit-$NSP4_{150\text{-}175}$ and a biotinylated goat anti rabbit antibody. Samples were precipitated with streptavidin agarose. The cell lysates and precipitated surface proteins were separated by SDS-PAGE and analyzed by Western blot using anit-$NSP4_{150\text{-}175}$. 1 = Cell lysates from biotinylated cells, 2 = Streptavidin pull down of biotinylated exofacial proteins, 3 = Cell lysate from live cell antibody treated cells, 4 = Streptavidin pull down of live cell antibody treated cells, 5 = Cell lysate from live cell treated (no RV) antibody treated cells, 6 = Streptavidin pull down of live cell treated (no RV) antibody treated cells

3.4.5 FRET analysis and exclusive colocalization of individual cells revealed exofacial exposure of NSP4 at the PM of RV infected cells

Biochemical analysis, whether it be by surface biotinylation or by live cell staining with an antibody yielded information on the exposure of NSP4 at the PM of a pool of cells grown in a 6 or 12 well tissue culture dishes. The exposure of NSP4 and not RV NSP5 or the PM located but endofacial oriented caveolin-1, revealed the relative integrity of the PM of the same pool of cells that we found exofacial NSP4. We then utilized confocal microscopy to assess for the exposure of NSP4 on an individual cell basis while simultaneously analyzing the PM integrity of the cell in question. Given that the PM is about 5 nm in width and a positive colocalization result of NSP4 and the PM only localizes NSP4 within a 200 nm region of the PM, a more sensitive FRET method to detect NSP4 exposure at the PM by confocal microscopy was used. Because FRET can resolve the Cy3 and Cy5 fluorophores to within a 10-nm distance (60) we developed and utilized a novel method to corroborate our biochemical findings with regards to the exposure of NSP4 at 7 hpi but not at 4 hpi in MDCK cells (Figure 3.5, and see material and methods). We were able to limit our analysis to cells in which the membrane appeared to be intact by monitoring Cy3 labeled proteins that had been surface biotinylated that gave a distinct morphologic appearance upon confocal analysis of cells with PM integrity versus those to which the membrane was not intact and therefore allowed for biotinylation of intracellular proteins. During confocal analysis of cells, any field containing cells that appeared to be biotinylated throughout the cell versus just at the exofacial PM were not utilized for FRET anlysis, for example the top left cell in

Figure 3.6 J appears to contain a cell which was biotinylated throughout versus just at the PM for the cells in the rest of the field. Utilizing the acceptor photobleaching method, a negative FRET reaction occurred between the Cy3 labeled exofacial PM proteins and Cy5 labeled NSP4 at 4 hpi (Fig 3.6 A-C). By 7 hpi in MDCK cells, photobleaching Cy5 resulted in an increase in the Cy3 signal of the labeled proteins at the PM resulting in a positive FRET reaction (Fig 3.6 D – F). Repeated evaluations of MDCK cells at both time points resulted in a positive FRET for NSP4 at 7 hpi in MDCK cells and negative FRET for NSP4 at 4 hpi (Table 3.2). All controls, to include Cy5 labeling caveolin-1 instead of NSP4 resulted in a negate FRET as well (Fig 3.6 graph). Since caveolin-1 is not exposed, but known to be expressed on the endofacial leaflet of the PM, the width of PM separated the Cy3 labeled surface biotinylated proteins from the Cy5 labeled caveolin-1.

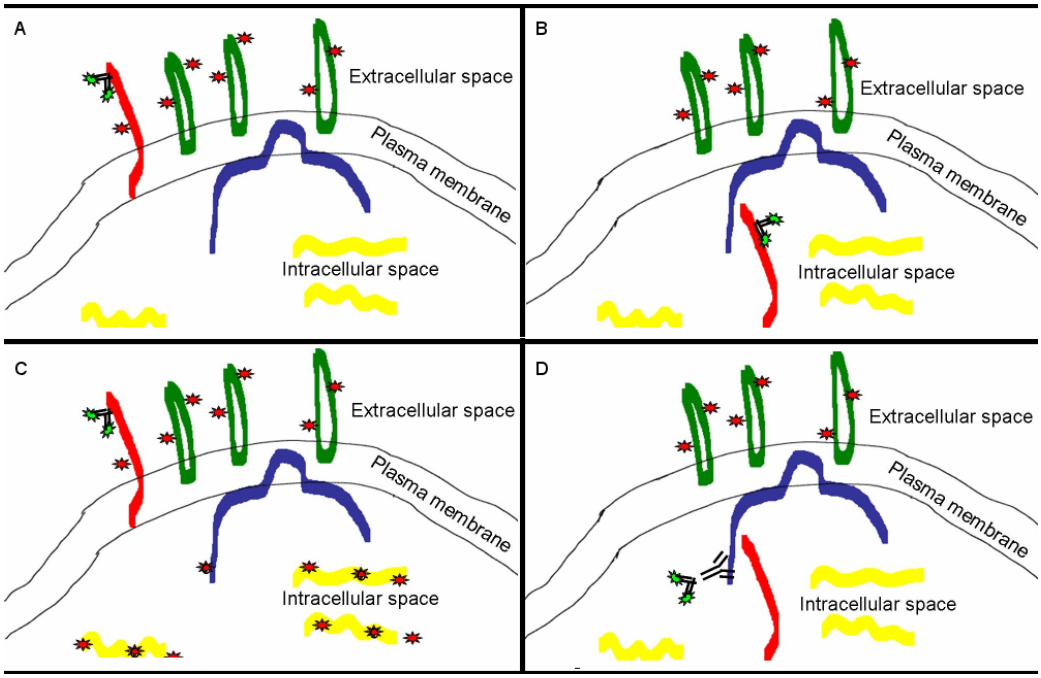

Figure 3.5. FRET analysis by acceptor photobleaching allows for simultaneous assessment of NSP4 exposure and PM integrity. If NSP4 is exposed it will be biotinylated and Cy3 and Cy5 labeled (A), if NSP4 is not exposed it is only Cy5 labeled (B). When PM loses its integrity proteins are biotinylated and Cy3 labeled throughout the cell (C) and refer to top left cell in 3.6 J. As an additional control caveolin-1 which is inserted into the endofacial PM is Cy5 labeled but because it is not exposed at the exofacial PM it is not biotinylated and therefore not Cy3 labeled. Green star = Cy5, Red star = Cy3, Red line = NSP4, Green ovals = exofacial PM proteins, blue = caveolin-1 and yellow = intracellular proteins.
A. = Positive FRET (Cy3 and Cy5 are in close enough proximity for a FRET to occur)
B. = Negative FRET (Cy3 and Cy5 are not in close enough proximity for a FRET to occur)
C. = FRET not assessed for, Cy3 throughout the cell indicates loss of PM integrity
D. = Negative FRET (Cy3 and Cy5 are not in close enough proximity for a FRET to occur)

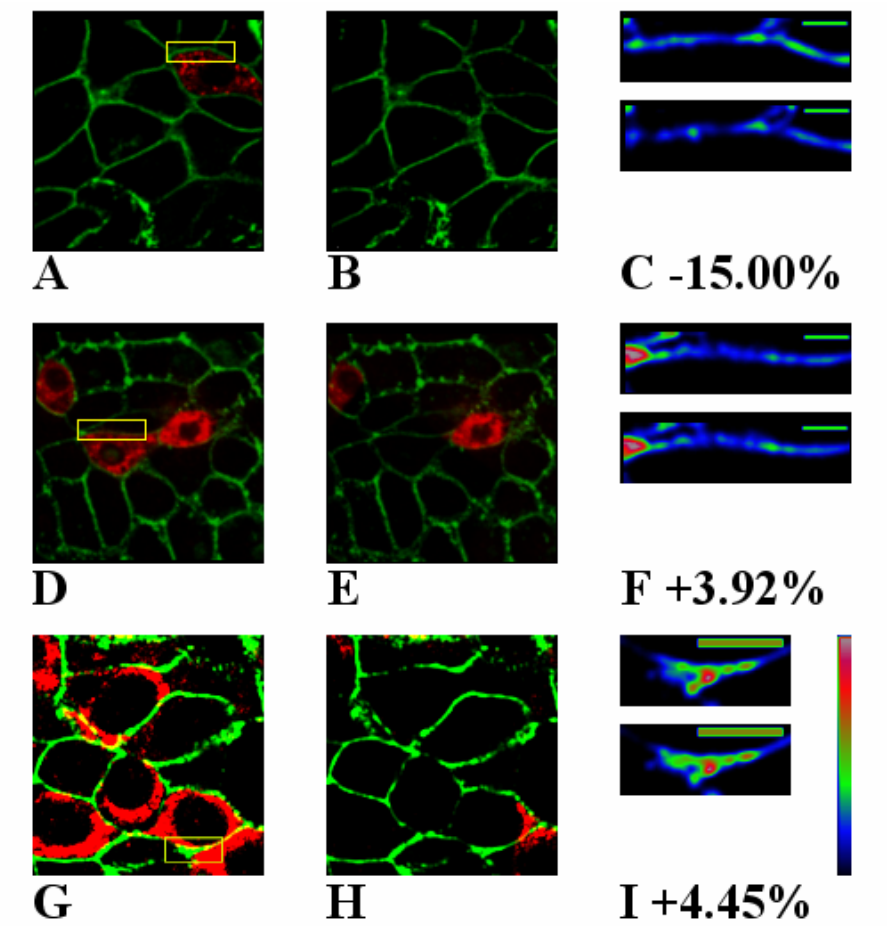

Figure 3.6 FRET analysis by acceptor photobleaching. Live cells were surface biotinylated prior to fixing and permeabilization. Streptavidin-Cy3 was utilized to label surface biotinylated proteins of the exofacial PM including NSP4 if exposed. NSP4 was labeled with Cy5-linked $F(ab)_2$ prepared from anti-$NSP4_{150\text{-}175}$. Cy5 (NSP4) and Cy3 (PM) images were acquired with the 647-nm and 568-nm-wavelentgh lasers both prior to and after bleaching NSP4. The percent FRET was calculated from the fluorescence intensity of selected areas of the PM both before and after bleaching NSP4, i.e. [(PM intensity in outlined yellow box post NSP4 bleaching –PM intensity pre NSP4 bleaching)/ PM intensity post NSP4 bleaching)]. A, D, and G = merged PM (Cy3) and NSP4 (Cy5) images prior to photobleaching NSP4 in MDCK at 4hpi, MDCK at 7 hpi and HT29.f8 cells at 7 hpi respectively. B, E, and H = same as A, D, and G, but post NSP4 photobleaching. C, F, and I are magnified regions of PM pseudo colored to show relative intensity with its respective calculated FRET value from outlined region in A, D, and G showing relative intensity of PM both before (top) and after (bottom) NSP4 photobleaching. Bar graph and table 3.2 show FRET values with error bars for MDCK cells at 4 and 7 hpi. Values were calculated from 10 different regions taken from two separate experiments for each time point, controls for each region were calculated from a region of PM in which NSP4 was not present. As an additional control caveolin-1 was Cy5 labeled and FRET calculated at 7 hpi. Horizontal bar = 5 microns, Vertical bar = relative intensity scale with red > green > blue. J = Streptavidin-Cy3 labeled PM with a cell in the top left corner that was biotinylated throughout due to loss of PM integrity.

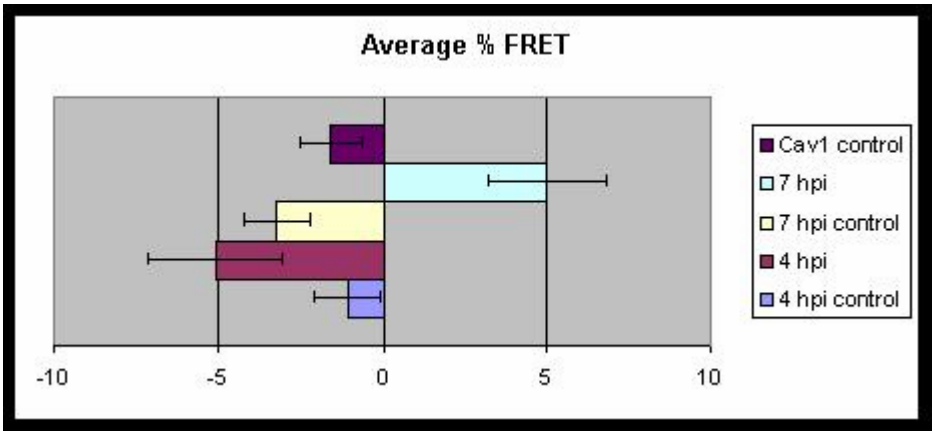

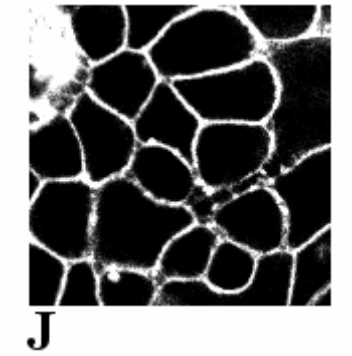

Figure 3.6 Continued.

TABLE 3.2 Average FRET values for MDCK cells at 4 and 7 hpi.

% FRET from Cy3 labeled exofacial PM to Cy5 labeled NSP4 in MDCK's	
7 hpi	**(+)** 3.21 – 6.79%
7 hpi control	**(-)** 2.2 – 4.22%
4 hpi	**(-)** 3.03 – 7.15%
4 hpi control	**(-)** 0.1 – 2.04%
*7 hpi control Cy3 PM to Cy5 Cav1	(-) 0.66 – 2.52%

An example of a positive FRET between Cy3 labeled exofacial PM proteins and Cy5 labeled NSP4 was also observed in HT29.f8 cells at 7 hpi (Fig. 3.6 G-I). NSP4 appeared to be exposed on the exofacial surface of RV infected HT29.f8 cells prior to 3 hpi, however it was technically difficult to conduct a FRET analyses during these very early time points post infection. NSP4 was detectable at these early time points by confocal microscopy, but the amounts were insufficient for acceptor photobleaching.

We developed and utilized an IFA exclusive colocalization image analysis technique for HT29.f8 cells to evaluate extremely early time point post infection and compared it to a much later time point post infection. Although NSP4 is translated within the ER, the ER spreads throughout the eukaryotic cell and in many cases towards the inner surface of the PM. Instead of merely colocalizing NSP4 and the PM we quadrupled labeled HT29.f8 cells at 3 and 11 hpi. Cells were labeled for NSP4, cyclophilin A which is a cytosolic protein, the ER and the PM. Colocalized signals corresponding to NSP4 and the PM were selected and pseudo-colored green, NSP4 and

cyclophilin A = red, NSP4 and ER = blue. These green, red, and blue colocalized signals were overlaid with each other so that colocalization corresponding to green, red and blue could be visualized. This resulted in red and green labeled pixels (NSP4 and PM merged with NSP4 and cyclophilin A) appeared yellow, whereas the red and blue labeled pixels (NSP4 and cyclophilin A with NSP4 and ER) appeared magenta. Merging of blue and green (NSP4 and ER with NSP4 and PM) appeared light blue and red and blue and green appeared white. For example, light blue indicated NSP4 waseither localized at the PM or the ER. This can readily occur given the inability to resolve differences less than 200 nm and the

ER can easily come within 50 nm of the PM. At 11 hpi NSP4 at the PM (green) at the exclusion of any NSP4 at the ER (blue) as well as NSP4 colocalized with cyclophilin A was noted, while at 3 hpi NSP4 was noted to colocalize with the PM (white and yellow pixels) but not at the exclusion of the ER or cyclophilin A (Table 3.3 Fig. 3.7).

TABLE 3.3.Exclusive colocalization color key for 3 and 11 hpi HT29.f8 cells

Color	**Co-Location(s)**
Green	NSP4 Exofacial PM
red	NSP4 Cyclophilin A
blue	NSP4,ER
yellow	NSP4 Exofacial PM Cyclophilin A
magenta	NSP4, ER Cyclophilin A
light blue	NSP4, ER Exofacial PM Cyclophilin A
White	NSP4, ER Exofacial PM Cyclophilin A

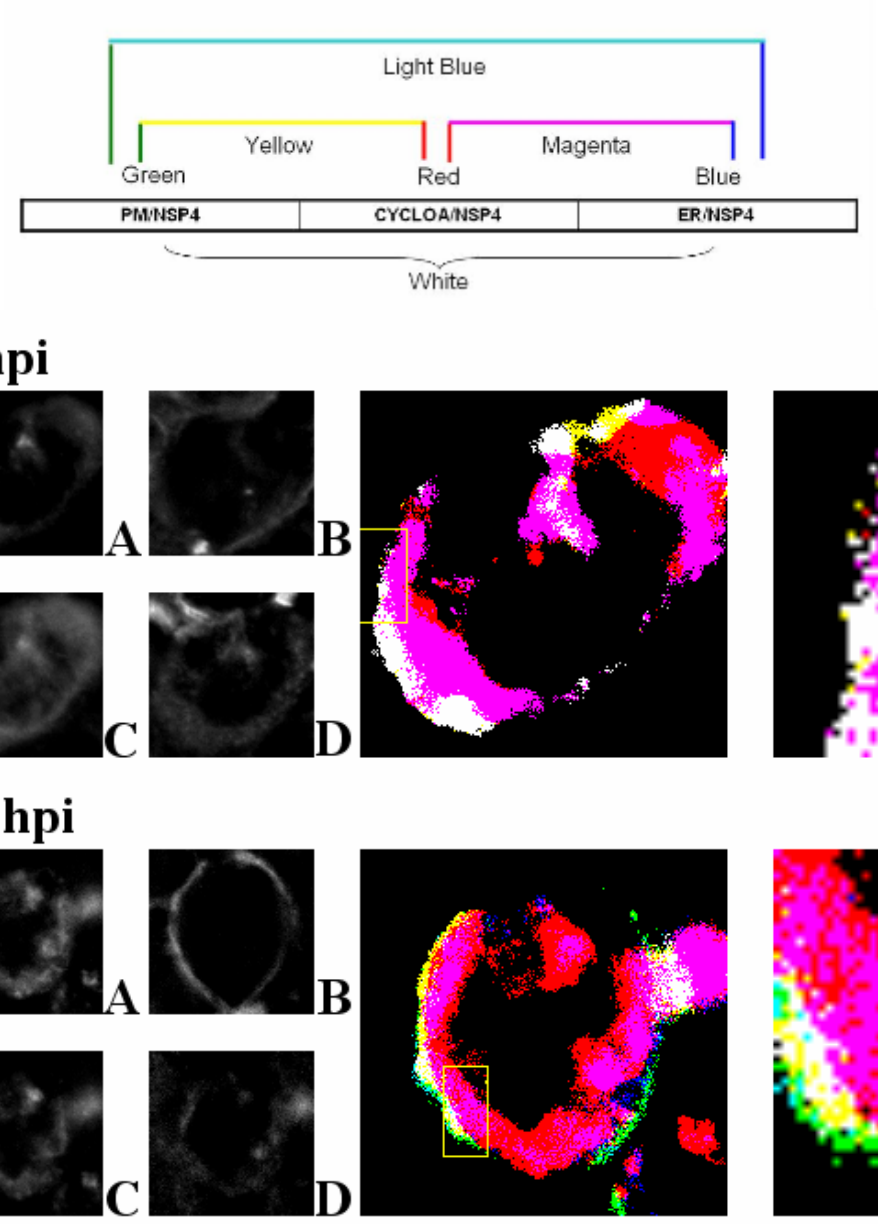

Figure 3.7. IFA of NSP4, ER, cyclophilin A and the PM. Localization of NSP4 to the exofacial PM by exclusive colocalization. HT29.f8 cells were RV infected for 3 and 11 hpi and labeled for A = NSP4, B = PM C = cyclophilin A and D = ER. NSP4 was colocalized with the PM (green) cyclophilin A (red) and the ER (blue) and respective colocalized pixels were colocalized again, see table 3, chart and material and methods. Pseudo-colored pictures of individual cells and magnified region of PM at far right shows NSP4 at the PM (yellow and white pixels) at both 3 and 11 hours post infection. NSP4 at the PM at the exclusion of all other proteins (green pixels) was only noted at 11 hours post infection.

3.4.6 NSP4 was released into the media from intact RV infected cells

To ascertain when NSP4 is secreted into the media of RV infected MDCK and HT29.f8 cells, we collected and analyzed the media by western blot analyses at the same time points and MOI that we conducted our growth curve analysis. At 6 hpi the media was negative for the presence of NSP4 by Western blot, but at 8 hpi NSP4 was detected in both cell lines.

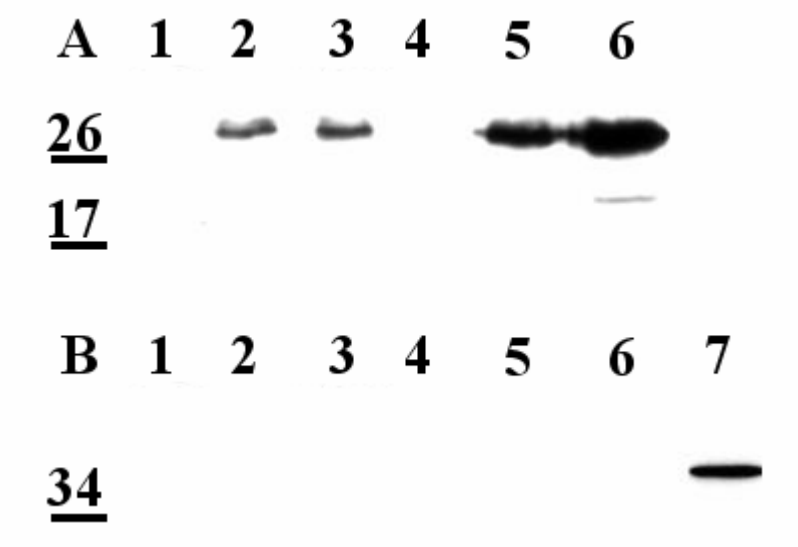

Figure 3.8 Western blot analyses of media from RV infected MDCK and HT29.f8 cells. Cells were infected with RV SA11.4F at a moi of 2 for 6, 8 and 12 hours. The media was collected and separated by SDS-PAGE and analyzed by Western blot using anti-$NSP4_{150\text{-}175}$ (A) and anti GAPDH (B) as a membrane integrity control. Lane 1 = 6 hpi media MDCK @ 10x concentration, 2 = 8 hpi media MDCK, 3 = 12 hpi media MDCK, 4 = 6 hpi media HT29.f8 @ 10x concentration, 5 = 8 hpi media HT29.f8, 6 = 12 hpi media HT29.f8, and lane 7 = HT29.f8 cell lysate GAPDH pos control.

The media analyzed at 6 hpi was concentrated approximately 10 times to increase our ability to detect small amounts of NSP4 secreted into the media, but was

still found to be negative (Fig. 3.8 A). GAPDH was analyzed in the media at all time points to assess for loss of the integrity of the PM. In agreement with our previous biochemical studies and our confocal studies regarding the integrity of the PM, GAPDH was not detected in the media even at 12 hpi (Fig. 3.8 B).

3.4.7 Exogenous addition of soluble NSP4 bound to the exofacial PM of MDCK and HT29.f8 cells

In agreement with the Bugarcic study (19), we found the soluble form of NSP4 in the media of RV infected cells. We also showed that this soluble form of NSP4 can be isolated from RV infected MA104 cells and that this portion of NSP4 from RV infected MA104's will bind to the PM of non-infected cells (data not shown). To determine a possible interaction of NSP4 with MDCK and HT29.f8 cells, soluble NSP4 interacted with these cells lines as well. Soluble NSP4 (see materials and methods) was first concentrated and then diluted again in DMEM and added in equal amounts to MDCK and HT29.f8 cells for 90 minutes under normal cell culture conditions. The cells were then washed with fresh DMEM, surface biotinylated and the precipitated surface proteins along with the cell lysates were analyzed by Western blot (see material and methods). Western blot data for both the MDCK and HT29.f8 cells exhibited a 28 and 56 kd band present at the exofacial surface of the PM corresponding to the molecular weight of the double glycosylated NSP4 and a dimmer thereof (Fig. 3.9 lane 2 and 7). The control cell lysates, which were not surface biotinylated, of both cell lines exposed to soluble NSP4 also revealed a similar 28 kd band (Fig 3.9 lane 3 and 8). Regarding the lysates of both cell lines which had there exofacial PM proteins removed, only the

lysates from HT29.f8 cells, exhibited the presence of NSP4, compare lane 1 of Fig 3.9 to lane 6. Similar results were found in 3 repeats of this experiment.

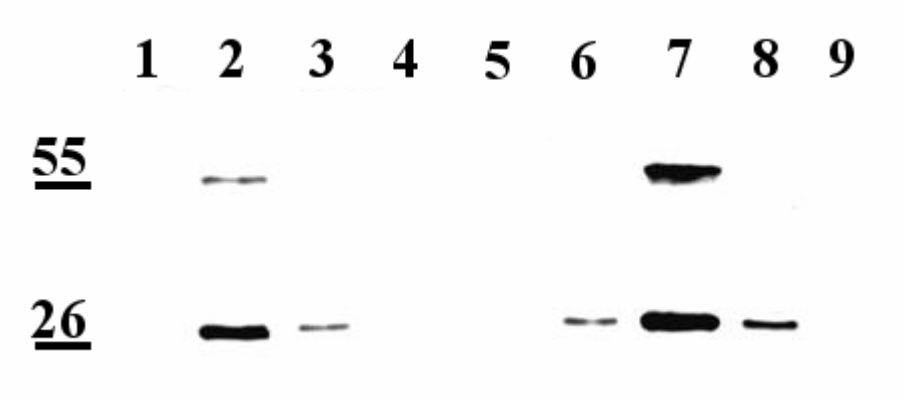

Figure 3.9 Western blot of surface biotinylated proteins from MDCK and HT29.f8 cells. Cells were incubated for 1.5 hours with equal amounts of NSP4 clarified of virus by centrifugation at 192,000g for 3 hours. The precipitated surfaces proteins were separated by SDS-PAGE and analyzed by Western blot using anti-$NSP4_{150\text{-}175}$.
Lanes as follows:
1 = MDCK cell lysate with exofacial proteins removed by streptavidin pull down
2 = MDCK exofacial PM
3 = MDCK cell lysate from no biotin control
4 = MDCK exofacial PM (no biotin control)
5 = no RV MDCK cell lysate
6 = HT29.f8 cell lysate with exofacial proteins removed by streptavidin pull down
7 = HT29.f8 exofacial PM
8 = HT29.f8 cell lysate from no biotin control
9 = HT29.f8 exofacial PM (no biotin control)

3.4.8 Confocal analysis revealed NSP4 at the PM of non-infected HT29.f8 cells and at the surface of MDCK cells

The biochemical results showing NSP4's interaction with the PM of non RV infected cells led us to re examine confocal data. In HT29.f8 cells, occasionally as early as 3 hpi (data not shown), and often at 7 hpi, NSP4 at the PM of cells that lacked any

intracellular pools of NSP4 was noted (Figure 3.10 yellow arrows in color panel). This pattern of staining was not evident in non RV infected cells treated with the same concentrations of antibodies.

We previously showed the association of full-length, endo H-sensitive NSP4 with caveolin-1 (95) and the presence of NSP4 in caveolae membranes isolated from the PM (132). To determine the extent to which the enterotoxin is exposed on the exofacial surface of infected cells, live cell confocal imaging was employed. Live MDCK cells were reacted with NSP4-specific antibody at 24 hpi (Fig. 3.10). To ensure the PM was intact at this late stage of infection, a giantin-specific (Golgi marker) counterstain was used. Any cell(s) that displayed a giantin-specific signal was discarded as the NSP4 staining may have included intracellular as well as surface-specific signals in these cells. In fixed and permeabilized MDCK control cells, giantin displayed a punctate and reticular signal pattern, whereas NSP4 predominantly was visualized in perinuclear and peripheral sites. In the live cells, giantin was not visible indicating the PM was intact and patches of NSP4-specific signal was seen at the cell surface. Given that antibodies specific to NSP4 aa 150 to 175 was used to stain the enterotoxin in these images, the results suggested that at least the carboxyl terminus of the enterotoxin was exposed on the cells' surface.

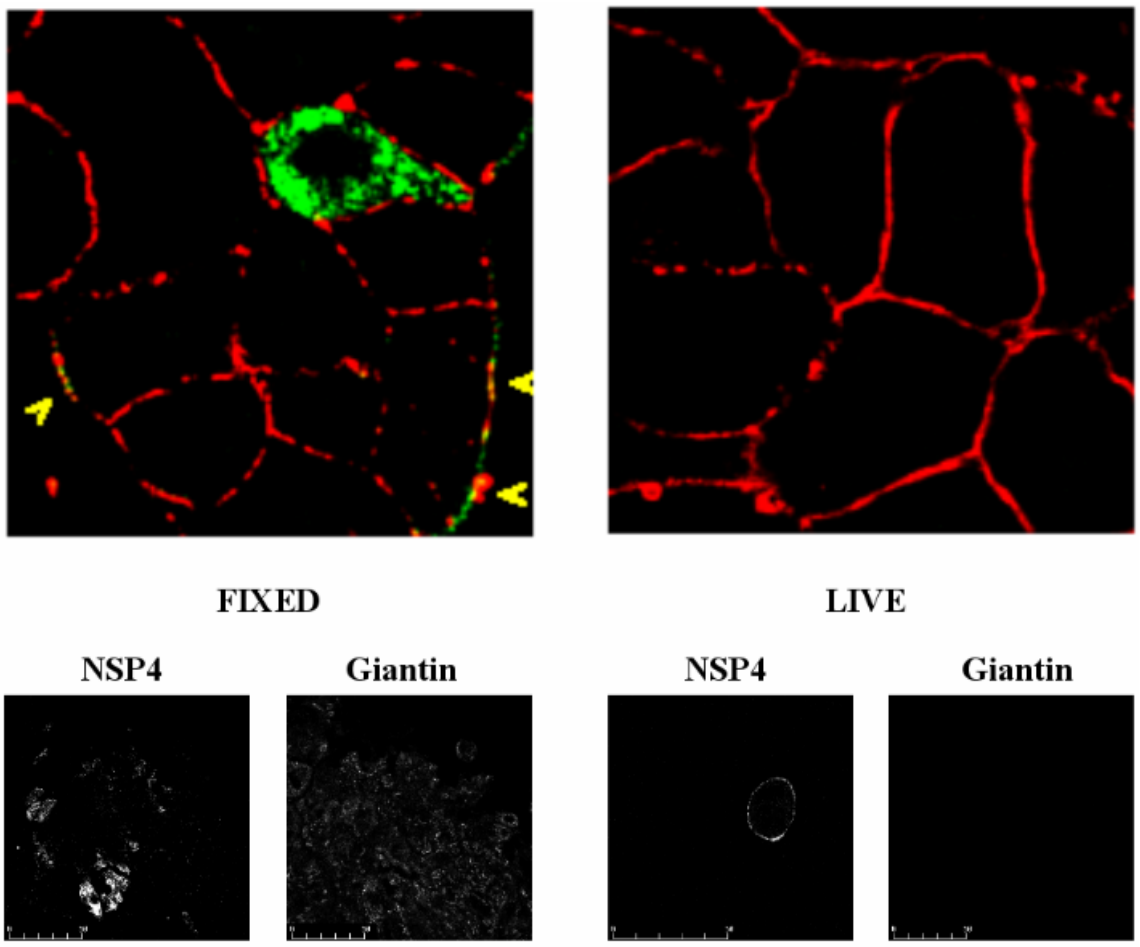

Figure 3.10 Confocal analysis of fixed HT29.f8 at 7 hpi and live cell staining of MDCK at 24 hpi. Left colored panel: Live HT29.f8's were surface biotinylated prior to fixing and permeabilization. Streptavidin-Cy2 was utilized to label surface biotinylated proteins of the exofacial PM (red). NSP4 was labeled with Cy5-linked $F(ab)_2$ prepared from anti-$NSP4_{150\text{-}175}$. (green). Arrows point to areas of the PM where NSP4 appears to be located in the absence NSP4 within the cell. Right colored panel is mock infected control labeled the same as the left colored panel. Black and white panels: MDCK cells at 24 hpi were fixed and permeabilized prior to the addition of primary antibodies (FIXED) or live, unfixed cells (LIVE) were reacted with the same antibodies at 4°C prior to fixation to visualize surface staining. Antibodies to the Golgi marker protein, giantin, were similarly treated.

3.5 Discussion

The results of this study showed full-length, endo H-sensitive NSP4 is secreted from rotavirus-infected epithelial cells shortly after its exposure on the cellular exofacial surface. Several recent reports indicate that the NSP4 enterotoxin is secreted from infected cells, yet each study describes a unique form of the enterotoxin being released. Bugarcic et al. identifies an endo H-resistant form of NSP4 with an approximate molecular weight of 32kD that is released into the media of intestinal-derived Caco-2 cultures infected with the bovine UK rotavirus (MOI of 10) (19). While this form of the enterotoxin is not apparent in the infected lysates produced from the cultures, it is the predominant form of NSP4 secreted between 16 and 42 hours post inoculation. Zhang et al. however show only a fragment (aa 112-175) of NSP4 released from kidney-derived MA104 and intestine-derived HT-29 cultures early during infection with the simian SA11 rotavirus (MOI of 20) (146). Both indicate that NSP4 transport to or release from the PM of infected cells may be dependent on processing of the 28kD, endo H-sensitive (mature) form of NSP4. Yet our recent report of NSP4 trafficking to the PM in kidney-derived MDCK cultures reveal that the mature form of the enterotoxin is present in PM caveolae at 24 hours post SA11 inoculation (MOI of 2) and was even able to transport to the PM in the absence of other viral proteins (132). While our previous study addresses the enterotoxic protein's presence, form, and distribution with the PM of infected cells, it did not define the protein's orientation within the PM bilayer or its secretion.

Here we found that with the same infection conditions, full-length endo H-sensitive NSP4 was exposed on the surface of both intact kidney-derived MDCK and intestine-derived HT-29.f8 cells. This data revealed that NSP4 does not require loss or processing of its amino-

terminus to traffic to or transpose through the PM bilayer. It also suggested that the lack of detectable 32kD, endo H-resistant NSP4 observed by Bugarcic et al. may have been due to a 28 to 32kD alteration occurring directly at the PM (19). In order for the exposed 28kD NSP4 to be a potential precursor reservoir for production of the 32kD NSP4, the exposure must precede the 32kD enterotoxin's release. While we were able to show that NSP4 exposure on the cell surface occurs before secretion of the enterotoxin, we were unable to detect secretion of the 32kD NSP4 from either SA11-infected MDCK or HT-29.f8 cultures. Instead, the secreted NSP4 was predominately the same 28kD 'mature' form observed exposed on the cell surface. While very low intensity NSP4 bands were seen intermittently at molecular weights slightly higher than 28kD when our NSP4 Western blots were overexposed (data not shown), only the endo H-sensitive 28kD form was intense and reproducible in media from both SA11-infected MDCK and HT-29.f8 cultures. These data suggested that neither translocation nor release of NSP4 was dependent on further processing of the endo H-sensitive 28kD enterotoxin. While NSP4 did not require processing for secretion, it was possible that the enterotoxin was modified after release by interaction with neighboring, uninfected cells. In testing this hypothesis, we confirmed that soluble, endo H-sensitive, 28kD NSP4 was able to associate with the exofacial surface of uninfected cells when added exogenously and appeared to actually be internalized by HT-29.f8 cells. However, as the enterotoxin retained its endo H-sensitivity and 28kD molecular weight, no processing or cleavage of exogenous NSP4 was indicated. As the previous NSP4 secretion studies used different initial infection conditions (19, 146), it is possible that NSP4 exposure and secretion of the 32kD and aa 112-175 forms of NSP4 could be produced in MDCK and HT-29.f8 cells in addition to the 28kD enterotoxin.

Another possibility with regards to the lack of our study or the Zhang study noting the 32kD form could be due to the anti-NSP4 used by Bugarcic. Bugarcic utilized a polyclonal rat antibody made to the C terminal 90 amino acids (86-175) versus the rabbit polyclonal to the 150-175 region. Nonetheless, the exposure and secretion the endo H-sensitive, 28kD NSP4 shown here is of specific importance in the context of NSP4's potential role(s) in inducing intracellular calcium mobilization and chloride secretion during RV infection. It has been shown previously that exogenous addition of the 28kD enterotoxin induces PLC-mediated mobilization of intracellular calcium stores resulting in chloride secretion and liquid accumulation (9, 30, 86). Endogenous expression, as confirmed by the presence of the 28kD form of NSP4, induces a similar calcium mobilization and chloride secretion response in the presence of PLC inhibitors (138). The data presented here shows for the first time that the 28kD form of NSP4 is present at both intracellular and exofacial sites in infected cells could induce PLC-independent and -dependent signaling in infected and uninfected cells. Induction of these signaling events in uninfected cells would be via exposure on the surface of neighboring infected cells or PM association/internalization of secreted NSP4.

In conclusion, the experiments reported here show that in infected epithelial cells, NSP4 trafficking to the PM, translocation across the PM bilayer, and secretion do not require additional processing of the endo H-sensitive 28kD enterotoxic protein. Further examination of the mechanism used by NSP4 for translocation across the cell PM, its orientation of the enterotoxin within the PM bilayer (transmembrane versus peripheral, single protein versus chaperone or lipid annulus complex), and the enterotoxic signaling functions of

exposed/secreted NSP4 would provide invaluable insights into the function of the enterotoxin during RV infection and potentially provide an alternate target for vaccine and antiviral therapies.

4. ROTAVIRUS NSP4: RELATION TO SELECTED CELLULAR PROTEINS OF THE SECRETORY PATHWAY AND THE CAVEOLIN-1 CHAPERONE COMPLEX IN AN INTESTINAL CELL LINE

4.1 Introduction

To date, we have shown that NSP4 localizes to PM caveolae at 24 hpi. We have also shown that NSP4 is exposed at the exofacial PM surface by 3 hpi in HT29.f8 cells and 7 hpi in MDCK cells. During these same studies on HT29.f8 and MDCK cells, NSP4 was shown to enter the media of both cell lines by 8 hpi and NSP4 containing media added to uninfected cells bound the PM of the cells. Although it is evident that NSP4 is located at various locations in the cell, including the ER, viroplasm, plasma membrane (PM) and outside the cell in the media, the mechanism regarding how NSP4 traffics to these varied areas within and out of the cell has not been elucidated.

There are many strong associative findings between NSP4 and caveolin-1, including the specific binding of NSP4 to caveolin-1 (95), the localization of NSP4 to PM caveolae (132), the phospholipase C dependent signaling triggered by the exogenous addition of NSP4 (30) and the fact that caveolae are rich in multiple signal transduction molecules including PIP2 (107, 124). NSP4 and caveolin-1 both appear to be unusual in that they can exists as an integral membrane protein and also as a soluble protein in multiple cellular compartments at the same time within the RV infected cell. One of the reasons that an integral membrane protein, such as caveolin-1, is also soluble within the cell is that there appears to be other pools of caveolin-1 which traffic independently from

the secretory pathway that transits through the Golgi complex. The cytosolic pool of caveolin-1 is associated with cyclophilin A, cyclophilin 40 and heat shock protein 56, traffics newly synthesized cholesterol to the PM and is referred to as the caveolin-1 chaperone complex (CCC) (140). To examine how NSP4 associates with both pools of caveolin-1 in the RV-infected cells we first examined at NSP4 and its relation to caveolin-1 and selected proteins of the secretory pathway. We utilized confocal microscopy and image analysis software to construct three dimensional visualizations of RV infected and non-infected cells to image NSP4, the PM, cis, medial, and trans Golgi, the viroplasm, and ER. The goal of these experiments was to examine NSP4's relationship to the secretory proteins. Confocal microscopy also was utilized to build a three dimensional picture of NSP4 and its relationship with the proteins of the CCC. The relationship between NSP4 and the proteins of the CCC were further explored by conducting FRET analysis to determine how closely NSP4 interacts with these proteins. NSP4 and its relationship with the CCC proteins also was explored in the absence of other rotaviral proteins by transfecting cells with full length NSP4 and visualizing the CCC proteins. Western blot and quantitative real time PCR assays were employed to determine the extent to which RV infecting cells impact the amount of CCC proteins and co-immunoprecipitation studies were done on the soluble portion of RV infected cell lysates to evalutate the interaction of NSP4 with the CCC proteins.

4.2 Materials and Methods

4.2.1 Antibodies and reagents

Antibodies directed against rabbit caveolin-1 (anti-caveolin-1, Cell Signaling, Danvers, MA), mouse caveolin-1 and clathrin heavy chain (anti-caveolin-1 and anti-clathrin heavy chain, BD Transduction Laboratories, San Jose California) β-Cop, cyclophilin A, cyclophilin 40 or heat shock protein 56 (rabbit anti-βcop, anti-cyclophilin A, anti-cyclophilin 40 and anti-heat shock protein 56, Affinity Bioreaents, Golden, CO) giantin (rabbit anti-human giantin aa 1 to 469; Covance Research Products, Inc., Princeton, NJ), protein disulfide isomerase (mouse anti-PDI, Medical & Biological Laboratories Co. LTD., Woburn, MA), and horseradish peroxidase linked anti rabbit (HRP; goat anti-rabbit immunoglobulin G; Pierce Biotechnology, Rockford, IL), horseradish peroxidase linked anti mouse (HRP; goat anti-mouse immunoglobulin G; Zymed Laboratories, San Francisco, CA) were purchased commercially from the indicated sources. Linked antibodies and fluorescent molecules included, the $F(ab')_2$ fragment of goat anti-guinea pig antibody-Cy3, goat anti-mouse antibody-Cy5 conjugated and the $F(ab')_2$ fragment of goat anti-rabbit antibody-Cy2, $F(ab')_2$ fragment of goat anti-rabbit antibody-Cy3 and Cy3 conjugated Streptavidin (Jackson ImmunoResearch, West Grove, PA) which also were purchased from indicated sources. Antibodies specific to the NSP4 peptide aa 150 to 175 ($NSP4_{150-175}$; deduced from the simian rotavirus SA11 NSP4 sequence) were generated in rabbits by using $NSP4_{150-175}$ cross-linked to keyhole limpet hemocyanin as an antigen. Guinea pig anti-NSP5 was a

gift from Dr Oscar Burrone's laboratory at the International Center for Genetic Engineering and Biotechnology, Padrician 99, 34012 Trieste Italy.

4.2.2 Generation of anti-NSP4$_{150–175}$ F(ab)$_2$ segments

NSP4$_{150–175}$-specific antibodies were affinity purified before use in confocal microscopy, and F(ab)$_2$ fragments were generated for fluorescent resonance energy transfer (FRET) analyses to reduce the distances of the fluorophores from the target proteins. Rabbit anti-NSP4$_{150–175}$ was affinity purified on an NSP4$_{150–175}$ peptide column prepared with preactivated cyanogen bromide Sepharose 4B beads by following the instructions of the manufacturer (Pharmacia Biotech, Piscataway, NJ) (7). The bound peptide IgG was eluted by altering the pH (134). The ImmunoPure F(ab)2 preparation kit (Pierce, Rockford, IL) was utilized, and the recommended protocol was followed to produce F(ab)$_2$ (142). Cy5 and Cy3 monofunctional reactive dye was conjugated to the affinity-purified NSP4$_{150–175}$ F(ab)$_2$ to produce aliquots of Cy3 and Cy5 conjugated NSP4$_{150–175}$ F(ab)$_2$ for FRET and exclusive colocalization analyses exactly as described by the manufacturer (Amersham Bioscience, Piscataway, NJ).

4.2.3 Cultured cells and virus

MA104 cells were purchased from the American Type Culture Collection (Manassas, VA). The MA104 cells were maintained in maintenance media (Minimum Essential Medium [MEM] Mediatech, Inc. Herndon, VA) and supplemented with 2 mM L-glutamine (200 mM; BioWhittaker/Cambrex), 1 mM sodium pyruvate (Cambrex), 0.1 mM non-essential amino acids (Mediatech, Inc.), 100 U/L penicillin, 100 μg/L

streptomycin, 0.25 μg/L amphotericin (10,000 U penicillin-10,000 U of streptomycin-25 μg/liter amphotericin B; Cambrex), 26.1 mM sodium bicarbonate (GIBCO), 10mM HEPES (Amresco, Solon,OH) 5% fetal bovine serum, and 5% Serum Supreme (Cambrex) at 37^{o}C in 5% CO_2. HT29.f8 cells, a spontaneously polarizing cell line derived from the human adenocarcinoma HT29 intestinal line (83), were grown in maintenance media (Dulbecco's Modification of Eagle's media [DMEM] with 4.5 g/L glucose, L-glutamine, and sodium pyruvate; Mediatech, Inc., Herndon, VA) supplemented with 2 mM L-glutamine, 1 mM sodium pyruvate, 0.1 mM non-essential amino acids, 100 U/L penicillin, 100 μg/L streptomycin, 0.25 μg/L amphotericin, 43.9 mM sodium bicarbonate, 5% fetal bovine serum, and 5% Serum Supreme at 37^{o}C in 5% CO_2. Cells were infected with SA11 clone 4F (gift of Mary Estes, Baylor College of Medicine, Houston, TX) at a multiplicity of infection (MOI) of 2 PFU/cell. Briefly, the virus was sonicated (5 minutes using a cuphorn attachment ice bath in a Misonix Sonicator 3000; Misonix, Inc, Farmingdale, NY) and incubated in serum-free DMEM with 10 μg/ml trypsin for 30 minutes at 37^{o}C, then incubated with the cells for 60 min at 37^{o}C in 5% CO_2. The inoculum was replaced with serum-free DMEM and the cells incubated for 7 hours unless otherwise stated.

4.2.4 Western blot analyses

Equal amounts of total protein as assessed by BCA or Coomassie staining of gels were resolved on 12% polyacrylamide minigels and transferred to nitrocellulose filters (0.45 μ pure nitrocellulose; GE Osmonics) according to the manufacturer (Mini-PROTEAN II and Trans-Blot respectively; BioRad). The filters were blocked in 10%

(wt/vol) non-fat dry milk in PBS (10% BLOTTO) for 1 hour at RT and reacted with the primary antibody in 2.5% BLOTTO for 14 hours at 4^{o}C with rocking. The filters were incubated an additional 1 hour at RT with primary antibody, then washed once in PBS, twice in PBS with 0.05% Tween-20, and once in PBS with rocking (10 min per wash). Secondary antibodies were diluted in 2.5% BLOTTO and incubated with the filters for 1 hour at RT with rocking. The filters were washed as above, and reacted with Immobilon Western chemiluminescent substrates as per the manufacturer's protocols (Millipore, Billerica MA). The marker-specific bands were visualized by exposure to and development of x-ray film.

4.2.5 Protein quantification

Micro bicinchoninic acid (BCA) protein assay (Pierce) was utilized to quantify the protein concentrations with bovine serum albumin standards per manufacturer's protocol.

4.2.6 NSP4 transfection

MA104 cells were transiently transfected with pcDNA6.2 NSP4$_{1\text{-}175}$ plasmid DNA by electroporation. Briefly, 1x10^{6} MA104 cells were placed into a 4 mm gap cuvette with Delbecco's PBS and 5µg/ml plasmid DNA. Cells were electroporated with a ECM 830 Electro Square Porator (BTX, San Diego, CA) set at100V for 70 ms, after which they remained for 5 minutes at room temperature before plating on coverslips with maintenance media for 20 hours. A control vector pcDNA™6.2/V5/GW/CAT (Invitrogen, Carlsbad, CA.) expressing a C-terminal fusion of V5 with chloramphenicol acetyltransferase (CAT) was transfected with the same conditions as the NSP4

expressing plasmid to ensure the stress and or production of a transfected protein did not up-regulate the proteins of the caveolin-1 chaperone complex. At 20 hours after transfection, the cells were fixed and permeabilized with ice-cold methanol:acetone (1:1).

4.2.7 Confocal microscopy

Mock and SA11-infected cells were grown on glass coverslips and processed at specified times post infection for fluorescent imaging. The infected cells were rinsed in PBS, fixed and permeabilized in methanol:acetone (1:1, vol/vol) for 5 min at -20^{o}C, and non-specific binding sites were blocked with 4% BLOTTO(4% dry milk in PBS) at RT for 45 min. The infected and uninfected cells were incubated with primary antibodies diluted in 2% BLOTTO-PBS at RT for 45 min. The cells were washed four times in PBS for 10 min each and incubated with Cy2, Cy3, or Cy5-labeled secondary antibody diluted in 1% BLOTTO-PBS for 45 min in the dark. When applicable the biotinylated proteins located on the exofacial surface of the PM were labeled with streptavidin conjugated to Cy2 or Cy3. The cells were washed again as above, but in the dark and mounted with fluorescent mounting media (KPL Inc.) onto glass slides. The resulting fluorescent images were captured with a MRC-1024MP BioRad laser scanning confocal microscopy system (BioRad, Hercules, CA) using a Zeiss inverted Axiovert microscope (Carl Zeiss, Inc., Thronwood, NY), a 63 X Zeiss oil apochromat objective, and the 488-568- and 647-nm-wavelength excitation lines of an argon/krypton ion laser source. LaserSharp 3.0 (BioRad), Confocal Assistant 4.02 (Brelje TC/BioRad) and Image J were used to capture the pixilated fluorescent data, and to adjust contrast curves to construct the final images.

4.2.8 IFA analysis

Images were aquired with a Stallion Digital Imaging workstation (Carl Zeiss MicroImaging, Inc. Thornwood, NY) equipped with a 300W xenon fluorescent light source with rapid switching (<2 msec) between excitation wavelengths. Images were collected using a 63X objective, 0.75 N.A., and a ROPER CoolSnap HQ camera. The Stallion system includes excitation/emission filter sets suitable for color staining including DAPI and Hoechst (365:445/50 nm), FITC and Cy2 (470/20:505-530 nm) and TX Red and Cy3 (560/40:590 nm) and Cy5 (600/50:685/50 nm). The images were processed using Image J.

4.2.9 FRET by acceptor photobleaching

FRET is a process by which nonradiative energy transfer from one fluorophore to another occurs if the two fluorophores (or proteins) are within 10 nm of each other (60). Acceptor photobleaching is one of the simpler and more effective FRET techniques whereby the acceptor fluorophore is bleached and then an increase in the donor fluorophore is assessed to determine if two proteins interact (59). Individual proteins of the caveolin-1 chaperone complex (cyclophilin A, cyclophilin 40 or heat shock protein 56) were labeled with an epitope-specific antibody to the protein followed by $F(ab)_2$ specific IgG-Cy3, NSP4 was labeled with the $F(ab)_2NSP4_{150–175}$ directly conjugated to Cy5. A series of images were taken both before (568 and 647 nm; 10% power) and after the photobleaching of the Cy5 fluorophore. The cells were photobleached at 647 nm at 100% power for 3 min. An increase in the Cy3 signal (568 nm) was assessed following photobleaching to determine if the two fluorophores were in close proximity (less than

10 nm apart) and there was a positive FRET reaction (60). For each protein of the caveolin-1 chaperone complex, a minimum of 3 fields were analyzed and percent FRET was calculated by selecting the Cy3 (selected protein from the caveolin-1 chaperone complex) from 2 areas outside (to serve as an internal control) and 2 areas within the region undergoing photobleaching of Cy5 (NSP4). The percent FRET was calculated by taking the IDV for the Cy3 signal after Cy5 photobleaching (Cy3 post) and subtracting the Cy3 signal attained before Cy5 photobleaching (Cy3 pre) and dividing by the Cy3 post signal for each selected area. Image analysis was accomplished using Image J software, a public domain Java image-processing program inspired by NIH Image. Image J has a large and increasing number of plug-ins, which are functional programming updates to Image J designed to perform a specific task.

4.2.10 Surface biotinylation for isolation of cell surface proteins or visualization by confocal analysis

Mock and infected HT29.f8 cells were grown to %80 confluency on 8 well coverslips (NALGE Nunc International, Rochester, NY.) and reacted with 0.5mg/ml of membrane impermeable Sulfo-NHS-SS-Biotin (PIERCE #21331,) for 20 min at 4°C. Excess biotin was quenched with cold cell culture media (DMEM with serum). Following washes, cells grown on the 8 well coverslips were fixed and permeabilized for Cy3 and Cy5 labeling and FRET analysis by confocal microscopy. Mock biotinylated samples were used to control for non specific Streptavidin-Cy2 or (Cy3) signal in LSCM analysis.

4.2.11 Real time quantitative PCR

Total RNA from RV infected and uninfected HT29.f8 cells were collected and cDNA was produced utilizing the Cells-to-cDNA II kit (Ambion, Austin, TX) according to the manufacturer's instruction. Messenger RNA levels for the proteins of the caveolin-1 chaperone complex in RV infected cells were assessed for relative amounts as compared to uninfected cells on the RAPID thermocycler (Idaho Technology Inc., Salt Lake City, UT.) The PCR master Mix RT^2 Real-Time SYBR Green and primers for GAPDH, Cyclophilin 40, Cyclophilin A and HSP 56 (Super Array, Frederick MD. Primers (Cat#s = PPH00150A, PPH02848A, PPH01319A and PPH02889A) were utilized according to the manufacturers' protocols with the addition of a melting curve analysis to assess for the presence of a single product with similar melting temperatures for a given primer set. Cycle thresholds (Ct's) of the target sequence (selected mRNA from the caveolin-1 chaperone complex) and a housekeeping gene (GAPDH) were calculated. The relative amounts of the messenger RNA was calculated by comparing the Ct's of the infected and uninfected samples for the housekeeping gene and target sequence to standard curves from cDNA corresponding to the mRNA for each of the genes. The relative expression level of the mRNA from the caveolin-1 chaperone complex was divided by the relative expression level of the GAPDH mRNA from a RV infected sample and the same was done for a non RV infected sample. By comparing the the relative expression levels of mRNA from the RV infected and non-infected cells we determined if RV infection had an impact on the CCC mRNA levels.

4.2.12 Coimmunoprecipitation

Aliquots of protein fractions from RV infected cells were subjected to co-immunoprecipitation reactions with antibodies to selected proteins of the caveolin-1 chaperone complex. The, anti-cyclophilin A and anti-cyclophilin 40 was bound by protein A (Pierce, Rockfor IL.) attached to sepharose beads and pelleted by gentle centrifugation. The protein A beads were be washed then boiled with SDS-loading buffer, and the released proteins were separated by SDS-PAGE and detected by Western blot. The species of primary antibody used in Western blot analyses was different than that of the species of the antibody used in the initial precipitation to avoid non specific signals created by the secondary antibody.

4.3 Results

4.3.1 Golgi was redistributed in RV-infected HT29.f8 cells

Most studies agree that NSP4 bypasses the Golgi (2, 10-12, 15, 26), although there has been a recent study indicating that at least a portion of NSP4 may traffic by way of the Golgi (19). To investigate the impact on the Golgi apparatus, a Golgi localized marker, giantin, (71) was utilized to visualize RV infected and non-infected

HT29.f8 cells. 360 degree reconstructed representations of the cell were prepared from z-series images taken at 1 micron intervals to enable detailed analysis of the Golgi throughout the cell. Cells were infected for seven hours prior to fixation and permeabilization, and all cells were biotinylated to enable exofacial PM visualization of cells with fluorescent streptavidin. RV-infected cells were identified by the presence of NSP4. Confocal imaging revealed a distinctly different morphology of the Golgi in RV-infected versus non-infected cells. In RV-infected cells the giantin appeared in discrete globular segments dispersed in a hazy staining pattern throughout the cell. The giantin in cells not exhibiting NSP4 staining appeared in a normal Golgi ribbon pattern (Fig. 4.1 and supplementary material for video).

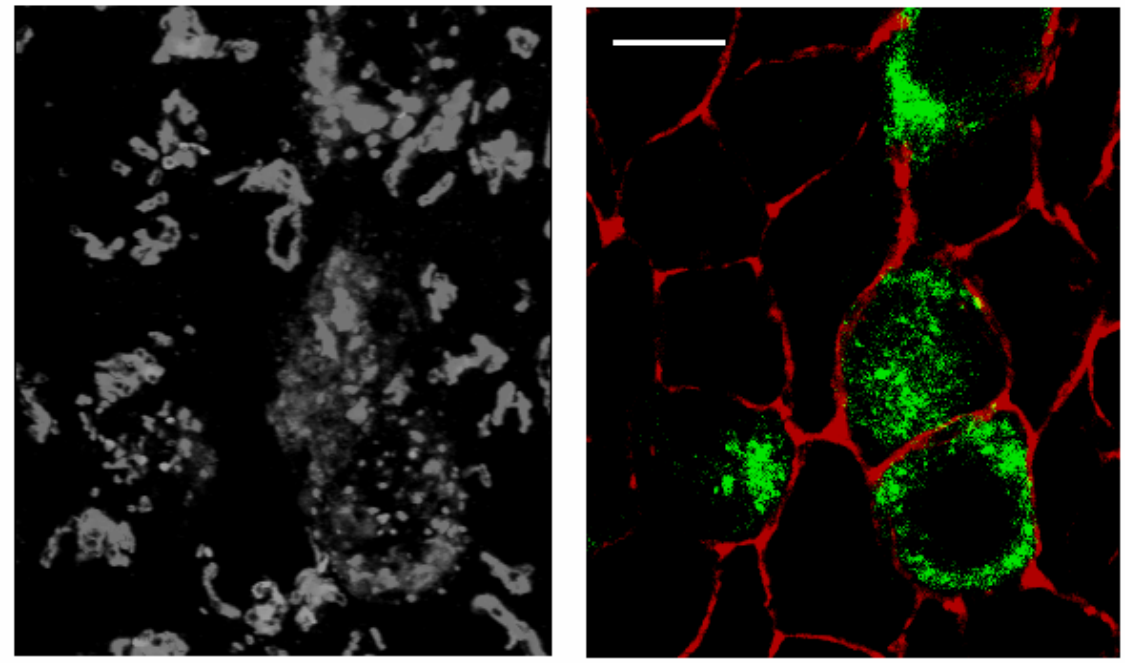

Figure 4.1. Golgi is redistributed in RV-infected HT29.f8 cells at 7 hpi. Live HT29.f8 cells were surface biotinylated prior to fixation and permeabilization. Streptavdin-Cy3 was utilized to label surface biotinylated proteins and served as a PM marker (red). NSP4 (green) was labeled with Mouse anti $NSP4_{150\text{-}175}$ and Goat α mouse-Cy5 and allowed for the identification of RV infected cells. The Golgi (black & white, left panel) was labeled with rabbit anti-giantin followed by the $F(ab)_2$ of Goat α rabbit-Cy2. To optimize the visualization of the Golgi distribution a set of 8 z-series images were taken at 1 µm intervals and the 360° 3D project plug-in from Image J was utilized (see supplementary material for video). Note the globular segments in a hazy background in cells with NSP4 versus the normal Golgi ribbon pattern in cells without NSP4. Bar = 10 microns.

4.3.2 Visualization of clathrin and Beta Cop in RV-infected and uninfected HT29.f8 cells

Clathrin coated vesicles internalize from the PM to endosomes as well as in budding from the trans-Golgi network to endosomes, therefore clathrin was explored in order to view any possible impact in the trans Golgi and distal to the PM (61). Beta Cop

is a protein that constitutes part of the COPI coat complex. COPI coated vesicles function primarily in retrograde transport from the ER-Golgi intermediate compartment to the ER as well as in forward transport within the cisternae of the Golgi (61, 106). Beta Cop was investigated to visualize the cis-Golgi and points proximal to the cis-Golgi back to the ER along the secretory pathway. At 7 hours post infection, 360° renditions of the cells showed no impact on clathrin in RV-infected cells versus non RV-infected cells (top versus bottom row of Fig 4.2A. and supplementary material). Beta Cop on the other hand was barely visible in uninfected cells while appearing quite prominently in RV infected cells (top versus bottom row of Fig 4.2B. and supplementary material). Because of the apparent redistribution of Beta Cop within the RV-infected cells, further confocal analysis was conducted to determine where the Beta Cop appeared to redistribute in relation to the ER and NSP4. The experiment was repeated and at 7 hpi, the cells were labled for an ER marker,by utilizing protein disulphide isomerase which is concentrated in the ER (65), Beta Cop and NSP4. 360° renditions of each of the proteins were constructed for RV-infected cells. Merging of these three proteins, revealed a substantial amount of Beta Cop and NSP4 colocalized, with most of the colocalization occuring with PDI as well. The appearance of most of the Beta Cop and NSP4 within the ER was confirmed by analysis of merged NSP4/Beta Cop and merged Beta Cop/PDI images. (Fig 4.3. and supplementary material).

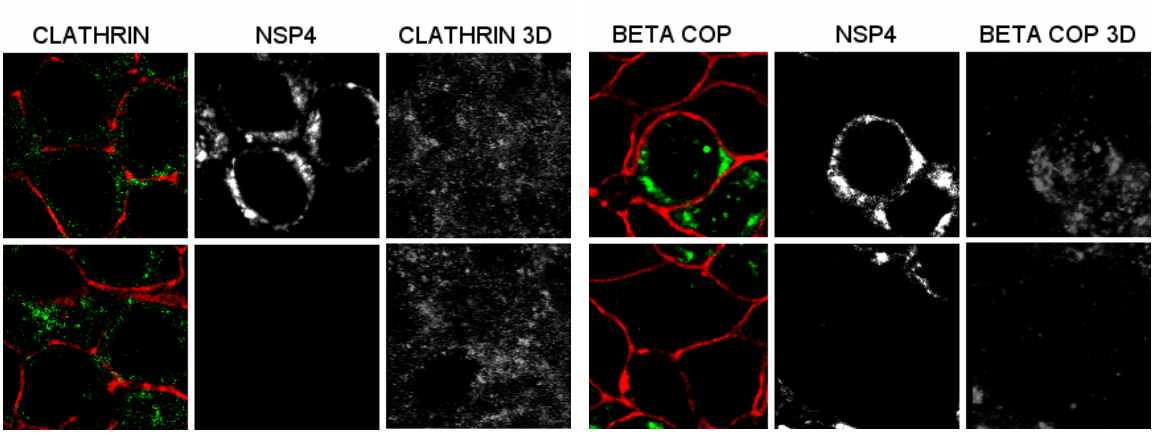

Figure 4.2. A retrograde transport marker from the Golgi (Beta Cop) but not a trans Golgi marker (clathrin) was redistributed in RV-infected cells. HT29.f8 cells were surface biotinylated prior to fixation and permeabilization. The PM (red) and NSP4 (black & white middle panel) were labeled as in 3.1 which enabeled the identification of RV infected cells. Rabbit $\alpha NSP4_{150\text{-}175}$ followed by $F(ab)_2$ goat α rabbit-Cy2 was utilized for the clathrin labeled cells. Clathrin (black & white of right panel in A) was labeled with mouse anti-clathrin followed by the $F(ab)_2$ of Goat α mouse-Cy5. Beta Cop (black & white of right panel B) was labeled with rabbit anti-Beta Cop followed by the $F(ab)_2$ of Goat α rabbit-Cy2. 360° renditions of Clathrin and Beta Cop were prepared as in 4.1 (see supplementary material for video).

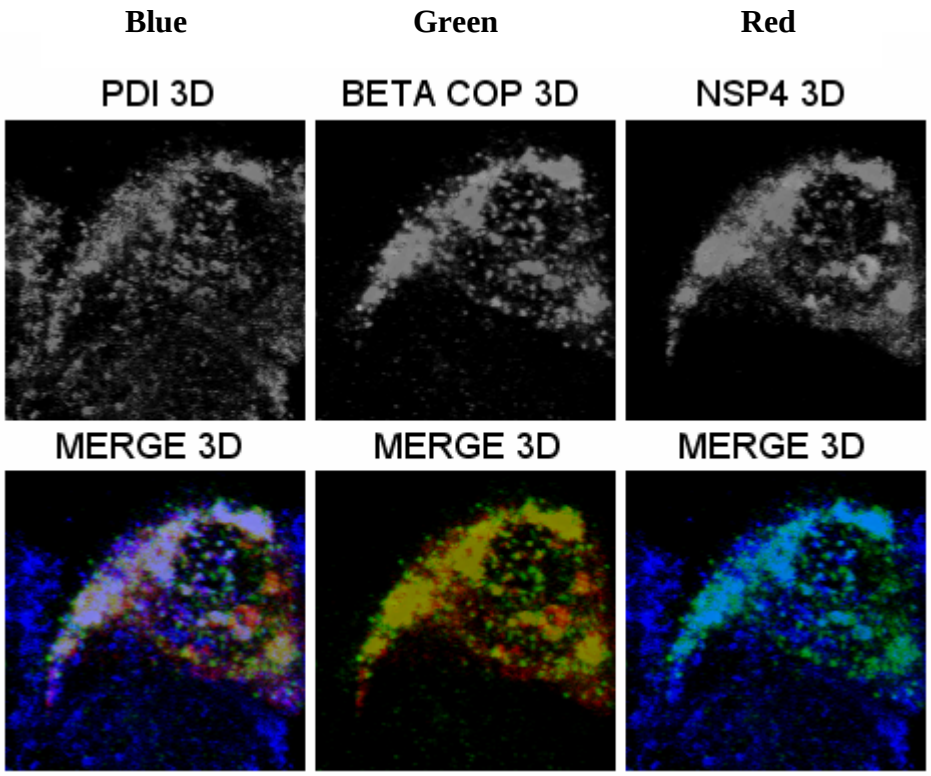

Figure 4.3. Beta Cop was redistributed to the ER in RV-infected HT29.f8 cells at 7 hpi. Cells were labeled with mouse α PDI (blue in merged images) followed by $F(ab)_2$ of Goat α mouse-Cy5, Beta Cop (green in merged images) was labeled with rabbit anti-Beta Cop followed by the $F(ab)_2$ of Goat α rabbit-Cy2 and NSP4 (red in merged images) was labeled with the Cy3 conjugated Fab of $\alpha NSP4_{150\text{-}175}$. Merged images: bottom left = PDI/Beta Cop/NSP4, bottom middle = Beta Cop/NSP4, bottom right = Beta Cop/PDI. 360° renditions as in 4.1 (see supplementary material for video).

4.3.3 Caveolin-1 was redistributed in RV infected HT29.f8 cells

A substantial portion of newly synthesized caveolin-1 is transported along the secretory network from the ER to the Golgi complex the PM (97, 98, 104). Because NPS4 has been shown to bind caveolin-1 as well as localize to PM caveolae (95, 132) and the Golgi appeared to be redistributed in RV infected cells, we investigated the extent to which caveolin-1 also underwent a similar redistribution pattern in infected

cells. RV-infected and non RV-infected cells were labeled for NSP4 and caveolin-1, and 360° renditions were constructed. As with giantin, confocal imaging revealed a distinct distribution of caveolin-1 in RV-infected versus non-infected cells. In RV-infected cells the caveolin-1 appeared in less discrete areas and dispersed in a hazy staining pattern throughout the cell as compared to the caveolin-1 staining in cells without NSP4 (compare the distribution of caveolin-1 in the top row (RV-infected) to the bottom row of (non RV-infected cells). Based on side by side comparisons with giantin labeled RV-infected versus non-infected cells, we concluded that the redistribution of caveolin-1 displayed similar characteristics as the redistributed Golgi. (Fig 4.4 and supplementary material)

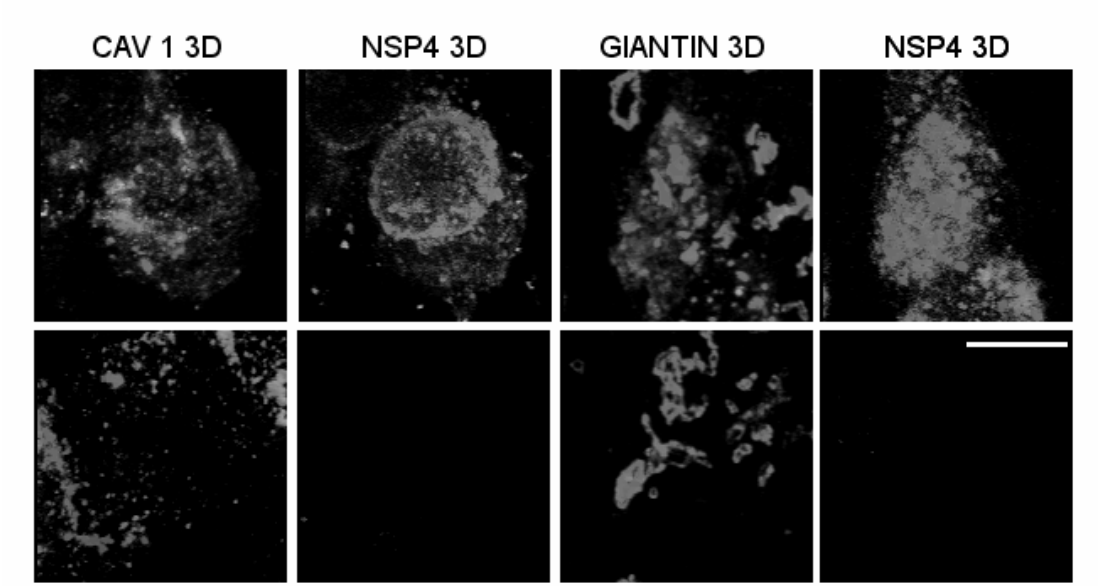

Figure 4.4. Caveolin-1 was redistributed in RV-infected cells. HT29.f8 cells were labeled with mouse α NSP4 followed by $F(ab)_2$ of Goat α mouse-Cy5 and either giantin or caveolin-1 was labeled with rabbit anti-giantin or caveolin-1 followed by the $F(ab)_2$ of Goat α rabbit-Cy2. 360° renditions were prepared as in 4.1 (see supplementary material for video). Top row = infected cells, bottom row = non-infected, giantin shown for comparison purposes.

4.3.4 The redistribution of caveolin-1 and giantin was distinctly different in relation to NSP4 and the NSP5 viroplasm marker

Because both caveolin-1 and giantin were redistributed in RV infected cells, we determined if these proteins, once redistributed, had similar locations with respect to the trafficking of NSP4. Cells were stained for NSP4, NSP5 and either caveolin-1 or giantin. Anti-NSP5 was chosen because it served as marker for viroplasms, (electron dense usually perinuclear located regions in RV-infected cells where nascent RNA and double layered particles are formed) (11, 42). Silencing NSP4 has been shown to prevent the formation of viroplasms (73, 121) and at least a portion of NSP4 has been shown to traffic to viroplasms (11). As previously reported by our laboratory, significant portions of NSP4 appeare to colocalize with caveolin-1, but very little of the NSP4 appeared to colocalize with giantin(132). With respect to NSP5, differences in NSP5 colocalization were even more pronounced, as none of the NSP5 appeared to colocalize with the giantin, whereas there was significant colocalization between NSP4 and caveolin-1 (Fig. 4.5. and supplementary material). Hence at least a portion of NSP4 in the cell was transferred to the viroplasm, which appeared to be a common destination for caveolin-1, but not for giantin. These differences were more evident after investigating the video representations of the 360° renditions of the cells. Our findings indicated that in RV-infected HT29.f8 cells, both caveolin-1 and the *cis* and *medial* Golgi were redistributed. This distribution was dependent on the presence of NSP4

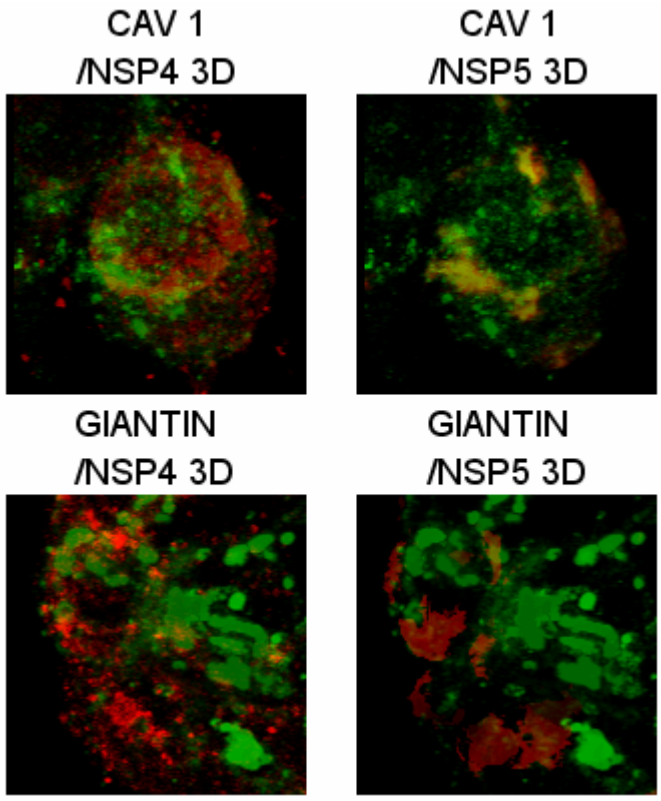

Figure 4.5. Caveolin-1 was redistributed in RV infected cells, but was distinct from that of giantin in relation to NSP4 and the viroplasm marker NSP5. HT29.f8 cells were labeled with mouse α NSP4 followed by $F(ab)_2$ of Goat α mouse-Cy5, guinea pig αNSP5 followed by $F(ab)_2$ of Goat α guinea pig-Cy3 and either giantin or caveolin-1 was labeled with rabbit anti-giantin or caveolin-1 followed by the $F(ab)_2$ of Goat α rabbit-Cy2. 360° renditions were prepared as in 4.1 (see supplementary material for video). Caveolin-1 or Giantin = green, NSP4 or NSP5 = red.

4.3.5 Cyclophilin A, cyclophilin 40 and HSP56 are redistributed in a similar fashion as caveolin-1 in RV infected cells

Given: i). The majority of caveolin-1 traffics via the secretory route through the Golgi complex from the ER to the PM (125), and ii). In RV-infected cells, the Golgi and caveolin-1 were redistributed in a different manner than the Golgi marker giantin in uninfected cells, additional studies were completed with proteins that have been shown

to occur with caveolin-1 in the cytosol. There is a pool of caveolin-1 in the cytosol that is soluble and is part of a complex composed of the proteins cyclophilin A, cyclophilin 40, heat shock protein 56 and caveolin-1. This complex transports newly synthesized cholesterol from the ER to the PM independent of the Golgi (140). The same confocal analysis that were conducted with NSP4 and caveolin-1 or NSP4 and giantin were conducted with each of the proteins of the caveolin-1 chapeonre complex (CCC). RV-infected cells were first analyzed for the redistribution of each of these proteins as compared to non-infected cells. The redistribution of each protein was also investigated in relation to NSP4 and the viroplasm marker NSP5. Akin to Beta Cop, but contrary to clathrin, cyclophilin 40, cyclophilin A and heat shock protein 56 proteins were much more visible in RV infected cells than in non (no NSP4) RV infected cells. The proteins were not only much more visible, but in each case, there was significant colocalization with NSP4 and NSP5 (Fig. 4.6 and supplementary material.), that is all of the CCC proteins colocalized with NSP4 and NSP5.

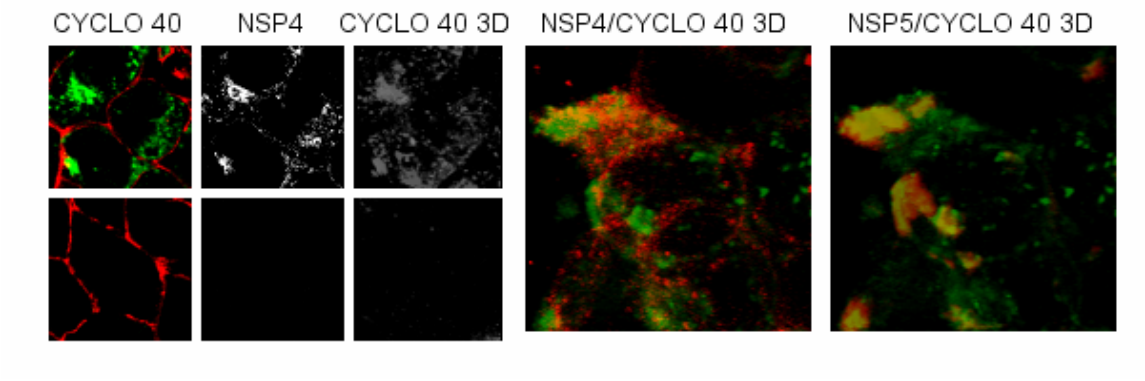

A.

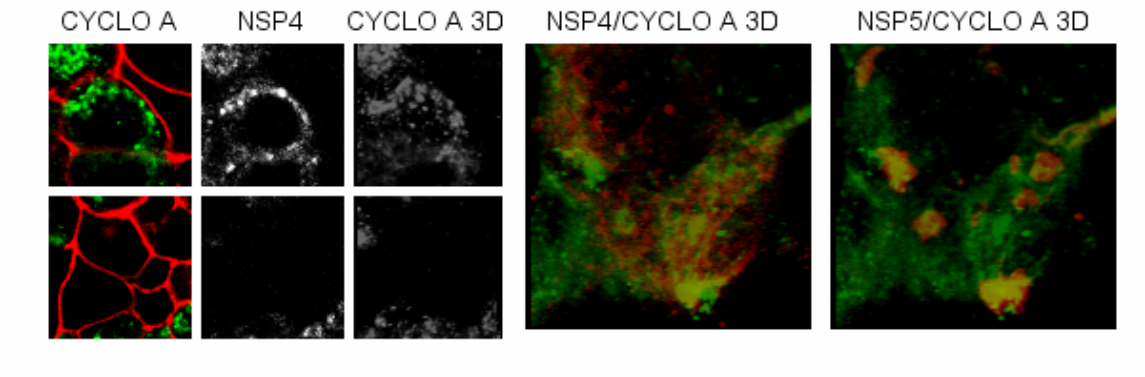

B.

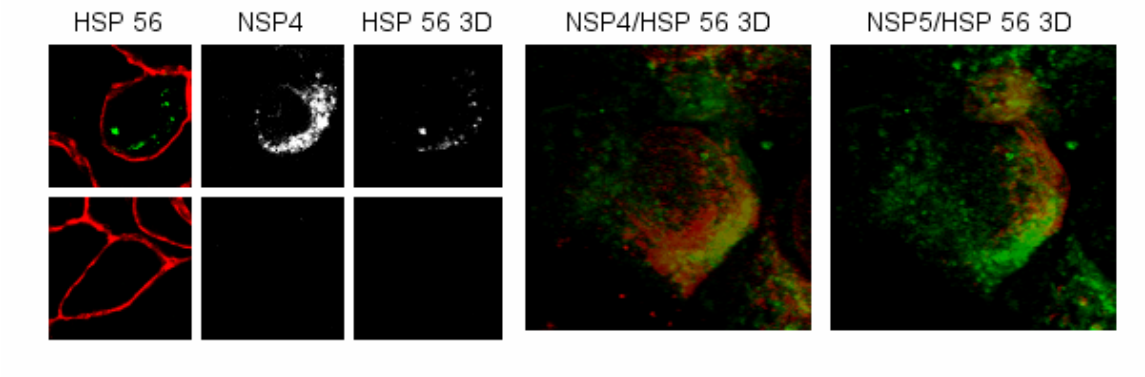

C.

Figure 4.6. The proteins of the caveolin-1 chaperone complex colocalized with NSP4 and NSP5 in RV-infected HT29.f8 cells at 7 hpi. Each of the proteins of the -1 chaperone complex are labeled for PM, NSP4 and either cyclophilin 40 (A), or cylcophilin A (B) or HSP 56 (C) as in figure 4.2. Relative redistribution of the proteins in relation to NSP4 and NSP5 are assessed.

4.3.6 Cy3 labeled cyclophilin A, cyclophilin 40 and HSP56 association resolved to within 10 nm of Cy5 labeled NSP4

The extensive colocalization of NSP4 and each of the caveolin-1 chaperone complex proteins prompted us to investigate the association of NSP4 may with this complex. To investigate a possible association between NSP4 and the CCC, FRET analyses with Cy5 labeled $F(ab)_2$ of anti $NSP4_{150\text{-}175}$ and Cy3 labeled antibodies to each of the proteins of the caveolin-1 chaperone complex (see materials and methods) were conducted in RV infected cells at 7 hpi. For each protein, there was a positive FRET reaction indicating that in each case NSP4 was associated with the complex proteins in a manner that resolved the probes within a 10-nm radius. Figure 4.7 depicts the Cy5 labeled NSP4 which is the acceptor both before (left panels) and after (middle panels) photobleaching. The top right panels show the selected caveolin-1 chaperone complex protein after photobleaching. The four outlined areas labeled A-D represent the area in which the fluorescence intensity of the selected caveolin-1 chaperone complex protein serving as the donor was measured both before and after acceptor photobleaching of NSP4. The resulting FRET calculation [(donor post – donor pre)/ donor post] is depicted just below each set of panels. These areas where chosen to include both a densely stained and sparsely stained region in which NSP4 was photobleached (areas C & D) as well as regions in which NSP4 was not photobleached (areas A & B) to serve as an internal control.

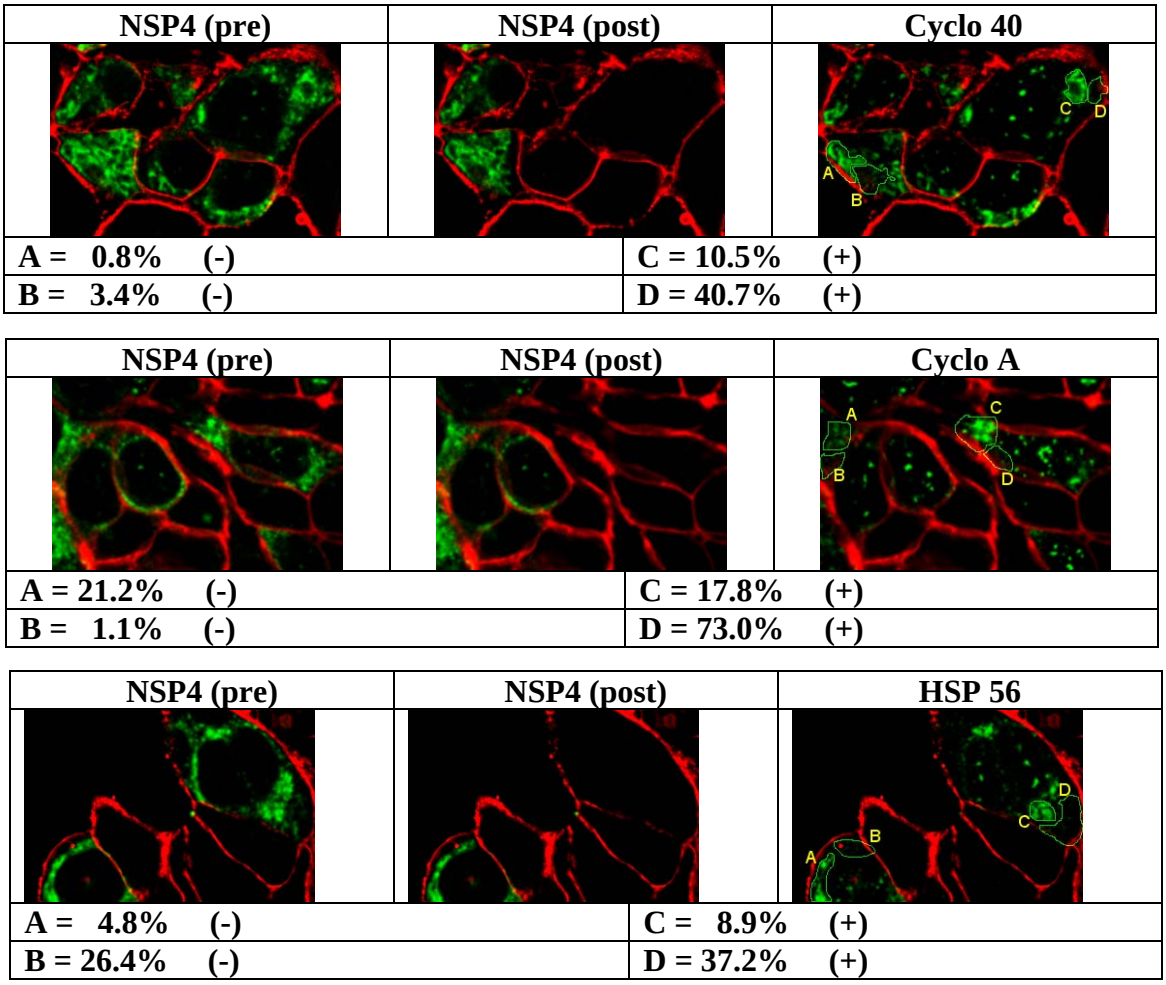

Figure 4.7. FRET analysis of NSP4 and respective CCC protein by acceptor photobleaching. Each row shows pre and postbleaching of NSP4 (left and center panel respectively), right panel shows respective CCC protein image post bleaching of NSP4. Top row shows NSP4/Cyclo 40 FRET example, middle NSP4/Cyclo A example and bottom row shows NSP4/HSP 56 FRET example. The PM was labeled as described in figure 4.1 accept that streptavidin-Cy2 was utilized instead of streptavidin-Cy3. The acceptor (NSP4) was labeled with a Cy5-linked F(ab)2 prepared from anti-$NSP4_{150-175}$. The caveolin-1 chaperone complex proteins (cyclophilin 40 or cyclophilin A or HSP 56) were labeled with the appropriate antibody followed by the F(ab)2 of goat anti-rabbit-Cy3. Cy5 (NSP4) and Cy3 (caveolin-1 chaperone complex protein) images were acquired with the 647-nm and 568-nm-wavelentgh lasers both prior to and after bleaching NSP4. The percent FRET was calculated from the fluorescence intensity of selected areas of the caveolin-1 chaperone complex protein both before and after bleaching NSP4, i.e. [(Cyclo 40 intensity in area outlined by A post NSP4 bleaching) – Cyclo 40 intensity in area A pre NSP4 bleaching) / (Cyclo 40 post NSP4 bleaching)]. FRET calculations shown in the table below each example were calculated for an intensely stained and sparsely stained area where NSP4 was and was not (to serve as an internal control) bleached (outlined A & B and C & D respectively) for each of the caveolin-1 chaperone complex proteins. Note, for illustrative purposes only the post caveolin-1 chaperone complex protein image with the areas selected for the FRET calculations are shown.

4.3.7 NSP4 coimmunoprecipitated with cyclophilin A and cyclophilin 40 from RV infected cells

We previously have reported the coimmunoprecipitation of NSP4 with caveolin-1 (95), so now we evaluated the Co-Ip of NSP4 with cyclophilin A and cyclophilin 40. At 18 hpi RV-infected HT29.f8 cells were lysed in TRIS-Lysine buffer and the soluble proteins were collected by high speed centrifugation. These soluble lysates which contained the caveolin-1 chaperone complex were immunoprecipitated with rabbit anti-cyclophilin A or anti-cyclophilin 40 or normal rabbit sera. Subsequent Western blot analyses with mouse anti-$NSP4_{150-175}$ revealed that NSP4-specific bands precipitated from the soluble portion of the infected cell lysates subjected to antibodies to cyclophilin A or cyclophilin 40 (Fig 4.8.).

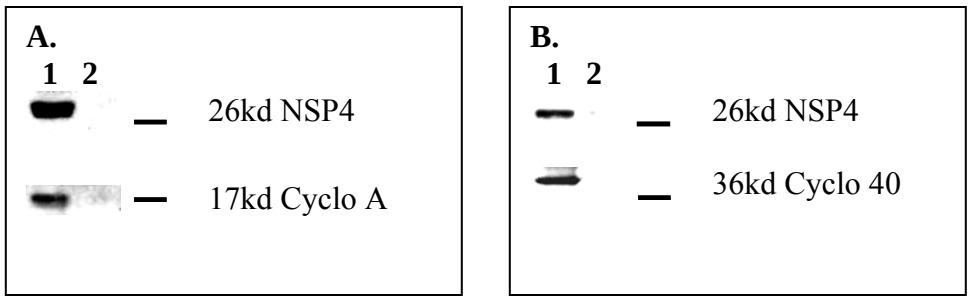

Figure 4.8. Co-IP of NSP4 and cyclophilin A (A) and NSP4 and cyclophilin 40 (B). Cyclophilin A and Cyclophilin 40 were precipitated from aliquots of soluble PNS of RV infected HT29.f8 cell lysates. The precipitated sample (lane 1) and a control (lane 2) precipitated with normal rabbit sera were subjected to SDS PAGE and transfer. Both samples were blotted with mouse anti-NSP4. The membrane for cyclophilin A (A) was cut at about the 20kd point and blotted for cyclophilin A. The membrane for cyclophilin 40 was washed and reblotted with mouse anti-cyclophilin 40.

4.3.8 NSP4 expression was sufficient to redistribute the caveolin-1 chaperone complex proteins, cyclophilin A, cyclophilin 40 and heat shock protein 56

The focus of this study was to explore NSP4 produced during RV infection in relation to selected secretory proteins and the proteins of the caveolin-1 chaperone complex. All results are shown from RV infected cells 7 hpi which corresponds to a point at which infective virus is just beginning to emerge from the cells according to our growth curve analysis studies previously conducted (Fig. 3.1). Our surface biotinylation studies on this cell line showed NSP4 at the exofacial PM as early as 3 hpi (Fig. 3.2 A.) and similar confocal studies (data not shown) conducted at 4 and 5 hpi produced similar results with regard to the redistribution and colocalization of NSP4 and the CCC proteins. Clearly these results occurred before virus release from the cell but they did occur in the presence of the other viral proteins within the cell. Previously we have shown that NSP4 expression in the absence of additional viral proteins colocalized with caveolin-1 (132).

To determine if this observation was consistent with the proteins of the caveolin-1 chaperone complex, epifluoressence was utilized with NSP4-transfected cells. Because HT29.f8 cells are difficult to transfect, we used MA104 cells which are much easier to transfect. MA104 cells were transiently transfected with a plasmid DNA to produce NSP4. In the transfected MA104 cells redistribution of the chaperone complex proteins in the transfected cells only was seen. In each case the pattern and distribution of the chaperone complex protein was very similar to the transfected NSP4. Control MA104 cells transfected with a V5-chloarmphenicol acetyltransferase fusion protein exhibited no redistribution in heat shock protein 56 (Fig. 4.9.).

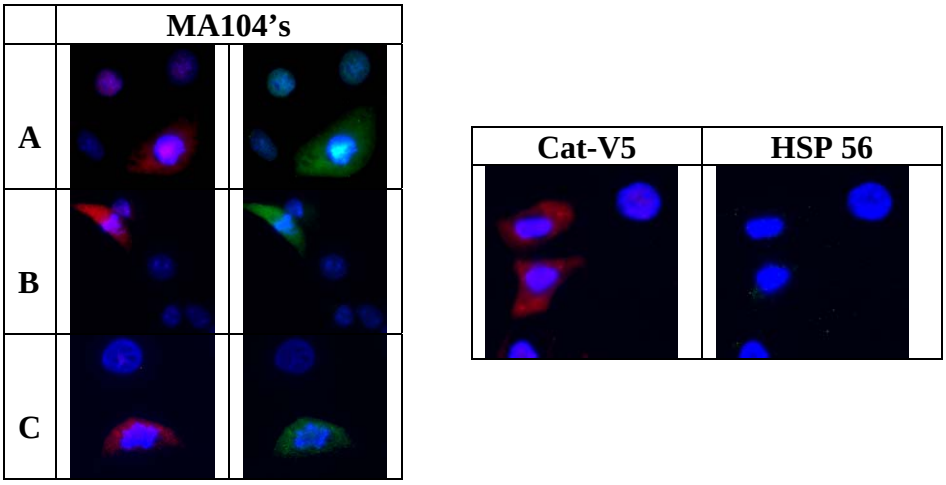

Figure 4.9. NSP4 transfected MA104 cells exhibited redistribution of the caveolin-1 chaperone complex proteins. MA104 cells were transfected with $NSP4_{1\text{-}175}$ plasmid DNA and probed with the antibodies of the caveolin-1 chaperone complex. Transfected NSP4 was labeled with a Cy3-linked Fab prepared from anti-$NSP4_{150\text{-}175}$. Cyclophilin A (A), Cyclophilin 40 (B) and HSP 56 (C) were labeled with their respective antibodies followed by F(ab)2 of goat anti-rabbit-Cy2. As a control MA104 cells were transfected with a chloramphenicol acetyltransferase-V5 epitope fusion protein and imaged for the V5-fusion protein (red) as well as HSP 56 (green).

4.3.9 Relative amounts of the caveolin-1 chaperone complex proteins (cyclophilin A, cyclophilin 40 and heat shock protein 56) were equal in RV-infected and uninfected cells

The confocal results regarding the CCC proteins in RV infected versus non-infected cells were striking. Even though the results were impressive, it is unclear if these results were due to a redistribution or reorientation of proteins that allowed for better visualization of the epitopes probed with our selected antibodies utilized to label the proteins as has been reported for caveoln-1 (104) or if it was due to an actual increase in protein levels. To determine if RV infection increased the amounts of the caveolin-1 chaperone complex proteins, the proteins were evaluated by Western blot analyses for protein levels from control mock infected cells and RV-infected cells at 7 hpi to coincide with the time-points in our confocal data. Protein analyses were conducted by utilizing both mock infected and infected cells. These respective cells were lysed and the PNS were subjected to high speed centrifugation to isolate soluble proteins. Equal amounts of the soluble proteins were loaded and separated by SDS PAGE before being transferred to nitrocellulose for western blotting. Utilizing GAPDH as a loading control, each of the proteins showed equal amounts in both mock infected and RV infected soluble cell lysates (Fig. 4.10).

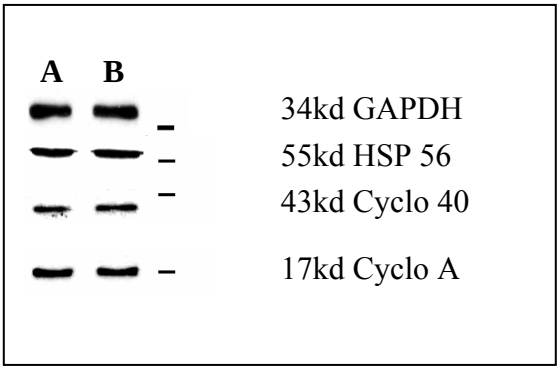

Figure 4.10. Relative distribution of the proteins of the caveolin-1 chaperone complex. Equal amounts of total protein from the soluble fraction of mock infected (A) and RV infected (B) HT29.f8 lysates were assayed. The same antibodies used for the respective proteins for microscopy studies were utilized to detect the proteins of the caveolin-1 chaperone complex by Western blotting. Results are shown side by side from four different sets of experiments in which equal amounts of protein were loaded from the same lysates (GAPDH shown as loading control).

4.3.10 Relative amounts of the mRNA for the caveolin-1 chaperone complex were equal in RV-infected and uninfected cells

Since the protein levels were equivalent, the relative levels of messenger RNA of the caveolin-1 chaperone complex in RV infected cells were assessed and compared to those of uninfected cells. Total RNA from infected and uninfected cells were collected, and cDNA produced from the total RNA. Primers for the housekeeping gene, glyceraldehyde-3-phosphate dehydrogenase (GAPDH), and for the genes of the caveolin-1 chaperone complex underwent real time PCR analysis with SYBR green as an indicator of the cycle threshold (Ct) of the target sequence. The comparison of the Ct's of the infected and uninfected samples to standard curves failed to reveal an increase in the relative amounts of the messenger RNA from RV infected cells. See example runs in figure 4.11. These results were conducted a minimum of three times

each at 3, 5 7 and 9 hpi and led us to postulate that the CCC imaging results were due to a redistribution of proteins upon RV infection and not an increase in the protein concentration.

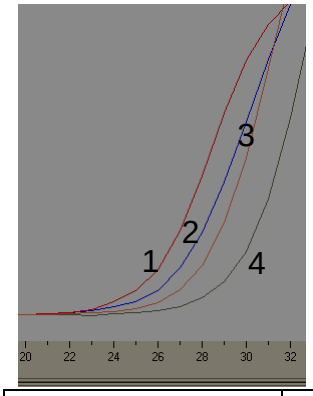

mRNA	Ct
1 = GAPDH (RV)	23.75
2 = GAPDH (no RV)	24.66
3 = Cyclo A (RV)	25.8
4 = Cyclo A (no RV)	27.32

1.4 fold mRNA in RV infected cells
Average = 1.3 (n=3)

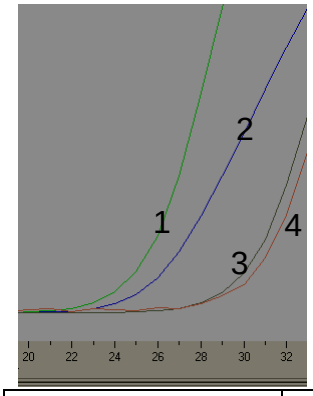

mRNA	Ct
1 = GAPDH (RV)	22.86
2 = GAPDH (no RV)	23.85
3 = Cyclo 40 (no RV)	28.05
4 = Cyclo A40(RV)	28.29

0.4 fold mRNA in RV infected cells
Average = 0.4 (n=3)

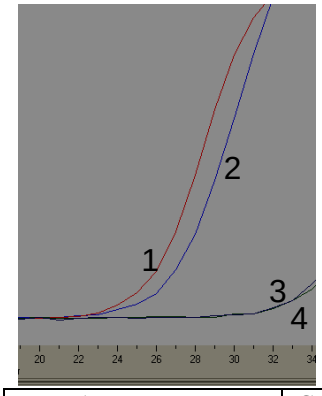

mRNA	Ct
1 = GAPDH (RV)	23.75
2 = GAPDH (no RV)	24.66
3 = HSP 56 (no RV)	32.16
4 =HSP 56 (RV)	32.33

0.47 fold mRNA in RV infected cells

Figure 4.11. mRNA levels of the caveolin-1 chaperone complex as assessed by real time PCR were not increased in RV-infected cells. Except for Cyclophilin A, which had an average of 1.3 times as much mRNA in RV infected cells as mock infected cells, mock infected cells have higher mRNA levels than that of RV infected cells. Examples above show cycle threshold values for GAPDH which was utilized as an internal control and cyclophilin A (left), cyclophilin 40 (middle) and HSP 56 (right).

4.4 Discussion

This study evaluated NSP4 produced by RV in relation to two sets of proteins. The first set of proteins were selected to investigate points along the secretory pathway

that traffics through the Golgi. The second set of proteins were those of the caveolin-1 chaperone complex that traffics directly from the ER to the PM (140).

With regard to the selected proteins along the secretory chain, our data showe giantin as the Golgi marker, appeared to be redistributed in RV infected cells at a relative early time post infection. Further exploration with Beta cop as a marker for anti-retrograde trafficking from the Golgi to the ER and clathrin as a trans Golgi and PM marker showed redistribution of the β-Cop to the ER with no impact on clathrin. NSP4 has been shown to bind microtubules, immobilize the secretory pathway, and redistribute β-Cop in transfected cells (143), but this is the first report on the impact of the Golgi apparatus as a whole in RV infected cells. ER export is important for maintenance of the Golgi apparatus (141) and their are several methods in addition to immobilization of the secretory pathway from the ER to the Golgi by which NSP4 and or the other RV proteins may impact the Golgi. Recently cholesterol has been shown to be required for efficient ER to Golgi traffic (111). NSP4 has been shown to preferentially interact with model membranes rich in cholesterol (51), and NSP4 which is initially an ER glycoprotein also has been shown to interact with caveolin-1 (95), which binds and traffics with cholesterol. Thus an interaction of NSP4 with cholesterol, be it directly or indirectly mediated by caveolin-1, may play a role in the redistribution of the Golgi. Alternatively, other structural proteins such as VP4 and the virus as a whole also have been shown to interact with cholesterol (114) and the interference with host cell translation by NSP3 (93) may contribute to the redistribution of the Golgi.

Because approximately 85-90% of newly synthesized caveolin-1 is transported along the secretory network from the ER to the Golgi complex and exits from the Golgi to the PM (97, 98, 104) we anticipated a redistribution of caveolin-1 in RV infected cells as well, which subsequently was shown experimentally. We compared the colocalization of NSP4 with giantin and NSP4 with caveolin-1 and found little no colocalization, suggesting that although NSP4 does interact with caveolin-1 (95, 132) it does not do so with the portion of caveolin-1 that is present within the Golgi.

In this study we utilized the viroplasm, the formation of which is dependent on expression of NSP4 (73, 121) as an intracellular marker. Because NSP4 has been shown to be present in the viroplasm (11), we highlighted another relative difference in the redistributed giantin and caveolin-1. Thus the viroplasm can be added to the list of associative properties of NSP4 and caveolin-1.

Since NSP4 does not appear to traffic through the Golgi, and hence doesn't traffic via th secretory pathway, we investigated its relative distribution with the proteins of the caveolin-1 chaperone complex, cyclophilin 40, cyclophilin A, and heat shock protein 56 that complex with caveolin-1 and newly synthesized cholesterol and do not traffic through the Golgi. Each of these proteins appeared to be redistributed in RV infected cells, colocalizing with NSP4 and the viroplasm suggesting that at least a portion of NSP4 may traffic with the caveolin-1 chaperone complex. This possibility could account for the delivery of NSP4 to the exofacial PM of HT29.f8 cells as early as 3 hpi. NSP4 and its association with the proteins of the caveolin-1 chaperone complex were also shown by FRET with each of the proteins and by co-immunoprecipitation of

NSP4 from the soluble fraction of RV infected cell lysates with either anti-cyclophilin 40 or anti-cyclophilin A.

The arrival of NSP4 at the exofacial surface of the PM at 3 hpi in HT29.f8 cells in our prior analysis clearly corresponded to a time post infection that was prior to virus release from the cell. This data suggested NSP4 does not require infective progeny virus to traffic from the ER to the exofacial PM. Expression of NSP4 by transfection in the absence of all other RV proteins did appear to redistribute the caveolin-1 chaperone complex proteins suggesting that a portion of NSP4 may travel with this complex without the assistance of RV or its proteins. Alternatively, NSP4 may inactivate a large portion of trafficking via the secretory process while simultaneously activating others required for the formation of the viroplasm as evidenced by the absence of the viroplasm when NSP4 is silenced (73, 121).

Our confocal data showed the caveolin-1chaperone complex proteins were upregulated in RV infected cells. Our real time PCR data did not detect an increase in messenger RNA for the caveolin-1 chaperone complex proteins, nor did our western blot data. We propose that during RV infection that protein trafficking via the secretory process is degraded causing the redistribution of other proteins including those of the caveolin-1 chaperone complex. The redistribution of the CCC proteins would give the appearance that they are more prevalent in RV infected cells by confocal analysis with the antibodies we utilized.

In summary, the data presented herein shows for the first time a redistribution of the Golgi complex during RV infection which supports previous findings of NSP4 and RV

trafficking independent of the Golgi. We also present for the first time evidence that the caveolin-1 chaperone complex are redistributed during RV infection and is likely utilized for the trafficking of NSP4 to various regions of the cell including the viroplasmand the PM.

5. CONCLUSION

5.1 Overview: The Research and Its Impact on an Increased Understanding of NSP4 and Its Functions During RV Infection

This study began with the presentation of evidence that suggested NSP4 is present outside of the ER in PM caveolae. Next it moved to show the temporal arrival of NSP4 at the exofacial surface of the PM in 2 cell lines in relation to the growth of virus in those cell lines. In addition the ability of NSP4 to interact with the PM of cells that have not been RV-infected was explored. This study concluded with an investigation of selected proteins from the secretory chain as well as proteins from the caveolin-1 chaperone complex providing for the first time preliminary evidence in the context of RV infection as to how NSP4 traffics throughout the cell to perform its many and varied functions.

Specifically this research has contributed to increasing the knowledge and understanding of some of the many and growing functions of NSP4. Details for each of the functions are described below and include: 1. A change from the paradigm that NSP4 is an ER glycoprotein and therefore is present only in the ER to function in viral morphogenesis by mediating the acquisition of a transient ER membrane as NSP4 pulls DLP's from the viroplasm into the ER (5, 6, 81). 2. NSP4 and its ability to induce age dependent diarrhea in mice and rats (9). 3. NSP4's ability to mobilize calcium from internal stores via a PLC dependent pathway upon exogenous addition to human intestinal cells (30) 4. and 5. NSP4 and its role in the formation of the viroplasm and modulation of transcription (11, 73, 121). This research also implies a role that has yet

to be suggested for NSP4 in the final maturation step for the incorporation of VP4 to progeny virus after leaving the ER (28).

5.1.1 NSP4 is present outside of the ER: Caveolae isolation

Although NSP4 had been shown to interact with caveolin-1, (95) this in itself did not provide evidence of the existence of a pool of NSP4 outside the ER in RV-infected cell. The development of the cavitation-sucrose chromatography caveolae isolation technique (Storey et. al.) was instrumental in setting the foundation for proof of NSP4 outside of the ER in RV infected cells. Prior to the development of this technique, finding NSP4 outside of the ER could have been interpreted as a false positive attributed to ER contamination. In addition to the isolation technique, which show NSP4 outside of the ER in caveolae, these data support the finding that NSP4 interacts with caveolin-1. The positive FRET reaction between NSP4 and caveolin-1 in RV-infected cells not only provided additional support for the interaction of NSP4 and caveolin-1, but laid the foundation for the utilization of FRET together with colocalization and biochemical methods to study how and when NSP4 was present at various locations throughout an RV infected cell.

5.1.2 Exofacial PM and Exogenous NSP4: diarrhea induction in mice and PLC dependent IP3 release of calcium from the ER

In our and other laboratories either a fragment of NSP4, or the intact NSP4 protein have been found in the media of RV-infected cultured cells (19, 146). Finding NSP4 in the media was significant because its presence was considered as evidence for a pool of NSP4 capable of interacting with the PM of cells, an interaction which had been

shown to lead to secretory diarrhea in neonatal mice and mobilization of intracellular calcium through receptor-mediated phospholipase C activation and IP_3 production resulting in Cl^- secretion causing water loss (9, 30). This work for the first time shows NSP4 present at the exofacial surface of the PM of RV-infected cells prior to virus release and loss of PM integrity. This provides a plausible mechanism for the pathogenesis of RV infection with regard to the activation of secretory diarrhea prior to the onset of pathological changes (109). The presence of NSP4 at the exofacial surface of the PM as early as 3 hpi in an intestinal cell line provided evidence that NSP4 could be the cause of this early secretory process. We also showed for the first time that soluble NSP4 clarified of virus by high speed centrifugation bound the PM of non-infected cells. These data provided further evidence for NSP4's contribution to the secretory process in RV infection. The simultaneous addition of NSP4 to both cell lines also corroborated differences regarding the trafficking of NSP4 in different cells lines, for example the earlier appearance at the exofacial PM in the intestinal cell line (HT29.f8) versus the kidney cell line (MDCK). Clearly NSP4 appeared to interact differently with the HT29.f8 versus the MDCK cells. These results suggest NSP4 may cross the PM of HT29.f8 cells which would provide at least a partial explanation for the appearance of NSP4 at the exofacial PM in the intestinal cell line much earlier than the kidney cell line.

Whe simultaneously investigated the temporal appearance of NSP4 at the exofacial surface of the PM and the impact of the exogenous addition of a virus clarified soluble NSP4 to MDCK and HT29.f8 cells. Because these 2 cell lines exhibited similar

RV growth curves, we further highlighted the important differences that can result from the use of different cell lines and how the cultured cells utilized needs to be considered when interpreting results regarding the trafficking of NSP4 and rotavirus. Notable is the appearance, as much as 4 hpi earlier, in the HT29.f8 cells the the MDCK cells even though both cell lines were RV-infected with the same MOI of the same passage of the same virus. The difference between these cell lines were further confirmed with the exogenous addition of equal amounts of NSP4 for an equal amount of time. Thus when considering NSP4 endogenously produced by RV infection or added exogenously to the PM of naïve cells, there appears to be a difference in how it traffics and interacts or possibly crosses the PM in HT29.f8 versus MDCK cells. Differences in the partitioning of NSP4 within the cell have even been noted when the same cell line was utilized. For example both Sapin et al. and Cuadras and Greenberg report the presence of NSP4 in the rafts of cells but one group found the NSP4 in rafts as early as 5 hpi, wheras the other did not detect NSP4 until 12 – 15 hpi (26, 114). One key difference was the stage at which the cells utilized (Caco-2) were infected. Cells grown for 10 days before RV infection exhibit the presence of NSP4 in rafts at 5 hpi, but cells grown for 21 days do not cosegregate NSP4 with rafts until 12- 15 hpi. We have noted similar differences with the relative amounts of NSP4 expressed in totally confluent monolayers of the spontaneously polarizing HT29.f8 cell line versus non confluent HT29.f8 cells. The differences in NSP4 trafficking throughout the cell could be due to the different states of membrane microdomains (122) both from cell line to cell line and within the same cell line dependent upon the stage of growth. These differences appear to impact the sorting

of proteins. Dependent upon how and when NSP4 and the other RV proteins were expressed appeared to impact how and when they are trafficked to the PM and whether or not NSP4 was able to cross rapidlyonce it arrived at the PM.

Three methods were utilized to determine if and when NSP4 was exposed at the exofacial surface of the PM. Two of these methods, surface biotinylation, and live cell staining, have been utilized for various cellular and viral proteins in the past and required only minor development and optimization for use. The third method involved the development and optimization of a novel technique. We utilized confocal microscopy, colocalizaton, and FRET to determine on a cell by cell basis if and when the C-terminus of NSP4 was exposed at the PM. All the proteins on the exofacial PM of live RV-infected cells were surface biotinylated, then fixed and permeabilized, subsequently the bioint was labeled with Cy3 and the NSP4 with Cy5. The PM's integrity was concurrently evaluated because the biotinylation agent we utilized was membrane impermeable. If the membrane lost its integrity the entire cell was biotinylated and subsequently Cy3 labeled. Any cells with intracellular biotin staining were disregarded. We then evaluated a FRET reaction between Cy3 and Cy5 by the acceptor photobleaching method. FRET should only occur if the Cy3 and Cy5 fluorophores are less than 10nm apart. Therefore, if NSP4 was not biotinylated because it was not exposed at the PM, the Cy3 labeling of the exofacial PM proteins did not place any Cy3 within 10nm of the Cy5. This method allowed the simultaneous evaluation of the integrity of the PM while determining if NSP4 was exposed in a particular cell. This was important not only in providing an additional means to support our findings

regarding NSP4 at the PM, but in ensuring that these findings were due to trafficking of NSP4 and not to cell lysis and rebinding of NSP4 to the PM.

5.1.3 NSP4 trafficking from the ER, its role in the formation of the viroplasm and modulation of transcription

The results indicating NSP4 at the exofacial surface of HT29.f8 cells at 3 hpi indicated rapid trafficking of an ER glycoprotein, but did reveal anything specific about the trafficking mechanism. Because we as well as others had shown that NSP4 appeared to traffic via a Golgi-independent pathway (10, 11, 15, 26, 91, 114, 132), we investigated NSP4 in relation to selected secretory proteins that transit the Golgi as well as the cavelin-1 chaperone complex proteins that traffic directly from the ER to the PM. The caveolin-1 chaperone complex proteins were chosen because of our previous results showing NSP4 binds caveolin-1 and traffics to caveolae as well as the fact that NSP4 and caveolin-1 are both integral membrane proteins that also exist in a soluble form in the cell (19, 140). The redistribution, colocalization, FRET and co-immunoprecipation studies of NSP4 with the proteins of the caveolin-1 chaperone complex strongly suggest that this is a method for the rapid trafficking of NSP4 from the ER to the PM.

The redistribution of the caveolin-1 chaperone complex proteins and colocalization with the viroplasm provided some additional insight as to the trafficking and or formation of the viroplasm. These results were especially intriguing because the redistribution of these proteins may be required for the formation of the viroplasm. The importance of NSP4 in both the formation of the viroplasm as well as in modulation viral transcription which largely takes place in the viroplasm has been previously

demonstrated (73, 121), but the mechanisms by which these events occur have remained elusive. Additionally NSP4 has been found to colocalize with an autophagosomal marker LC3 suggesting that NSP4 is responsible for inducing or hijacking the cellular autophagy membranes (11). Autophagic membranes are hypothesized to form either de novo or directly from the ER (62). Our results show for the first time that NSP4 may induce the trafficking of the caveolin-1 chaperone complex proteins to the viroplasm. Alternatively, if the viroplasm buds from the ER, NSP4 may be required, or cause portions of the ER also containing the proteins of the caveolin-1 chaperone complex to bud and form the viroplasm. It is also possible that the interference with the secretory pathway by NSP4 as evidenced by or data showing the redistribution of the Gogli as well as by Xu (143) could trigger the formation of the viroplasm. Regardless of the mechanism whereby NSP4 triggers the formation of the viroplasm, NSP4's appearance at the exofacial surface of the PM by 3 hpi in RV-infcted HT29.f8 cells requires a rapid Golgi-bypassing transport mechanism such as that of the caveolin-1 chaperone complex and suggests that this is the likely mechanism exploited by RV-infected HT29.f8 cells to traffic NSP4.

5.1.4 Other roles for NSP4

This study places a portion of NSP4 at the exofacial PM at a very early time point post infection. VP4 also has been shown to present at the exofacial PM early post infection and partitions to raft fractions of infected cell lysates independent of virus particles and NSP4 (26, 89, 114). We have shown a positive FRET reaction for VP4 and NSP4 and the same NSP4 and caveolin-1 at the cell periphery (data not shown)

suggestive of a role in a post ER site. Given that NSP4 binds both VP4 and VP6, and at least one group has provided evidence that VP4 addition to the TLP of RV is accomplished after the TLP has exited the ER (28), NSP4 may play additional roles in the final morphogenesis of RV as well, such as assisting with the addition of the VP4 spike to the TLP.

5.2 Pitfalls

Since 1996, when NSP4 was first shown to induce diarrhea in mouse pups, much of the research done to elucidate how a non structural ER glycoprotein can act at the PM to increase secretion from the cell has been associative in nature. For example, exogenous addition of NSP4 to cultured cells has been shown to induce a PLC to IP3 to calcium mediated chloride secretion from the cells, and NSP4 has been found in the media of cell culture which means it may associate with receptors triggering a secretory event. A second example is that NSP4 has been shown to bind caveolin-1 which is the defining protein of caveolae. Given caveolae are known areas at the PM rich in signal transduction proteins, NSP4 was shown to associate with a protein important to signal transduction across the PM. As with previous research, one of the potential weaknesses for this research is that much of the data are associative as well. Ideally, to show NSP4 leaves the ER and traffics to the exofacial PM of non-infected cells to trigger a secretory event we would show this happening real time in RV-infected cells. One way to accomplish this would require the design of a genetically modified RV with a fluorescent NSP4 and the ability to simultaneously monitor it as well the PM and any secretion from the cell across the PM where NSP4 is found. Additionally, similar

studies would be conducted with cells transfected with a fluorescent NSP4 to examine its activity in the absence of the other RV proteins. Although not technically impossible, reverse genetics with RV has only been recently achieved with limited success. One laboratory has demonstrated the ability to incorporate a genetically modified structural protein of RV (66) and another laboratory has demonstrated a technically demanding and cell line restricted procedure because it requires the simultaneous transfection of all the viral genes for a reovirus at once (64). Transfecting cells with NSP4 has proven difficult because of its toxicity to the cell with some recent success when utilizing an inducible system to control when NSP4 is expressed (11). So far the only fluorescent NSP4 that has been studied have utilized a fusion protein of NSP4 with green fluorescent protein, but this more that doubles the size of NSP4 and may interfere some of its normal interactions with the cell.

Our findings, (NSP4 is isolated with caveolae, NSP4 is at the exofacial surface of the PM prior to virus release in an intestinal cell line, NSP4 binds the PM of non RV infected cells, the Golgi is redistributed in RV infected cells and NSP4 does not colocalize with the Golgi, but does associate with the proteins of the caveolin-1 chaperone complex that traffics independent of the Golgi) are associative in nature as well, but do build upon prior findings. These findings suggest that NSP4 does traffic from the ER independent of the Golgi to the exofacial PM of non-infected cells where it may activate a receptor and induce secretion from yet uninfected cells. Each additional associative finding increases the possibility of further elucidating NSP4's importance in

the overall pathology caused by a RV infection as well as elucidate a mechanism by which a virally encoded protein hijacks a Golgi independent trafficking pathway.

5.3 Future Research

This research has provided evidence for the association of NSP4 and caveolin-1, not only at PM caveolae, but within the viroplasm as well. Given that RV and NSP4 appear to traffic via a Golgi independent pathway and RV appears to disrupt the Golgi we examined and found an impact on the caveolin-1 chaperone complex proteins in RV infected cells. Future studies should continue to focus on the caveolin-1 chaperone complex proteins and NSP4. In particular to investigate if any or all of the constituents of the caveolin-1 chaperone complex are required for the rapid transport of NSP4 to the exofacial PM and for the formation of the viroplasm. Several strategies including the use a pharmaceutical agents to manipulate the caveolin-1 chaperone complex and cholesterol, caveolin-1 negative and caveolin-1 mutant cell lines, cyclophilin A negative cell lines, and selected gene silencing studies have been developed and could be utilized to investigate further any specific and or required use of the caveolin-1 chaperone complex by NSP4. A brief outline of these studies follows.

5.3.1 Pharmaceutical agents

Methyl-β-cyclodextrin, lovastatin, cyclosporin A and rapamycin are agents that have the ability to alter the distribution of cholesterol in mammalian cells (90, 123, 140). These agents could be utilized in RV-infected cells to determine if they impact the trafficking of NSP4 and/or the formation of the viroplasm. Given that the PM is estimated to contain about 60-80% of total cellular cholesterol (80) and cyclodextrin has

been used to specifically remove PM cholesterol, (90) treatment of cells with cyclodextrin reduces the cholesterol content of the cells. Hydroxymethylglutaryl-coenzyme A (HMG-CoA) is a precursor for cholesterol synthesis. HMG-CoA reductase is the rate limiting enzyme that catalyzes the production of mevalonate from HMG-CoA for the eventual production of cholesterol (32). Lovastatin is an effective inhibitor of HMG-CoA reductase and thus decreases cholesterol biosynthesis in mammalian cells (123). The immunophilins, including cyclophilin A, cyclophilin 40 and HSP 56 are cytosolic enzymes that catalyze cis-trans isomerization of peptidylprolyl bonds as well as have a strong affinity for the immunosuppressant drugs cyclosporine A or rapamycin (54). Cyclophilin 40 and cyclophilin A are cyclophilins that have no affinity for rapamycin, while HSP 56 has no affinity for cyclosporin A (54). Cyclosporin A and rapamycin both have been used successfully to disrupt the caveolin-1 chaperone complex. Rapamycin prevents the association of HSP 56 and cyclophilin 40 with the complex and cyclosporin A prevents the association of cyclophilin A and cyclophilin 40 with the complex (140). Utilizing these agents, studies could be conducted to determine whether NSP4 can traffic with newly synthesized or previously synthesized cholesterol, as well as if it can traffic when the caveolin-1 chaperone complex is perturbed. These studies could be conducted by comparing the trafficking of NSP4 out of the ER in RV-infected HT-29.f8 cells versus drug treated RV-infected cells.

5.3.2 Caveolin-1 negative and caveolin-1 mutant cell lines

The lymphoid cell line, L1210-JF, is caveolin-1 negative and has been permanently transfected with caveolin-1 and mutants of caveolin-1 that confer a single

amino acid change from cysteine to alanine to prevent palmitoylation at position 133, 143, 156 or all three simultaneously (139). In the parent L1210-JF cell line, the caveolin-1 chaperone complex did not form, and therefore did not rapidly transport newly synthesized cholesterol from the ER to the PM. Transfecting the L1210-JF cell line with caveolin-1 enabled the formation of the caveolin-1 chaperone complex to include all of the protein constituents, HSP 56, cyclophilin A, and cyclophilin 40, which enabled the rapid transport of newly synthesized cholesterol to PM caveolae. When L1210-JF cells are transfected with the caveolin-1 143 mutant, cyclophilin A is no longer incorporated into the complex (139). When L1210-JF's are transfected with the caveolin-1 156 mutant, HSP 56 is not incorporated and when it was transfected with the caveolin-1 triple mutant both HSP 56 and cyclophilin A are lost from the caveolin-1 chaperone complex (139). Utilizing these cell lines would help determine if the caveolin-1 chaperone complex plays a role in NSP4 transport from the ER and if so which of the proteins of the complex are important for this transport.

5.3.3 Cyclophilin A negative cell line

A Cyclophilin A negative cell line has been produced by homologous recombination (18). This cell line has been utilized to study the impact on HIV replication versus the parent cell line with cyclophilin A. This same strategy could be employed to investigate whether or not the loss of cyclophilin A impacts the transport of NSP4 via the caveolin-1 chaperone complex.

5.3.4 Silencing studies

Silencing RNA strategies in conjunction with pharmaceutical agents or caveolin-1 negative, caveolin-1 mutant or cyclophilin A negative cell lines could be utilized to corroborate and further delineate NSP4 traffic in these various cell lines. One example would be silencing a specific immunophilin such as cyclophilin 40 from the L1210-JF line transfected with the triple caveolin-1 mutant that prevents the incorporation of HSP 56 and cyclophilin A but not cyclophilin 40 into the caveolin-1 chaperone complex. Another example entails utilizing cyclosporine A, which dissociates cyclophilin A and cyclophilin 40 from the caveolin-1 chaperone complex but does not decrease the levels produced in the cell. Silencing either or both of these proteins in conjunction with utilization of a pharmaceutical agent such as cyclosporine A could delineate whether or not the specified protein transports NSP4 only when incorporated in the caveolin-1 chaperone complex.

The results of this research continue to reveal the importance of NSP4 in the morphogenesis, trafficking and pathogensis of rotavirus. Future studies will undoubtedly continue to increase our knowledge of the cellular machinery including the many roles of caveolin-1 and trafficking of cholesterol, as well as reveal unique methods of utilizing NSP4 to impact the cellular machinery and possible mediate the pathology of rotavirus.

REFERENCES

1. **Abeliovich, H. D., W. A. Dunn Jr., J. Kim, and D. J. Klionsky.** 2000. Dissection of autophagosome biogenesis into distinct nucleation and expansion steps J. Cell Biol. **151:**1025-1034.
2. **Adachi, S., A. R. Cross, B. M. Babior, and R. A. Gottlieb.** 1997. Bcl-2 and the outer mitochondrial membrane in the inactivation of cytochrome c during Fas-mediated apoptosis. J Biol Chem **272:**21878-82.
3. **Anderson, R. G.** 1998. The caveolae membrane system. Annu Rev Biochem **67:**199-225.
4. **Anthony, I. D., S. Bullivant, S. Dayal, A. R. Bellamy, and J. A. Berriman.** 1991. Rotavirus spike structure and polypeptide composition. J Virol **65:**4334-40.
5. **Au, K. S., W. K. Chan, J. W. Burns, and M. K. Estes.** 1989. Receptor activity of rotavirus nonstructural glycoprotein NS28. J Virol **63:**4553-62.
6. **Au, K. S., N. M. Mattion, and M. K. Estes.** 1993. A subviral particle binding domain on the rotavirus nonstructural glycoprotein NS28. Virology **194:**665-73.
7. **Axen, R., J. Porath, and S. Ernback.** 1967. Chemical coupling of peptides and proteins to polysaccharides by means of cyanogen halides. Nature **214:**1302-4.
8. **Ball, J. M., D. M. Mitchell, T. F. Gibbons, and R. D. Parr.** 2005. Rotavirus NSP4: a multifunctional viral enterotoxin. Viral Immunology **18:**27-40.
9. **Ball, J. M., P. Tian, C. Q. Zeng, A. P. Morris, and M. K. Estes.** 1996. Age-dependent diarrhea induced by a rotaviral nonstructural glycoprotein. Science **272:**101-4.
10. **Bergmann, C. C., D. Maass, M. S. Poruchynsky, P. H. Atkinson, and A. R. Bellamy.** 1989. Topology of the non-structural rotavirus receptor glycoprotein NS28 in the rough endoplasmic reticulum. Embo J **8:**1695-703.
11. **Berkova, Z., S. E. Crawford, G. Trugnan, T. Yoshimori, A. P. Morris, and M. K. Estes.** 2006. Rotavirus NSP4 induces a novel vesicular compartment regulated by calcium and associated with viroplasms. J Virol **80:**6061-71.
12. **Berkova, Z., A. P. Morris, and M. K. Estes.** 2003. Cytoplasmic calcium measurement in rotavirus enterotoxin-enhanced green fluorescent protein (NSP4-EGFP) expressing cells loaded with Fura-2. Cell Calcium **34:**55-68.
13. **Bican, P., J. Cohen, A. Charpilienne, and R. Scherrer.** 1982. Purification and characterization of bovine rotavirus cores. J Virol **43:**1113-7.
14. **Bickel, P. E., P. E. Scherer, J. E. Schnitzer, P. Oh, M. P. Lisanti, and H. F. Lodish.** 1997. Flotillin and epidermal surface antigen define a new family of caveolae-associated integral membrane proteins. J Biol Chem **272:**13793-802.
15. **Boshuizen, J. A., J. W. Rossen, C. K. Sitaram, F. F. Kimenai, Y. Simons-Oosterhuis, C. Laffeber, H. A. Buller, and A. W. Einerhand.** 2004. Rotavirus enterotoxin NSP4 binds to the extracellular matrix proteins laminin-beta3 and fibronectin. J Virol **78:**10045-53.
16. **Both, G. W., L. J. Siegman, A. R. Bellamy, and P. H. Atkinson.** 1983. Coding assignment and nucleotide sequence of simian rotavirus SA11 gene segment 10:

location of glycosylation sites suggests that the signal peptide is not cleaved. J Virol **48:**335-9.

17. **Bowman, G. D., I. M. Nodelman, Levy, S. L. OLin, P. Tian, T. J. Zamb, S. A. Udem, B. Venkataraghavan, and C. E. Schutt.** 2000. Crystal structure of the oligomerization domain of NSP4 from rotavirus reveals a core metal-binding site J. Mol. Biol. **304:**861-891.
18. **Braaten, D., and J. Luban.** 2001. Cyclophilin A regulates HIV-1 infectivity, as demonstrated by gene targeting in human T cells. Embo J **20:**1300-9.
19. **Bugarcic, A., and J. A. Taylor.** 2006. Rotavirus nonstructural glycoprotein NSP4 is secreted from the apical surfaces of polarized epithelial cells. J. Virol. **80:**12343-12349.
20. **Burke, B., and U. Desselberger.** 1996. Rotavirus pathogenicity. Virology **218:**299-305.
21. **Chan, W. K., K. S. Au, and M. K. Estes.** 1988. Topography of the simian rotavirus nonstructural glycoprotein (NS28) in the endoplasmic reticulum membrane. Virology **164:**435-42.
22. **Chun, M., U. K. Liyanage, M. P. Lisanti, and H. F. Lodish.** 1994. Signal transduction of a G protein-coupled receptor in caveolae: colocalization of endothelin and its receptor with caveolin. Proc Natl Acad Sci U S A **91:**11728-32.
23. **Cohen, A. W., R. Hnasko, W. Schubert, and M. P. Lisanti.** 2004. Role of caveolae and caveolins in health and disease. Physiol Rev **84:**1341-79.
24. **Collins, J., W. G. Starkey, T. S. Wallis, G. J. Clarke, K. J. Worton, A. J. Spencer, S. J. Haddon, M. P. Osborne, D. C. Candy, and J. Stephen.** 1988. Intestinal enzyme profiles in normal and rotavirus-infected mice. J Pediatr Gastroenterol Nutr **7:**264-72.
25. **Cuadras, M. A., B. B. Bordier, J. L. Zambrano, J. E. Ludert, and H. B. Greenberg.** 2006. Dissecting rotavirus particle-raft interaction with small interfering RNAs: insights into rotavirus transit through the secretory pathway. J Virol **80:**3935-46.
26. **Cuadras, M. A., and H. B. Greenberg.** 2003. Rotavirus infectious particles use lipid rafts during replication for transport to the cell surface in vitro and in vivo. Virology **313:**308-21.
27. **Cunliffe, N. A., P. E. Kilgore, J. S. Bresee, A. D. Steele, N. Luo, C. A. Hart, and R. I. Glass.** 1998. Epidemiology of rotavirus diarrhoea in Africa: a review to assess the need for rotavirus immunization. Bull World Health Organ **76:**525-37.
28. **Delmas, O., A. M. Durand-Schneider, J. Cohen, O. Colard, and G. Trugnan.** 2004. Spike protein VP4 assembly with maturing rotavirus requires a postendoplasmic reticulum event in polarized caco-2 cells. J Virol **78:**10987-94.
29. **Devaux, P. F., and R. Morris.** 2004. Transmembrane asymmetry and lateral domains in biological membranes. Traffic **5:**241-6.
30. **Dong, Y., C. Q. Zeng, J. M. Ball, M. K. Estes, and A. P. Morris.** 1997. The rotavirus enterotoxin NSP4 mobilizes intracellular calcium in human intestinal cells by stimulating phospholipase C-mediated inositol 1,4,5-trisphosphate production. Proc Natl Acad Sci U S A **94:**3960-5.

31. **Drenan, R. M., X. Liu, P. G. Bertram, and X. F. Zheng.** 2004. FKBP12-rapamycin-associated protein or mammalian target of rapamycin (FRAP/mTOR) localization in the endoplasmic reticulum and the Golgi apparatus. J Biol Chem **279:**772-8.
32. **Endo, A.** 1981. 3-Hydroxy-3-methylglutaryl-CoA reductase inhibitors. Methods Enzymol **72:**684-9.
33. **Ericson, B. L., D. Y. Graham, B. B. Mason, and M. K. Estes.** 1982. Identification, synthesis, and modifications of simian rotavirus SA11 polypeptides in infected cells. J Virol **42:**825-39.
34. **Ericson, B. L., D. Y. Graham, B. B. Mason, H. H. Hanssen, and M. K. Estes.** 1983. Two types of glycoprotein precursors are produced by the simian rotavirus SA11. Virology **127:**320-32.
35. **Fabbretti, E., I. Afrikanova, F. Vascotto, and O. R. Burrone.** 1999. Two non-structural rotavirus proteins, NSP2 and NSP5, form viroplasm-like structures in vivo. J Gen Virol **80 (Pt 2):**333-9.
36. **Fujimoto, T.** 1993. Calcium pump of the plasma membrane is localized in caveolae. J Cell Biol **120:**1147-57.
37. **Fujimoto, T., S. Nakade, A. Miyawaki, K. Mikoshiba, and K. Ogawa.** 1992. Localization of inositol 1,4,5-trisphosphate receptor-like protein in plasmalemmal caveolae. J Cell Biol **119:**1507-13.
38. **Gallegos, A. M., S. M. Storey, A. B. Kier, F. Schroeder, and J. M. Ball.** 2006. Structure and cholesterol dynamics of caveolae/raft and nonraft plasma membrane domains. Biochemistry **45:**12100-16.
39. **Gardet, A., M. Breton, P. Fontanges, G. Trugnan, and S. Chwetzoff.** 2006. Rotavirus spike protein VP4 binds to and remodels actin bundles of the epithelial brush border into actin bodies. J Virol **80:**3947-56.
40. **Gelderblom, H. R., H. Renz, and M. Ozel.** 1991. Negative staining in diagnosic virology. Micron and microscopica acta **22:**435-477.
41. **Glass, R. I., P. E. Kilgore, R. C. Holman, S. Jin, J. C. Smith, P. A. Woods, M. J. Clarke, M. S. Ho, and J. R. Gentsch.** 1996. The epidemiology of rotavirus diarrhea in the United States: surveillance and estimates of disease burden. J Infect Dis **174 Suppl 1:**S5-11.
42. **Gonzalez, R. A., R. Espinosa, P. Romero, S. Lopez, and C. F. Arias.** 2000. Relative localization of viroplasmic and endoplasmic reticulum-resident rotavirus proteins in infected cells. Arch. Virol. **145:**1963-1973.
43. **Gottschalk, A.** 1972. Glycoproteins: their composition, structure, and function. Elseveir Publishing Company, New York.
44. **Gumbleton, M., A. G. Abulrob, and L. Campbell.** 2000. Caveolae: an alternative membrane transport compartment. Pharm Res **17:**1035-48.
45. **Gurwith, M., W. Wenman, D. Hinde, S. Feltham, and H. Greenberg.** 1981. A prospective study of rotavirus infection in infants and young children. J Infect Dis **144:**218-24.
46. **Gustavsson, J., S. Parpal, M. Karlsson, C. Ramsing, H. Thorn, M. Borg, M. Lindroth, K. H. Peterson, K. E. Magnusson, and P. Stralfors.** 1999.

Localization of the insulin receptor in caveolae of adipocyte plasma membrane. Faseb J **13:**1961-71.

47. **Heerklotz, H., H. Szadkowska, T. Anderson, and J. Seelig.** 2003. The sensitivity of lipid domains to small perturbations demonstrated by the effect of Triton. J Mol Biol **329:**793-9.
48. **Hope, H. R., and L. J. Pike.** 1996. Phosphoinositides and phosphoinositide-utilizing enzymes in detergent-insoluble lipid domains. Mol Biol Cell **7:**843-51.
49. **Hoshino, Y., and A. Z. Kapikian.** 1996. Classification of rotavirus VP4 and VP7 serotypes. Arch Virol Suppl **12:**99-111.
50. **Hua, J., X. Chen, and J. T. Patton.** 1994. Deletion mapping of the rotavirus metalloprotein NS53 (NSP1): the conserved cysteine-rich region is essential for virus-specific RNA binding. J Virol **68:**3990-4000.
51. **Huang, H., F. Schroeder, M. K. Estes, T. McPherson, and J. M. Ball.** 2004. Interaction(s) of rotavirus non-structural protein 4 (NSP4) C-terminal peptides with model membranes. Biochem J **380:**723-33.
52. **Huang, H., F. Schroeder, C. Zeng, M. K. Estes, J. K. Schoer, and J. M. Ball.** 2001. Membrane interactions of a novel viral enterotoxin: rotavirus nonstructural glycoprotein NSP4. Biochemistry **40:**4169-80.
53. **Hubbard, S. C., and R. J. Ivatt.** 1981. Synthesis and processing of asparagine-linked oligosaccharides. Annu Rev Biochem **50:**555-83.
54. **Ivery, M. T.** 2000. Immunophilins: switched on protein binding domains? Med Res Rev **20:**452-84.
55. **Jackson, M. R., T. Nilsson, and P. A. Peterson.** 1990. Identification of a consensus motif for retention of transmembrane proteins in the endoplasmic reticulum. Embo J **9:**3153-62.
56. **Jayaram, H., M. K. Estes, and B. V. Prasad.** 2004. Emerging themes in rotavirus cell entry, genome organization, transcription and replication. Virus Research **101:**67-81.
57. **Kabcenell, A. K., and P. H. Atkinson.** 1985. Processing of the rough endoplasmic reticulum membrane glycoproteins of rotavirus SA11. J Cell Biol **101:**1270-80.
58. **Kapikian, A. Z.** 1993. Viral gastroenteritis. Jama **269:**627-30.
59. **Karpova, T. S., C. T. Baumann, L. He, X. Wu, A. Grammer, P. Lipsky, G. L. Hager, and J. G. McNally.** 2003. Fluorescence resonance energy transfer from cyan to yellow fluorescent protein detected by acceptor photobleaching using confocal microscopy and a single laser. J Microsc **209:**56-70.
60. **Kenworthy, A. K.** 2001. Imaging protein-protein interactions using fluorescence resonance energy transfer microscopy. Methods **24:**289-96.
61. **Kirchhausen, T.** 2000. Three ways to make a vesicle. Nat Rev Mol Cell Biol **1:**187-98.
62. **Kirkegaard, K., M. P. Taylor, and W. T. Jackson.** 2004. Cellular autophagy: surrender, avoidance and subversion by microorganisms. Nat Rev Microbiol **2:**301-14.

63. **Kluck, R. M., E. Bossy-Wetzel, D. R. Green, and D. D. Newmeyer.** 1997. The release of cytochrome c from mitochondria: a primary site for Bcl-2 regulation of apoptosis. Science **275:**1132-6.
64. **Kobayashi, T., Antar, A., Boehme, K.W., Danthi, P., Eby, E.A., Guglielmi, K.M., Holm, G.H., Johnson, E.M., Maginnis, M.S., Naik, S., Skelton, W.B., Wetzel, J.D., Wilson, G.J., Chappel, J.D., and Dermody, T.S.** 2007. A plasmid-based reverse genetics system for animal double-stranded RNA viruses. Cell Host & Microbe **1:**147-157.
65. **Koch, G. L., D. R. Macer, and M. J. Smith.** 1987. Visualization of the intact endoplasmic reticulum by immunofluorescence with antibodies to the major ER glycoprotein, endoplasmin. J Cell Sci **87 (Pt 4):**535-42.
66. **Komoto, S., J. Sasaki, and K. Taniguchi.** 2006. Reverse genetics system for introduction of site-specific mutations into the double-stranded RNA genome of infectious rotavirus. Proc Natl Acad Sci U S A **103:**4646-51.
67. **Kurzchalia, T. V., P. Dupree, R. G. Parton, R. Kellner, H. Virta, M. Lehnert, and K. Simons.** 1992. VIP21, a 21-kD membrane protein is an integral component of trans-Golgi-network-derived transport vesicles. J Cell Biol **118:**1003-14.
68. **Lennarz, W. J.** 1980. The biochemistry of glycoproteins and proteoglycans. Plenum Press, New York.
69. **Li, S., J. Couet, and M. P. Lisanti.** 1996. Src tyrosine kinases, Galpha subunits, and H-Ras share a common membrane-anchored scaffolding protein, caveolin. Caveolin binding negatively regulates the auto-activation of Src tyrosine kinases. J Biol Chem **271:**29182-90.
70. **Li, S., K. S. Song, S. S. Koh, A. Kikuchi, and M. P. Lisanti.** 1996. Baculovirus-based expression of mammalian caveolin in Sf21 insect cells. A model system for the biochemical and morphological study of caveolae biogenesis. J Biol Chem **271:**28647-54.
71. **Linstedt, A. D., and H. P. Hauri.** 1993. Giantin, a novel conserved Golgi membrane protein containing a cytoplasmic domain of at least 350 kDa. Mol Biol Cell **4:**679-93.
72. **Lisanti, M. P., P. E. Scherer, J. Vidugiriene, Z. Tang, A. Hermanowski-Vosatka, Y. H. Tu, R. F. Cook, and M. Sargiacomo.** 1994. Characterization of caveolin-rich membrane domains isolated from an endothelial-rich source: implications for human disease. J Cell Biol **126:**111-26.
73. **Lopez, T., M. Camacho, M. Zayas, R. Najera, R. Sanchez, C. F. Arias, and S. Lopez.** 2005. Silencing the morphogenesis of rotavirus. J Virol **79:**184-92.
74. **Lopez, T., M. Rojas, C. Ayala-Breton, S. Lopez, and C. F. Arias.** 2005. Reduced expression of the rotavirus NSP5 gene has a pleiotropic effect on virus replication. J Gen Virol **86:**1609-17.
75. **Lu, L., G. Tai, and W. Hong.** 2004. Autoantigen Golgin-97, an effector of Arl1 GTPase, participates in traffic from the endosome to the trans-golgi network. Mol Biol Cell **15:**4426-43.

76. **Lundgren, O., and L. Svensson.** 2001. Pathogenesis of rotavirus diarrhea. Microbes and Infection **3:**1145-1156.
77. **Lynch, M., W. J. Shieh, K. Tatti, J. R. Gentsch, T. Ferebee-Harris, B. Jiang, J. Guarner, J. S. Bresee, M. Greenwald, S. Cullen, H. D. Davies, C. Trevenen, S. R. Zaki, and R. I. Glass.** 2003. The pathology of rotavirus-associated deaths, using new molecular diagnostics. Clin Infect Dis **37:**1327-33.
78. **Malek, M. A., A. T. Curns, R. C. Holman, T. K. Fischer, J. S. Bresee, R. I. Glass, C. A. Steiner, and U. D. Parashar.** 2006. Diarrhea- and rotavirus-associated hospitalizations among children less than 5 years of age: United States, 1997 and 2000. Pediatrics **117:**1887-92.
79. **Manders, E. M. M., F. J. Verbeck, and J. A. Aten.** 1993. Measurement of colocalization of objects in dual-color confocal images. Journal of Microscopy **169:**375-382.
80. **Maxfield, F. R., and D. Wustner.** 2002. Intracellular cholesterol transport. J Clin Invest **110:**891-8.
81. **Meyer, J. C., C. C. Bergmann, and A. R. Bellamy.** 1989. Interaction of rotavirus cores with the nonstructural glycoprotein NS28. Virology **171:**98-107.
82. **Mirazimi, A., M. Nilsson, and L. Svensson.** 1998. The molecular chaperone calnexin interacts with the NSP4 enterotoxin of rotavirus in vivo and in vitro. J. Virol. **72:**8705-8709.
83. **Mitchell, D. M., and J. M. Ball.** 2004. Characterization of a spontaneously polarizing HT-29 cell line, HT-29/cl.f8. In Vitro Cell Dev Biol Anim **40:**297-302.
84. **Montero, H., C. F. Arias, and S. Lopez.** 2006. Rotavirus nonstructural protein NSP3 is not required for viral protein synthesis. J Virol **80:**9031-8.
85. **Moremen, K. W., R. B. Trimble, and A. Herscovics.** 1994. Glycosidases of the asparagine-linked oligosaccharide processing pathway. Glycobiology **4:**113-25.
86. **Morris, A. P., J. K. Scott, J. M. Ball, C. Q. Y. Zeng, W. K. O'Neal, and M. K. Estes.** 1999. NSP4 elicits age-dependent diarrhea and Ca2+mediated I- influx into intestinal crypts of CF mice. Am J Physiol Gastrointest Liver Physiol **277:**G431-444.
87. **Morrow, I. C., S. Rea, S. Martin, I. A. Prior, R. Prohaska, J. F. Hancock, D. E. James, and R. G. Parton.** 2002. Flotillin-1/reggie-2 traffics to surface raft domains via a novel golgi-independent pathway. Identification of a novel membrane targeting domain and a role for palmitoylation. J Biol Chem **277:**48834-41.
88. **Murata, M., J. Peranen, R. Schreiner, F. Wieland, T. V. Kurzchalia, and K. Simons.** 1995. VIP21/caveolin is a cholesterol-binding protein. Proc Natl Acad Sci U S A **92:**10339-43.
89. **Nejmeddine, M., G. Trugnan, C. Sapin, E. Kohli, L. Svensson, S. Lopez, and J. Cohen.** 2000. Rotavirus spike protein VP4 is present at the plasma membrane and is associated with microtubules in infected cells. J Virol **74:**3313-20.
90. **Neufeld, E. B., A. M. Cooney, J. Pitha, E. A. Dawidowicz, N. K. Dwyer, P. G. Pentchev, and E. J. Blanchette-Mackie.** 1996. Intracellular trafficking of cholesterol monitored with a cyclodextrin. J Biol Chem **271:**21604-13.

91. **Newton, K., J. C. Meyer, A. R. Bellamy, and J. A. Taylor.** 1997. Rotavirus nonstructural glycoprotein NSP4 alters plasma membrane permeability in mammalian cells. J Virol **71:**9458-65.
92. **Ovchinnikov Yu, A., N. M. Luneva, E. A. Arystarkhova, N. M. Gevondyan, N. M. Arzamazova, A. T. Kozhich, V. A. Nesmeyanov, and N. N. Modyanov.** 1988. Topology of Na+,K+-ATPase. Identification of the extra- and intracellular hydrophilic loops of the catalytic subunit by specific antibodies. FEBS Lett **227:**230-4.
93. **Padilla-Noriega, L., O. Paniagua, and S. Guzman-Leon.** 2002. Rotavirus protein NSP3 shuts off host cell protein synthesis. Virology **298:**1-7.
94. **Parashar, U. D., E. G. Hummelman, J. S. Bresee, M. A. Miller, and R. I. Glass.** 2003. Global illness and deaths caused by rotavirus disease in children. Emerg Infect Dis **9:**565-72.
95. **Parr, R. D., S. M. Storey, D. M. Mitchell, A. L. McIntosh, M. Zhou, K. D. Mir, and J. M. Ball.** 2006. The rotavirus enterotoxin NSP4 directly interacts with the caveolar structural protein caveolin-1. J Virol **80:**2842-54.
96. **Parton, R. G.** 1994. Ultrastructural localization of gangliosides; GM1 is concentrated in caveolae. J Histochem Cytochem **42:**155-66.
97. **Parton, R. G., M. Hanzal-Bayer, and J. F. Hancock.** 2006. Biogenesis of caveolae: a structural model for caveolin-induced domain formation. J Cell Sci **119:**787-796.
98. **Parton, R. G., and K. Simons.** 2007. The multiple faces of caveolae. Nat Rev Mol Cell Biol **8:**185-194.
99. **Patton, J. T., V. D. Carpio, and E. Spencer.** 2004. Replication and transcription of the rotavirus genome. Current Pharmaceutical Design **10:**3769-3777.
100. **Patton, J. T., and D. Chen.** 1999. RNA-binding and capping activities of proteins in rotavirus open cores. J Virol **73:**1382-91.
101. **Pike, L. J.** 2005. Growth factor receptors, lipid rafts and caveolae: an evolving story. Biochim Biophys Acta **1746:**260-73.
102. **Pike, L. J.** 2003. Lipid rafts: bringing order to chaos. J Lipid Res **44:**655-67.
103. **Pike, L. J., and L. Casey.** 1996. Localization and turnover of phosphatidylinositol 4,5-bisphosphate in caveolin-enriched membrane domains. J Biol Chem **271:**26453-6.
104. **Pol, A., S. Martin, M. A. Fernandez, M. Ingelmo-Torres, C. Ferguson, C. Enrich, and R. G. Parton.** 2005. Cholesterol and fatty acids regulate dynamic caveolin trafficking through the Golgi complex and between the cell surface and lipid bodies. Mol. Biol. Cell **16:**2091-2105.
105. **Prasad, B. V., G. J. Wang, J. P. Clerx, and W. Chiu.** 1988. Three-dimensional structure of rotavirus. J Mol Biol **199:**269-75.
106. **Puri, S., and A. D. Linstedt.** 2003. Capacity of the golgi apparatus for biogenesis from the endoplasmic reticulum. Mol Biol Cell **14:**5011-8.
107. **Quest, A. F., L. Leyton, and M. Parraga.** 2004. Caveolins, caveolae, and lipid rafts in cellular transport, signaling, and disease. Biochem Cell Biol **82:**129-44.

108. **Rajagopalan, S., Y. Xu, and M. B. Brenner.** 1994. Retention of unassembled components of integral membrane proteins by calnexin. Science **263:**387-90.
109. **Ramig, R. F.** 2004. Pathogenesis of intestinal and systemic rotavirus infection. J Virol **78:**10213-20.
110. **Razani, B., S. E. Woodman, and M. P. Lisanti.** 2002. Caveolae: from cell biology to animal physiology. Pharmacol Rev **54:**431-67.
111. **Ridsdale, A., M. Denis, P. Y. Gougeon, J. K. Ngsee, J. F. Presley, and X. Zha.** 2006. Cholesterol is required for efficient endoplasmic reticulum-to-Golgi transport of secretory membrane proteins. Mol Biol Cell **17:**1593-605.
112. **Rothberg, K. G., J. E. Heuser, W. C. Donzell, Y. S. Ying, J. R. Glenney, and R. G. Anderson.** 1992. Caveolin, a protein component of caveolae membrane coats. Cell **68:**673-82.
113. **Sabanayagam, C. R., J. S. Eid, and A. Meller.** 2005. Using fluorescence resonance energy transfer to measure distances along individual DNA molecules: corrections due to nonideal transfer. J Chem Phys **122:**061103.
114. **Sapin, C., O. Colard, O. Delmas, C. Tessier, M. Breton, V. Enouf, S. Chwetzoff, J. Ouanich, J. Cohen, C. Wolf, and G. Trugnan.** 2002. Rafts promote assembly and atypical targeting of a nonenveloped virus, rotavirus, in Caco-2 cells. J Virol **76:**4591-602.
115. **Scheiffele, P., P. Verkade, A. M. Fra, H. Virta, K. Simons, and E. Ikonen.** 1998. Caveolin-1 and -2 in the exocytic pathway of MDCK cells. J Cell Biol **140:**795-806.
116. **Scherer, P. E., R. Y. Lewis, D. Volonte, J. A. Engelman, F. Galbiati, J. Couet, D. S. Kohtz, E. van Donselaar, P. Peters, and M. P. Lisanti.** 1997. Cell-type and tissue-specific expression of caveolin-2. Caveolins 1 and 2 co-localize and form a stable hetero-oligomeric complex in vivo. J Biol Chem **272:**29337-46.
117. **Schmid, S. L.** 1997. Clathrin-coated vesicle formation and protein sorting: an integrated process. Annu Rev Biochem **66:**511-48.
118. **Schnitzer, J. E., D. P. McIntosh, A. M. Dvorak, J. Liu, and P. Oh.** 1995. Separation of caveolae from associated microdomains of GPI-anchored proteins. Science **269:**1435-9.
119. **Schnitzer, J. E., P. Oh, B. S. Jacobson, and A. M. Dvorak.** 1995. Caveolae from luminal plasmalemma of rat lung endothelium: microdomains enriched in caveolin, Ca(2+)-ATPase, and inositol trisphosphate receptor. Proc Natl Acad Sci U S A **92:**1759-63.
120. **Schroeder, F., A. M. Gallegos, B. P. Atshaves, S. M. Storey, A. L. McIntosh, A. D. Petrescu, H. Huang, O. Starodub, H. Chao, H. Yang, A. Frolov, and A. B. Kier.** 2001. Recent advances in membrane microdomains: Rafts, caveolae, and intracellular cholesterol trafficking. Exp. Biol. Med. **226:**873-890.
121. **Silvestri, L. S., M. A. Tortorici, R. Vasquez-Del Carpio, and J. T. Patton.** 2005. Rotavirus glycoprotein NSP4 is a modulator of viral transcription in the infected cell. J Virol **79:**15165-74.
122. **Simons, K., and E. Ikonen.** 1997. Functional rafts in cell membranes. Nature **387:**569-72.

123. **Sinensky, M., L. A. Beck, S. Leonard, and R. Evans.** 1990. Differential inhibitory effects of lovastatin on protein isoprenylation and sterol synthesis. J Biol Chem **265:**19937-41.
124. **Smart, E. J., G. A. Graf, M. A. McNiven, W. C. Sessa, J. A. Engelman, P. E. Scherer, T. Okamoto, and M. P. Lisanti.** 1999. Caveolins, liquid-ordered domains, and signal transduction. Mol Cell Biol **19:**7289-304.
125. **Smart, E. J., Y. Ying, W. C. Donzell, and R. G. Anderson.** 1996. A role for caveolin in transport of cholesterol from endoplasmic reticulum to plasma membrane. J Biol Chem **271:**29427-35.
126. **Smart, E. J., Y. S. Ying, C. Mineo, and R. G. Anderson.** 1995. A detergent-free method for purifying caveolae membrane from tissue culture cells. Proc Natl Acad Sci U S A **92:**10104-8.
127. **Song, K. S., S. Li, T. Okamoto, L. A. Quilliam, M. Sargiacomo, and M. P. Lisanti.** 1996. Co-purification and direct interaction of Ras with caveolin, an integral membrane protein of caveolae microdomains. Detergent-free purification of caveolae microdomains. J Biol Chem **271:**9690-7.
128. **Sot, J., M. Isabel Collado, Jose L. R. Arrondo, Alicia Alonso, Felix M. Foni.** 2002. Triton X-100-resitant bilayers: Effect of lipid composition and relevance to the raft phenomenon. Langmuir **18:**2828-2835.
129. **Souto, R. P., G. Vallega, J. Wharton, J. Vinten, J. Tranum-Jensen, and P. F. Pilch.** 2003. Immunopurification and characterization of rat adipocyte caveolae suggest their dissociation from insulin signaling. J Biol Chem **278:**18321-9.
130. **Spisni, E., V. Tomasi, A. Cestaro, and S. C. Tosatto.** 2005. Structural insights into the function of human caveolin 1. Biochem Biophys Res Commun **338:**1383-90.
131. **Stoorvogel, W., V. Oorschot, and H. J. Geuze.** 1996. A novel class of clathrin-coated vesicles budding from endosomes. J Cell Biol **132:**21-33.
132. **Storey, S. M., T. F. Gibbons, C. V. Williams, R. D. Parr, F. Schroeder, and J. M. Ball.** 2007. Full-length, glycosylated NSP4 is localized to plasma membrane caveolae by a novel raft isolation technique. J. Virol. **81:**5472-5483.
133. **Tafazoli, F., C. Q. Zeng, M. K. Estes, K. E. Magnusson, and L. Svensson.** 2001. NSP4 enterotoxin of rotavirus induces paracellular leakage in polarized epithelial cells. J Virol **75:**1540-6.
134. **Tan-Wilson, A. L., M. Reichlin, and R. W. Noble.** 1976. Isolation and characterization of low and high affinity goat antibodies directed to single antigenic sites on human hemoglobin. Immunochemistry **13:**921-7.
135. **Taniguchi, K., K. Nishikawa, N. Kobayashi, T. Urasawa, H. Wu, M. Gorziglia, and S. Urasawa.** 1994. Differences in plaque size and VP4 sequence found in SA11 virus clones having simian authentic VP4. Virology **198:**325-30.
136. **Taylor, J. A., J. C. Meyer, M. A. Legge, J. A. O'Brien, J. E. Street, V. J. Lord, C. C. Bergmann, and A. R. Bellamy.** 1992. Transient expression and mutational analysis of the rotavirus intracellular receptor: the C-terminal methionine residue is essential for ligand binding. J Virol **66:**3566-72.

137. **Taylor, J. A., J. A. O'Brien, and M. Yeager.** 1996. The cytoplasmic tail of NSP4, the endoplasmic reticulum-localized non-structural glycoprotein of rotavirus, contains distinct virus binding and coiled coil domains. Embo J **15:**4469-76.
138. **Tian, P., M. K. Estes, Y. Hu, J. M. Ball, C. Q. Zeng, and W. P. Schilling.** 1995. The rotavirus nonstructural glycoprotein NSP4 mobilizes Ca2+ from the endoplasmic reticulum. J. Virol. **69:**5763-5772.
139. **Uittenbogaard, A., and E. J. Smart.** 2000. Palmitoylation of caveolin-1 is required for cholesterol binding, chaperone complex formation, and rapid transport of cholesterol to caveolae. J Biol Chem **275:**25595-9.
140. **Uittenbogaard, A., Y. Ying, and E. J. Smart.** 1998. Characterization of a cytosolic heat-shock protein-caveolin chaperone complex. Involvement in cholesterol trafficking. J Biol Chem **273:**6525-32.
141. **Ward, T. H., R. S. Polishchuk, S. Caplan, K. Hirschberg, and J. Lippincott-Schwartz.** 2001. Maintenance of Golgi structure and function depends on the integrity of ER export. J Cell Biol **155:**557-70.
142. **Wines BD, E.-S. S.** 1991. The Fab/c fragment of IgG produced by cleavage at cyanocysteine residues. Molecular Immunology **28:**855-863.
143. **Xu, A., A. R. Bellamy, and J. A. Taylor.** 2000. Immobilization of the early secretory pathway by a virus glycoprotein that binds to microtubules. Embo J **19:**6465-74.
144. **Yarbrough, T. L., T. Lu, H. C. Lee, and E. F. Shibata.** 2002. Localization of cardiac sodium channels in caveolin-rich membrane domains: regulation of sodium current amplitude. Circ Res **90:**443-9.
145. **Zeng, C. Q., M. J. Wentz, J. Cohen, M. K. Estes, and R. F. Ramig.** 1996. Characterization and replicase activity of double-layered and single-layered rotavirus-like particles expressed from baculovirus recombinants. J Virol **70:**2736-42.
146. **Zhang, M., C. Q. Zeng, A. P. Morris, and M. K. Estes.** 2000. A functional NSP4 enterotoxin peptide secreted from rotavirus-infected cells. J Virol **74:**11663-70.

APPENDIX A

Supplementary videos accompany this dissertation as separate files available for downloading.

Figure		**Link**
4.1		
	Giantin	
4.2		
	Clathrin 3D (RV-infected HT29.f8 cells)	
	Clathrin 3D (uninfected HT29.f8 cells)	
	Beta Cop 3D (RV-infected HT29.f8 cells)	
	Beta Cop 3D (uninfected HT29.f8 cells)	
4.3		
	PDI 3D	
	Beta Cop 3D	
	NSP4 3D	
	Merge 3D (PDI, Beta Cop, NSP4)	
	Merge 3D (Beta Cop, NSP4)	
	Merge 3D (PDI, Beta Cop)	
4.4		
	Cav-1 3D (RV-infected HT29.f8 cells)	
	Cav-1 3D (uninfected HT29.f8 cells)	
	Giantin 3D (RV-infected HT29.f8 cells)	
	Giantin 3D (uninfected HT29.f8 cells)	
4.5		
	Cav-1/NSP4 3D (RV-infected HT29.f8 cells)	
	Cav-1/NSP5 3D (RV-infected HT29.f8 cells)	
	Giantin/NSP4 3D (RV-infected HT29.f8 cells)	
	Giantin/NSP5 3D (RV-infected HT29.f8 cells)	
4.6		
	NSP4/Cyclo 40 3D	
	NSP5/Cyclo 40 3D	
	NSP4/Cyclo A 3D	
	NSP5/Cyclo A 3D	
	NSP4/HSP 56 3D	
	NSP5/HSP 56 3D	

VITA

Captain Thomas Field Gibbons, USAF, BSC

Phone: 210-536-5882
Address 2484 Gillingham Drive, B-175 West, Brooks City-Base, TX 78235-5109
E-mail: Thomas.Gibbons@Brooks.af.mil

Captain Gibbons is an Air Force Biomedical Science Corps Laboratory Officer, currently assigned as the chief military scientist at the Applied Technology Cell, Air Force Institute for Operational Health, Brooks city-base, TX. His previous assignment was as an Air Force Institute of Technology (AFIT) student pursuing a Ph.D. in Microbiology at Texas A&M University. Prior to his AFIT assignment he was Chief of Microbiology, Air Force Institute for Operational Health, Brooks city-base, TX. There, he directed the USAF's only reference services for microbiology and parasitology. Captain Gibbons also served as the Air Force Laboratory Response Network Gatekeeper, directing the Air Forces' lead national Laboratory Response Network biowarfare laboratory facility and coordinating testing with the CDC and Federal Bureaus of Investigations for the Air Force.

Captain Gibbons received an associates degree in Instructor of Technology and Military Science, from the Community College of the Air Force in 1995, his Bachelors of Applied Arts and Science from Midwestern State University in 1992 and his Master of Science in Clinical Laboratory Science from the University of North Dakota in 2002.